UNCLASSIFIED

AD NUMBER
AD839274
NEW LIMITATION CHANGE
TO Approved for public release, distribution unlimited
FROM Distribution authorized to DoD only; Administrative/Operational Use; AUG 1968. Other requests shall be referred to Air Force Rocket Propulsion Lab., Edwards AFB, CA 93523.
AUTHORITY
AFRPL ltr 27 Oct 1971

THIS PAGE IS UNCLASSIFIED

AFRPL-TR-63-124-Vol II

Copy No. 32

AD 839274

FLEXIBLE EXIT CONE NOZZLE DEVELOPMENT PROGRAM PHASE II REPORT

VOLUME II COLD FLOW TESTS

August 1968

STATEMENT #4 UNCLASSIFIED

Each tran[illegible]ent outside the Department of Defense must have prior approval of _____

Prepared for

Air Force
Rocket Propulsion Laboratory
Research and Technology Division
Air Force Systems Command
Edwards, California 93523

attn: RPPR/ST INFO

Thiokol
CHEMICAL CORPORATION
WASATCH DIVISION

DDC
SEP 17 1968
A

DISCLAIMER NOTICE

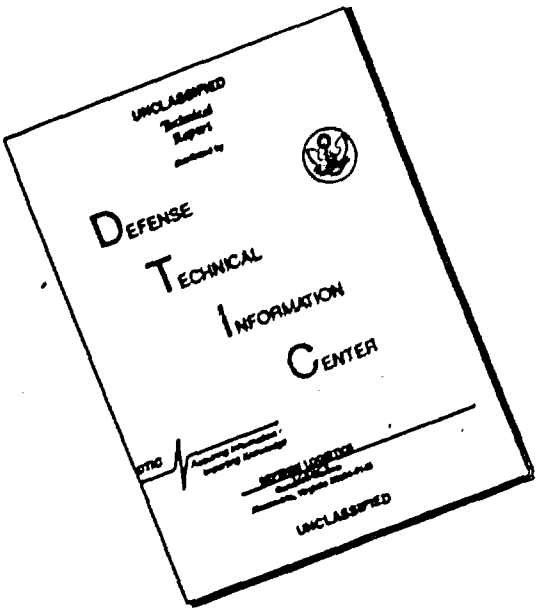

THIS DOCUMENT IS BEST QUALITY AVAILABLE. THE COPY FURNISHED TO DTIC CONTAINED A SIGNIFICANT NUMBER OF PAGES WHICH DO NOT REPRODUCE LEGIBLY.

TWR-3050

FINAL REPORT

COLD FLOW TESTS
FLEX-X NOZZLE

August 1968

Prepared by

R. Lavery
Aero-Thermo Analysis Section

Sa: AD392452L (c), Vol. 1

18 19 AFRPL-TR-68-124-Vol[redacted]-2

14 TWR-3050-Vol-2.

9 Final rept. 15 Mar 67-31 Jul 68, on Phase 2,

AD V.1 AD 392 452L

6

FLEXIBLE EXIT CONE NOZZLE DEVELOPMENT PROGRAM.

[redacted]

VOLUME II. COLD FLOW TESTS.

10 R. Lavery

11 Aug[redacted] [redacted]68

12 93p.

15 F04611-68-C-0004 AD V.1 AD 392 452 L

Prepared by

THIOKOL CHEMICAL CORPORATION
WASATCH DIVISION
Brigham City, Utah

Publications No. 0868-19523

829 727

TABLE OF CONTENTS

		Page
I	INTRODUCTION AND SUMMARY	1
	A. Introduction	1
	B. Summary	2
II	TEST OBJECTIVES	3
III	TECHNICAL APPROACH	4
	A. Scope	4
	B. Test Plan	5
	C. Nomenclature	5
IV	FACILITY	9
V	TEST PROCEDURE	17
	A. Calibration	17
	B. Test Models	26
	C. Instrumentation	32
	D. Testing	35
VI	TEST RESULTS	37
	A. Data Presentation	37
	B. Discussion of Test Data	40
	1. Side Force and Torque	40
	2. Axial Force Data	61
	3. Pressure Data and Flow Visualization Data	66
VII	CONCLUSIONS	73
VIII	RECOMMENDATIONS	

LIST OF ILLUSTRATIONS

Figure		Page
1	Basic Flex-X Cold Flow Nozzle Nomenclature	7
2	Cold Flow Laboratory Layout (TUL 11175)	10
3	Arrangement of Test Tank	11
4	Ejector System for Thrust Stand Cold Flow	12
5	Thrust Stand and Piping	13
6	Flex-X Model in Thrust Stand	15
7	Flexible Joint Thrust Stand	16
8	Channel 5 Calibration	19
9	Channel 6 Calibration	20
10	Chanel 7 Calibration	21
11	Channel 5, Second Calibration	23
12	Channel 6, Second Calibration	24
13	Channel 7, Second Calibration	25
14	Flex-X Cold Flow Model Details	27
15	Flex-X Cold Flow Model Assembly	28
16	Flex-X Cold Flow Model Details at Exit Expansion ϵ 10	29
17	Flex-X Cold Flow Model Details, 15 Degree Nozzle Angle, Exit Expansion ϵ 10, 16, and 25	30

LIST OF ILLUSTRATIONS (Cont)

Figure		Page
18	Flex-X Cold Flow Model Details, 25 Degree Nozzle Angle, Exit Expansion ϵ 10, 16, and 25	31
19	Sketch of Eroded Nozzles (30 and 60 Sec)	33
20	Three Component Balance System Gage Installation	34
21	Photograph of the Mercury Manometer Board Run No. 1, 5 Degree Vector, Hg 25.71	36
22	Effect of Pivot Location on Side Force and Torque Amplification ($\epsilon = 10$, $\epsilon_s = 1.5$)	42
23	Effect of Pivot Location on Side Force and Torque Amplification ($\epsilon = 10$, $\epsilon_s - 2.5$)	43
24	Effect of Pivot Location on Side Force and Torque Amplification ($\epsilon = 10$, $\epsilon_s = 4.0$)	44
25	Effect of Pivot Location on Side Force and Torque Amplification ($\epsilon = 25$, $\epsilon_s = 1.5$)	45
26	Effect of Pivot Location on Side Force and Torque Amplification ($\epsilon = 25$, $\epsilon_s = 2.5$)	46
27	Effect of Pivot Location on Side Force and Torque Amplification ($\epsilon = 25$, $\epsilon_s = 4.0$)	47
28	Effect of Joint Location on Side Force and Torque Amplification ($\epsilon = 10$, Pivot 1)	49
29	Effect of Joint Location on Side Force and Torque Amplification ($\epsilon = 10$, Pivot 2)	50
30	Effect of Joint Location on Side Force and Torque Amplification ($\epsilon = 10$, Pivot 3)	51
31	Effect of Joint Location on Side Force and Torque Amplification ($\epsilon = 25$, Pivot 1)	52

LIST OF ILLUSTRATIONS (Cont)

Figure		Page
32	Effect of Joint Location on Side Force and Torque Amplification (ϵ = 25, Pivot 2)	53
33	Effect of Joint Location on Side Force and Torque Amplification (ϵ = 25, Pivot 3)	54
34	Effect of Nozzle Expansion Ration on Side Force and Torque Amplification (α = 15 Deg)	56
35	Effect of Nozzle Expansion Ration on Side Force and Torque Amplification (α = 25 Deg)	57
36	Effect of Nozzle Cone Angle on Side Force and Torque Amplification	59
37	Effect of Nozzle Erosion on Side Force and Torque Amplification	60
38	Axial Thrust Efficiency vs Nozzle Vector Angle	62
39	Axial Thrust Efficiency vs Nozzle Vector Angle	63
40	Axial Thrust Efficiency vs Nozzle Vector Angle	64
41	Axial Thrust Efficiency vs Nozzle Vector Angle	65
42	Comparison of Test Data with Theory, Compression Side of Nozzle	67
43	Comparison of Test Data with Theory, Expansion Side of Nozzle	68
44	Flow Visualization Showing Separation Upstream of the Joint (Test 19)	69
45	Flow Visualization Showing Separation Upstream of the Joint (Test 20)	70
46	Flow Visualization Showing Separation Upstream of the Joint (Test 21)	71

LIST OF TABLES

Table		Page
I	Cold Flow Test Matrix	6
II	Calibration Data (Ten Pound Increments)	18
III	Calibration Data (Fifty Pound Increments)	22

SECTION I

INTRODUCTION AND SUMMARY

A. INTRODUCTION

The flexible exit cone nozzle is a new concept being developed by Thiokol Chemical Corporation to provide improved rocket motor system performance and reliability. This concept consists of replacing a section of the exit cone with a flexible joint which will permit vectoring of the supersonic section of the exit cone.

This document is a report of the cold flow testing and analysis performed at Thiokol to establish nozzle design and performance criteria.

The Flex-X concept provides thrust vector control (TVC) by turning the exhaust gases in the supersonic portion of the nozzle, resulting in complex flow patterns which are difficult to evaluate analytically. These flow conditions are similar to those of the supersonic splitline nozzle. Therefore the data acquired in this program is applicable to both the supersonic splitline and the flexible exit cone designs.

This report supersedes results presented in the Phase I report.* Analysis revealed some faulty data and it was therefore necessary to repeat some runs to obtain consistent reliable results.

*AFRPL-TR-68-66 Flexible Exit Cone Nozzle Development Program Phase I Report dated April 1968.

B. SUMMARY

This report documents the cold flow testing conducted on the flexible exit cone nozzle. The cold flow program was conducted to establish the performance characteristics of the Flex-X nozzle. The influence of various geometric parameters on nozzle side force, actuation torque, and axial thrust were investigated.

The flexible exit cone nozzle turns the gas in the supersonic portion of the nozzle. With proper design this concept can produce side forces greater than those realized with conventional vector nozzle systems.

The maximum side force amplification achieved in this program was approximately 1.65 on the 10:1 expansion ratio nozzle and 1.95 on the 25:1 expansion ratio nozzle. Torque amplifications were 3.6 and 2.9 respectively. Axial thrust losses for these configurations were from one to two percent. The maximum thrust loss measured was approximately eight percent.

Between five and ten degrees nozzle vector, the compression side shock intersected the expansion wall and moved into the nozzle far enough to cause a decrease in side force amplification. Where high vector angles are required, the seal could be moved aft to prevent this shock intersection.

SECTION II

TEST OBJECTIVES

The objectives of this program were:

1. Characterize the performance of the flexible exit cone nozzle as a function of nozzle geometric design variables.
2. Evaluate flow conditions in the supersonic portion of the nozzle so an analytical model could be developed and verified.
3. Provide data to support the design of flexible exit cone demonstration nozzles.
4. Provide data for refinement of the TVC Computer Program.

SECTION III

TECHNICAL APPROACH

A. SCOPE

The nozzle axial thrust, side force, and actuation torque were measured on all test configurations. The effects of the following design variables on these parameters were investigated.

1. Joint Location
2. Pivot Location
3. Cone Angle
4. Nozzle Expansion Ratio
5. Vector Angle

A contoured nozzle also was tested for comparison with the conical nozzle designs.

Two eroded configurations were tested to evaluate the effect of firing time on nozzle performance. A 30 and a 60 second firing time configuration were tested. These configurations were predicted using measured erosion data from the fixed nozzle materials evaluation tests.

B. TEST PLAN

The test program was conducted in accordance with the test matrix presented in Table I. A total of 27 tests were conducted. Each test consisted of four runs at vector angles of 0, 2.5, 5.0, and 10.0 degrees.

Nozzle thrust, side force, and torque were measured on all test runs. Exit cone pressures were measured at several axial locations in the 0, 45, 90, 135, and 180 deg radial planes.

The cold flow program was conducted in four parts. Part 1 consisted of nine tests in which the effect of joint location, pivot location, and vector angle were evaluated for a 20 deg half angle exit cone having a 10:1 expansion ratio. Part 2 was identical to Part 1 except that a 25:1 expansion ratio nozzle was tested. Part 3 consists of seven tests in which the effect of exit cone divergence angle and expansion ratio are evaluated. The contoured nozzle was tested in this portion of the test. In Part 4, the effects of exit cone erosion are investigated.

C. NOMENCLATURE

The basic Flex-X cold flow model is shown in Figure 1. Pertinent nomenclature to be referenced in this report are shown in this figure.

All axial locations are measured along the centerline of the unvectored nozzle. Pressure data measured on the vectored nozzle are presented at the respective unvectored axial locations to ease data presentation.

The joint location is presented as the axial coordinate of the upstream side of the joint in this report. Joint thickness is held constant throughout the test.

All force data are presented nondimensionally for convenience in scaling.

TABLE I

COLD FLOW TEST MATRIX

Test	Station Location of Flexible Section	Hinge Location	Exit Cone Divergence Angle (deg)	Expansion Ratio of Nozzle	Nozzle Vector Angle	Purpose of Test Series
1	1	1	20	25		Determine the effect of flexible section location at various nozzle skirt hinge locations at an expansion ratio of 25.
2	2	1	20	25		
3	3	1	20	25		
4	1	2	20	25		
5	2	2	20	25	4 each	
6	3	2	20	25		
7	1	3	20	25		
8	2	3	20	25		
9	3	3	20	25		
10	1	1	20	10		Determine the effect of flexible section location at various nozzle skirt hinge locations at an expansion ratio of 10.
11	2	1	20	10		
12	3	1	20	10		
13	1	2	20	10		
14	2	2	20	10	4 each	
15	3	2	20	10		
16	1	3	20	10		
17	2	3	20	10		
18	3	3	20	10		
19	2	2	25	25		Determine the effect of exit cone divergence angle and expansion ratio.
20	2	2	25	18		
21	2	2	25	10		
22	2	2	15	25		
23	2	2	15	18	4 each	
24	2	2	15	10		
25	2	2	contour	10		
26	2	2	20	10	4 each	Check the effect of erosion at 30 sec after motor ignition.
27	2	2	20	10		Check the effect of erosion at 60 sec after motor ignition.

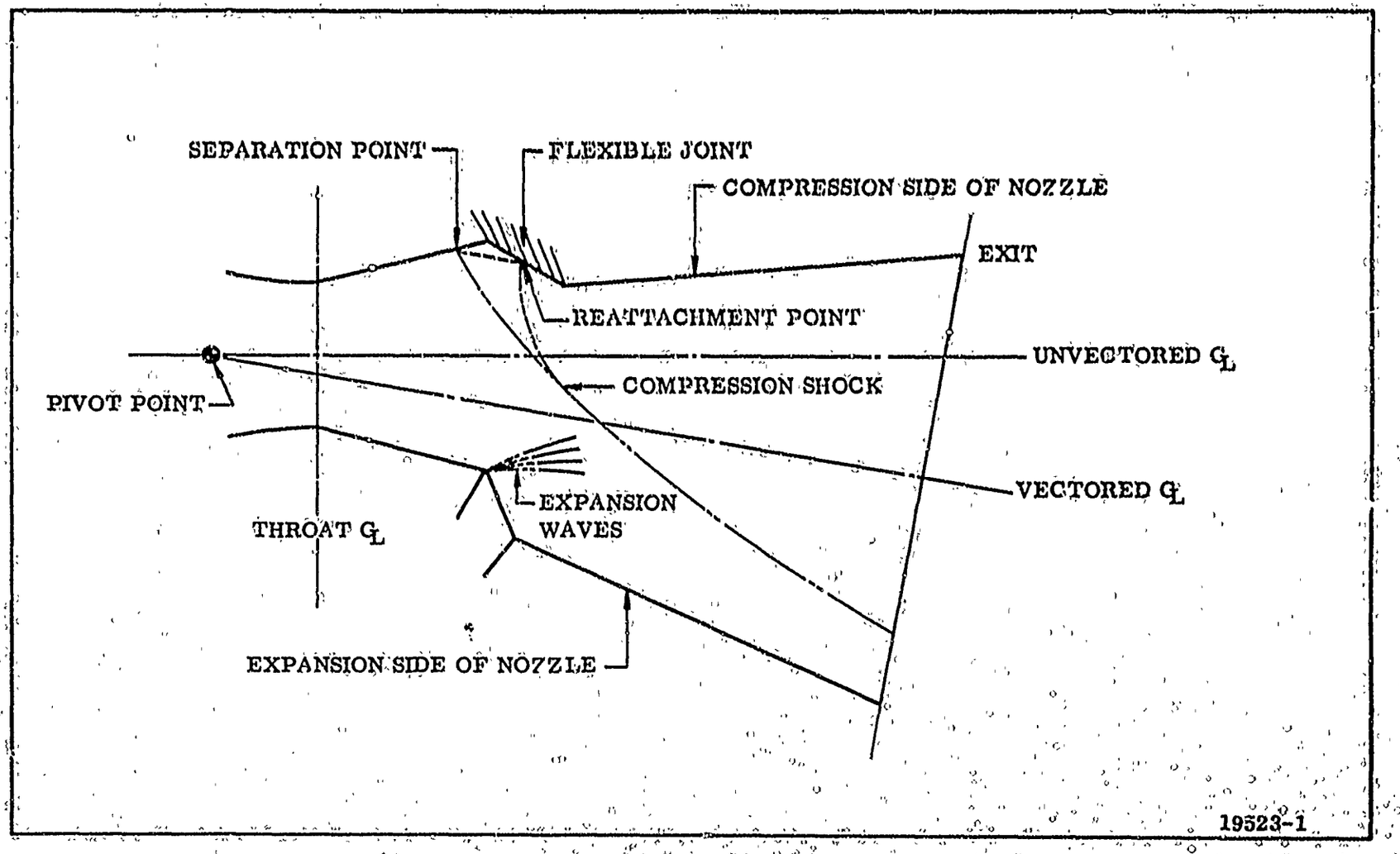

Figure 1. Basic Flex-X Cold Flow Nozzle Nomenclature

The following symbols and definitions are used in this report.

Symbol	Definition
P_o or P_t	Total Pressure
P and P_s	Static Pressure
ϵ_s	Joint Expansion Ratio
ϵ_e	Exit Expansion Ratio
γ	Specific Heat Ratio
C_f	Thrust Coefficient
δ	Vector Angle (deg)
P_a	Back Pressure
P_e	Exit Static Pressure
A_t	Throat Area
F_s	Side Force
Tamp	Torque Amplification
AF	Force Amplification
λ	Divergence Angle Correction Factor

SECTION IV

FACILITY

The Cold Flow Test Program was conducted at the Thiokol Wasatch Division Aerodynamics Laboratory. A complete description of this facility is presented in Reference 1.

Figure 2 shows the basic laboratory layout. The air supply is generated by a 3,000 psig compressor having a 200 cfm flow rate. The compressor exhausts directly into two 3,000 psi air receivers having a combined volume of 50 cubic feet. These tanks serve as surge tanks for the compressor. The main storage volume is provided by four Stage I Minuteman "Battleship" motor cases. The volume of each tank is 500 cubic feet. Thus the total system capacity is 2,000 cu ft of air at 400 psig (4,076 lb) and 50 cu ft at 3,000 psig (764 lb).

The air is piped from the large air receiver to a 10 in. flow control and shutoff valve located immediately upstream of the test cell.

The test cell consists of a three component thrust stand, an orifice metering tube, a plenum chamber with flexible seal connection to the air supply, a vacuum chamber enclosing the plenum chamber, an exhaust diffuser, and an ejector system. Figure 3 shows the general arrangement of the test cell and Figure 4 shows the ejector system.

The orifice meter accurately measures the weight flow delivered to the thrust stand by measuring the pressure loss across the orifice plate.

The air supply from the metering tube is split through a tee into a yoke and then to the plenum chamber (Figure 5). This configuration eliminates the inlet air momentum from the plane of the force measurement and balances the pressure area force of the air inlets.

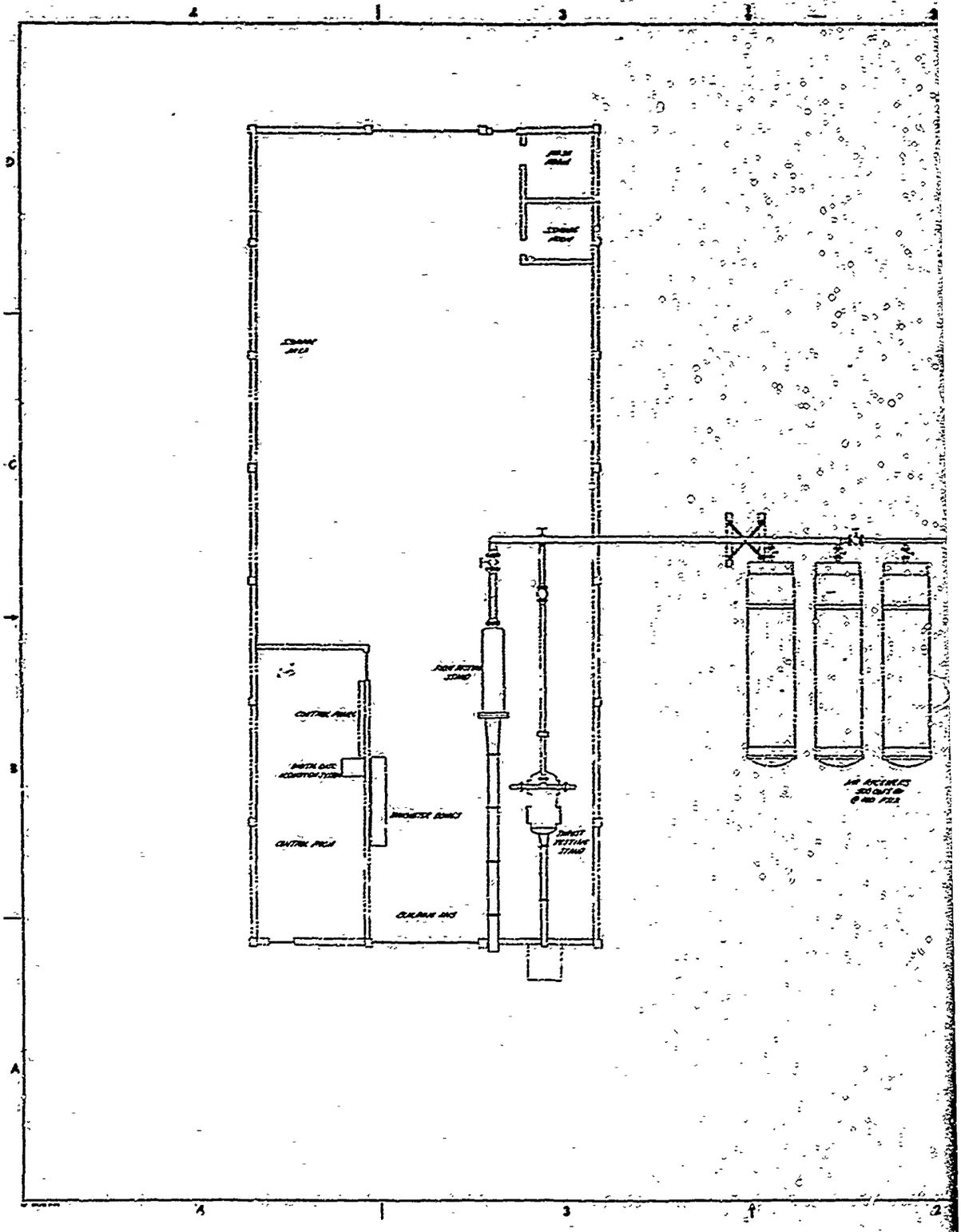

F

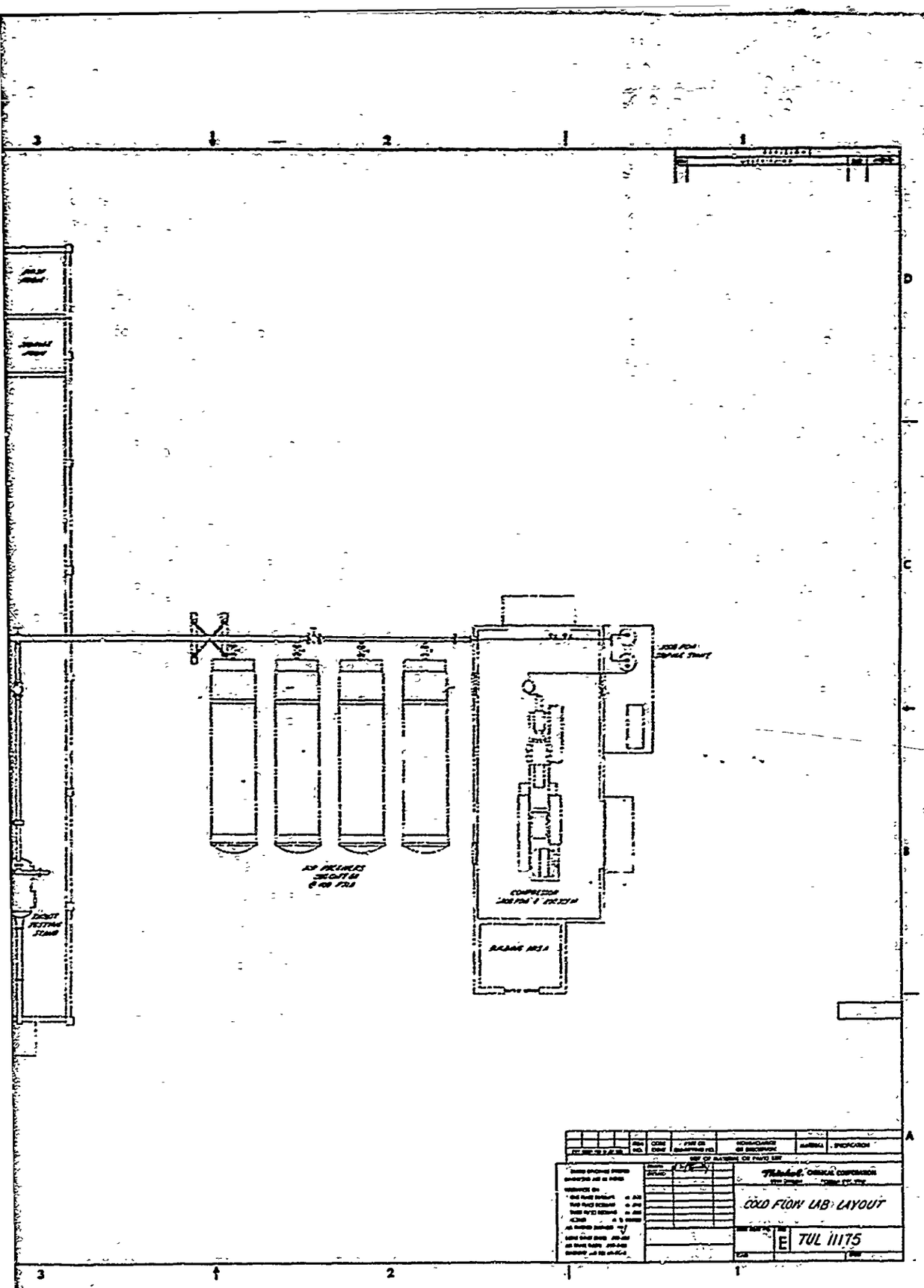

Figure 2. Cold Flow Laboratory Layout (TUL 11175)

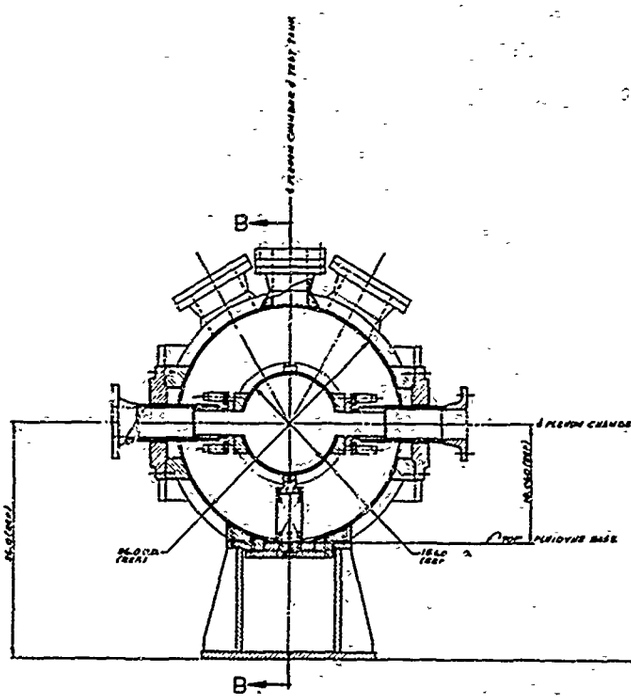

SECTION A-A

NO.	REVISIONS	CHECKED BY	DATE	DRAWN	DESIGN	NO.	REVISIONS	CHECKED BY	DATE	DRAWN	DESIGN	NO.	REVISIONS	CHECKED BY

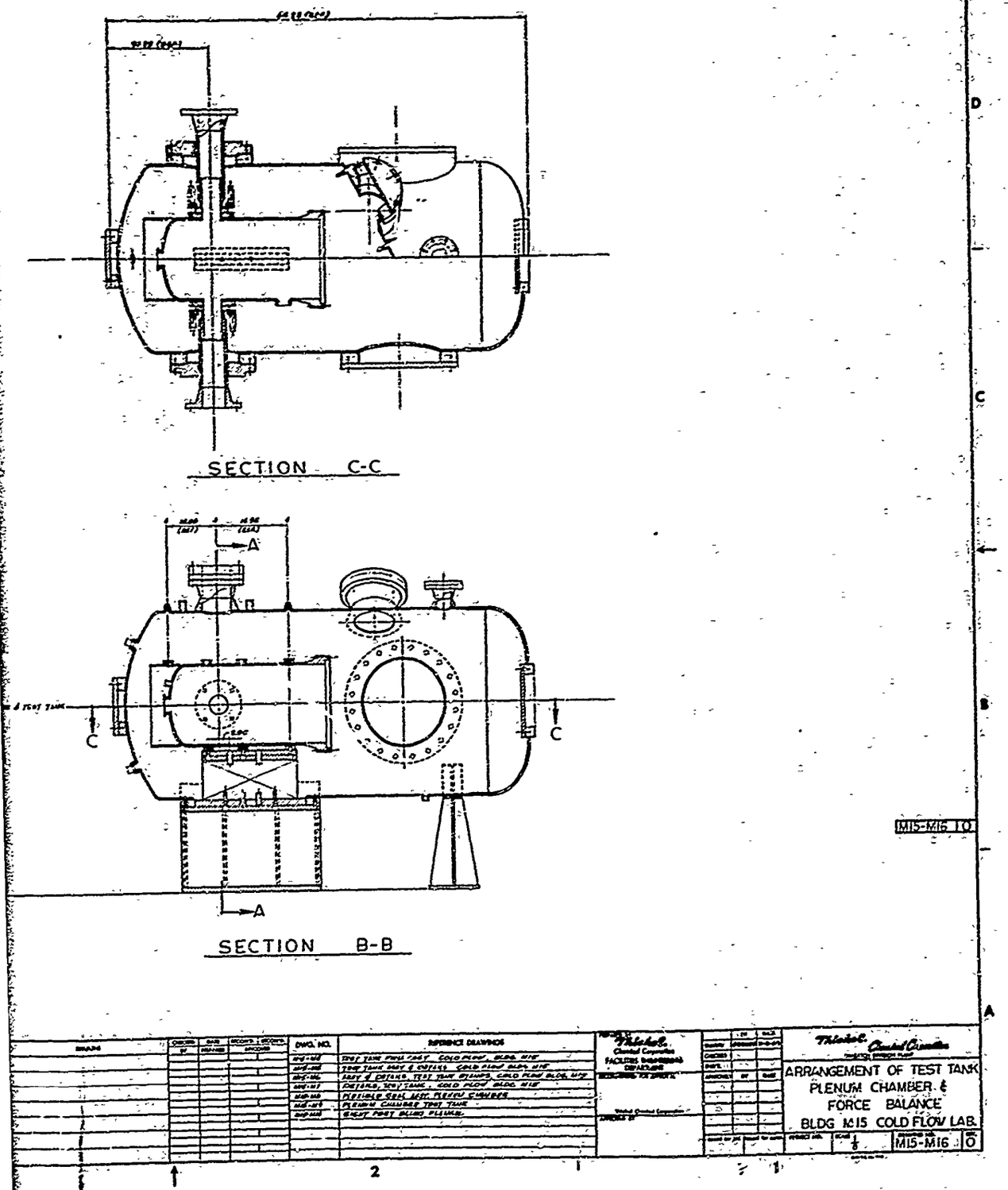

Figure 3. Arrangement of Test Tank

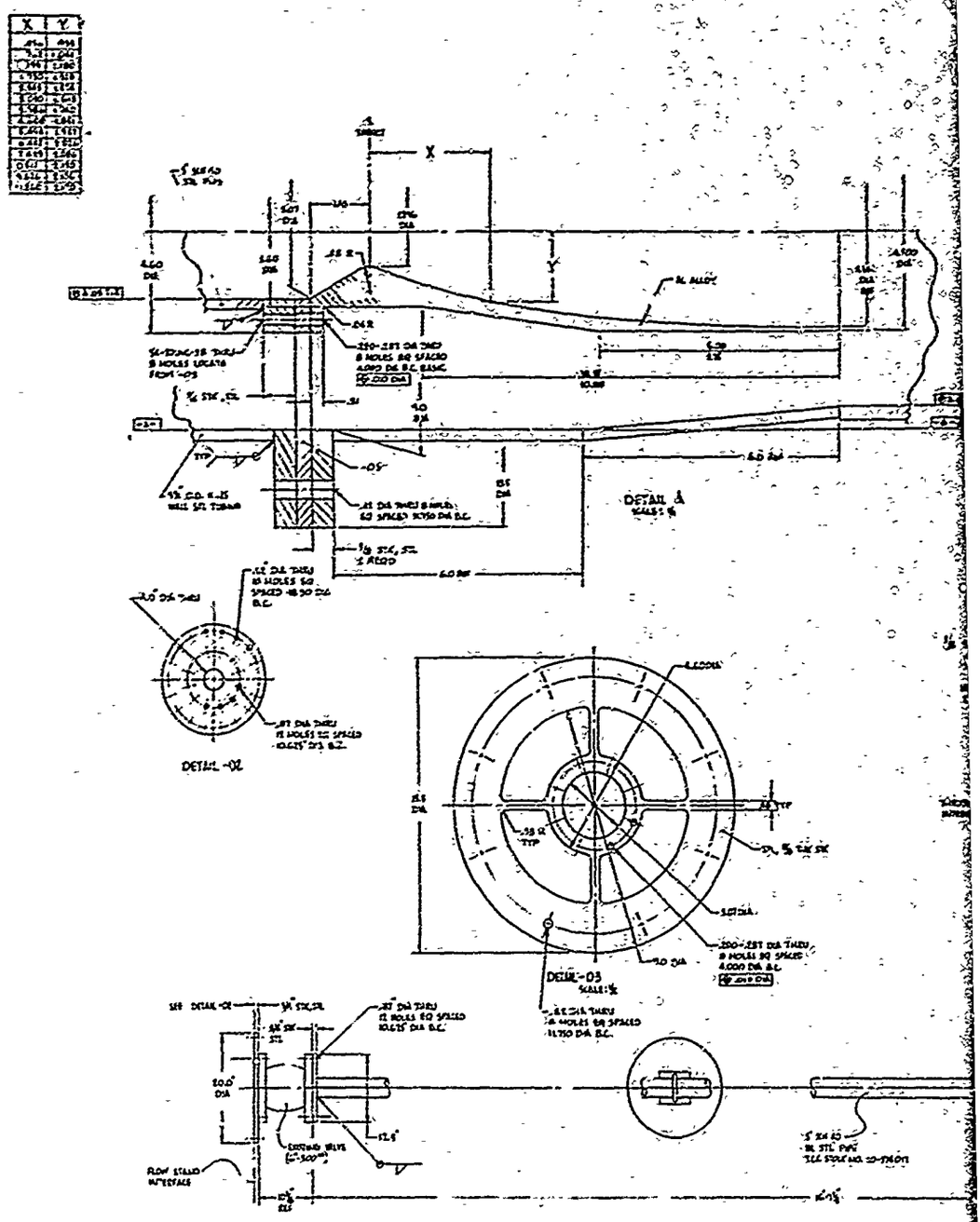
DETAIL A
DETAIL -02
DETAIL -03

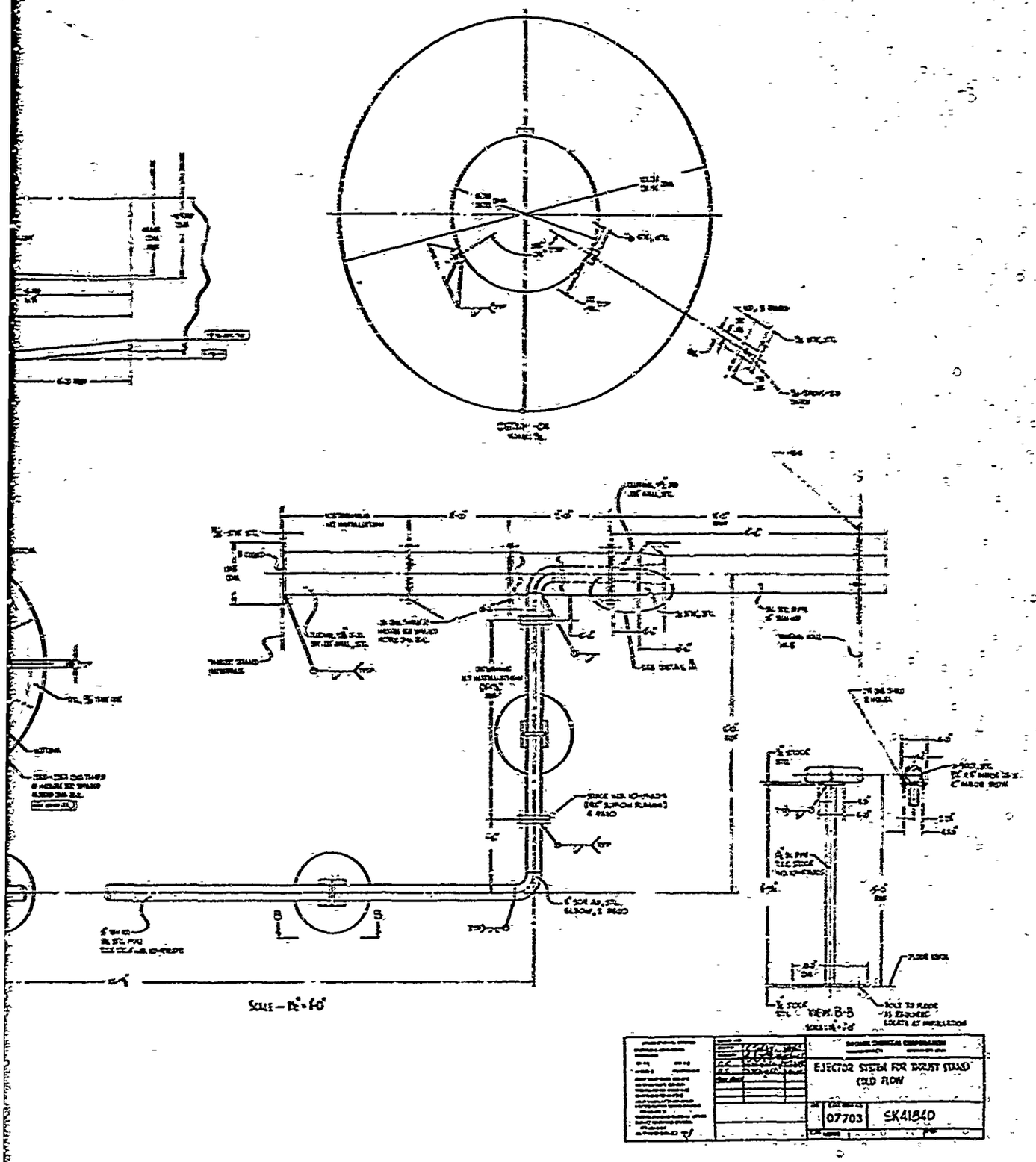

Figure 4. Ejector System for Thrust Stand Cold Flow

Figure 5. Thrust Stand and Piping

The plenum chamber supports the test model and supplies high pressure, zero velocity air to the test nozzle (Figure 6). The surrounding vacuum chamber allows the test nozzle to exhaust into a low pressure quiescent atmosphere for altitude simulation.

The exhaust diffuser serves to reduce the pressure in the vacuum chamber to the desired level to assure a fully flowing nozzle. The high expansion ratio nozzles require a lower back pressure such that the ejector system is necessary to achieve the desired conditions.

The vacuum chamber supports the instrumentation flanges and the air supply piping. The multicomponent force balance supports the plenum chamber and measures the three components of force in the vertical plane.

The flexible ducts replace the flexible seals described in Reference 1. The flexible ducts are constructed of alternate layers of rubber and steel (Figure 7). The force exerted on the plenum by the flexible ducts is very small and repeatable. The magnitude of force is proportional to the thrust load and is approximately 0.1 percent of the axial thrust. Calibration of the force balance removes the error induced by the ducts since the error is linear and repeatable.

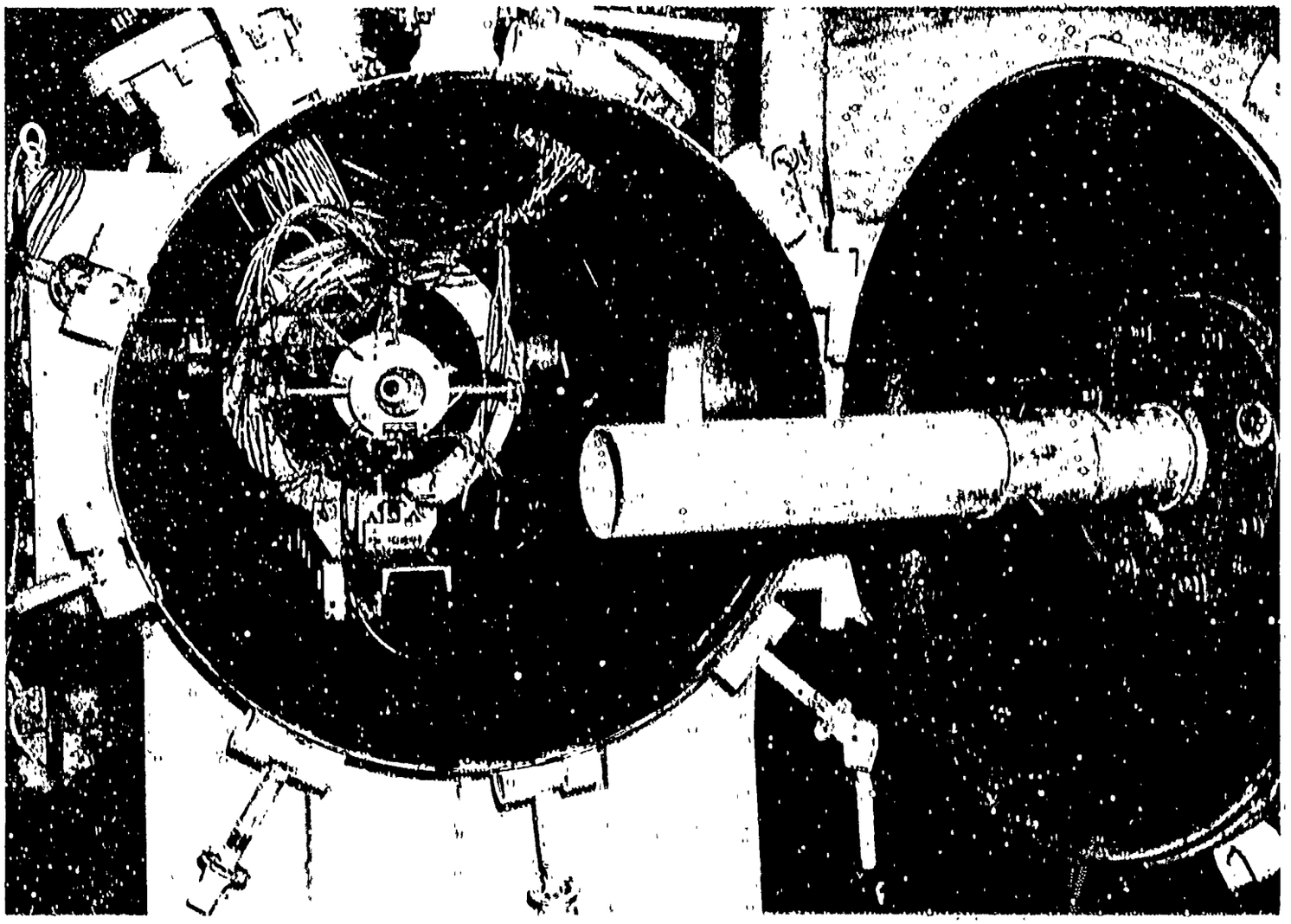

Figure 6. Flex-X Model in Thrust Stand

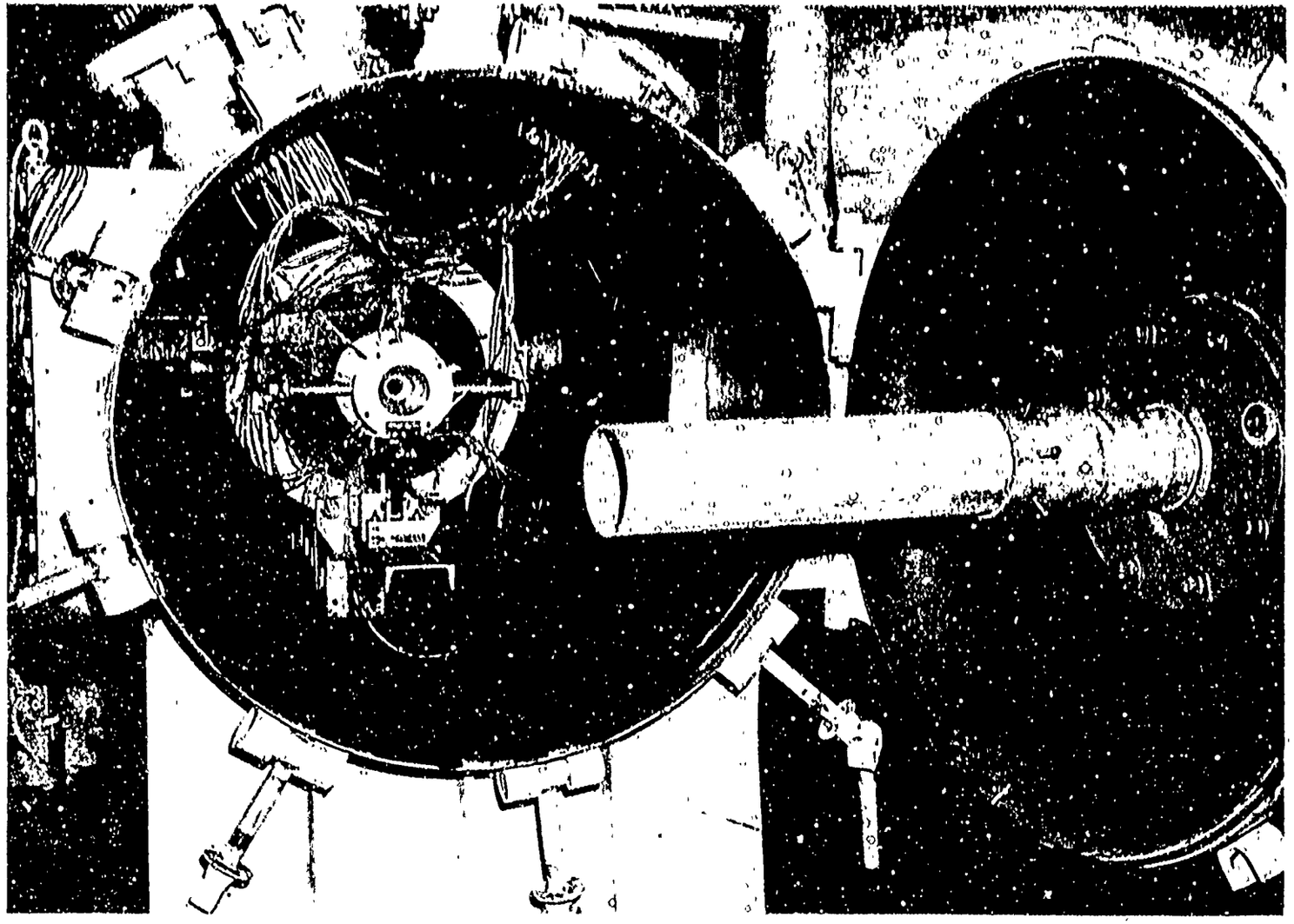

Figure 6. Flex-X Model in Thrust Stand

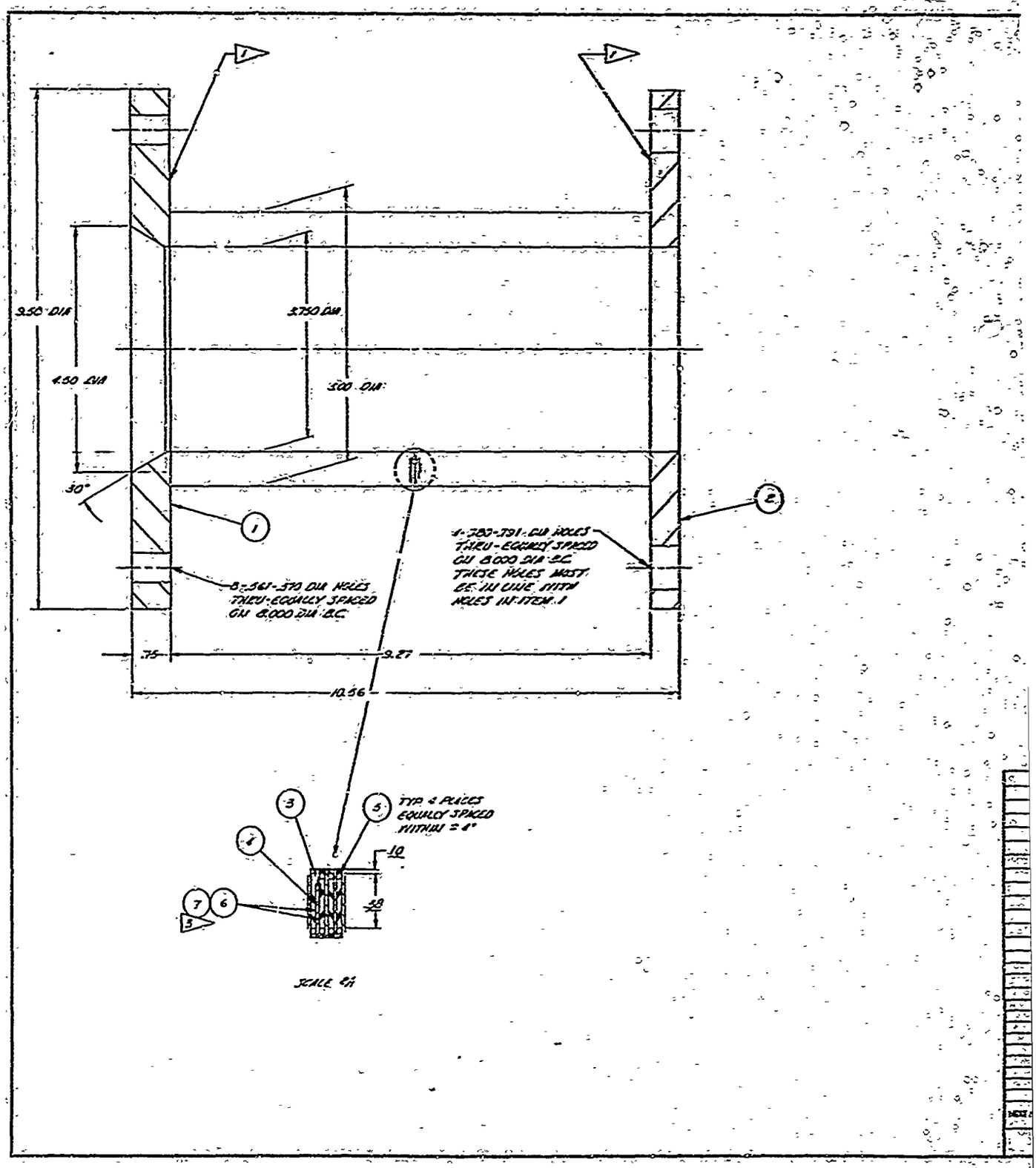
9.50 DIA
4.50 DIA
3.750 DIA
3.00 DIA
30°
1
2
8-.561-.570 DIA HOLES THRU-EQUALLY SPACED ON 8.000 DIA B.C.
4-.380-.391 DIA HOLES THRU-EQUALLY SPACED ON 8.000 DIA B.C. THESE HOLES MUST BE IN LINE WITH HOLES IN ITEM 1
.75
9.27
10.56
3
5
TYP 4 PLACES EQUALLY SPACED WITHIN ± 4°
4
10
7
6
5
.38
SCALE 2/1

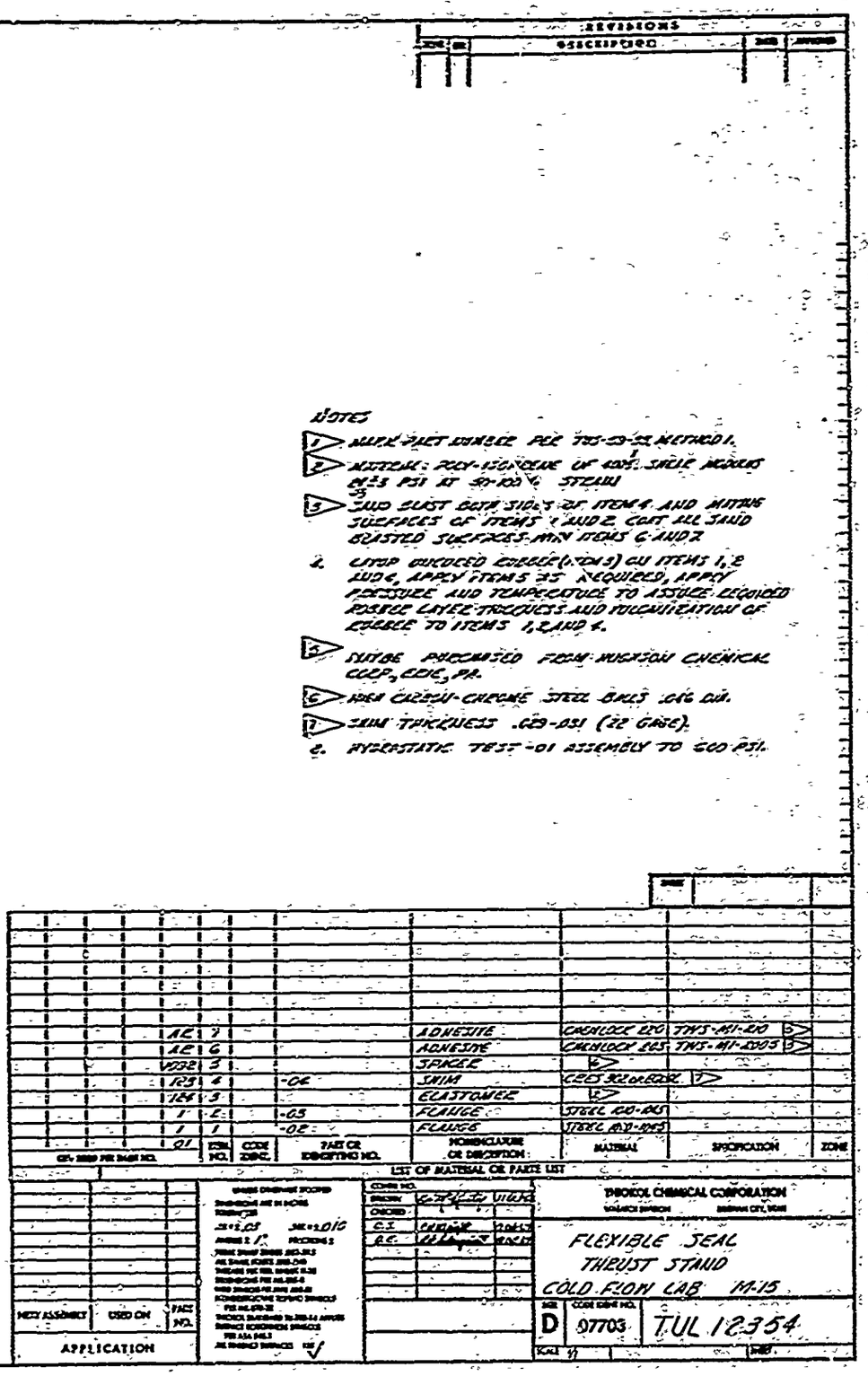

Figure 7. Flexible Joint Thrust Stand

SECTION V

TEST PROCEDURE

A. CALIBRATION

The force balance was calibrated electrically prior to each of the first nine tests. The deviation in these calibrations was so slight that the procedure was deemed unnecessary. It was therefore abandoned for the remainder of the program.

The force balance was calibrated using a dead weight. A cable on a pulley was attached to the upstream end of the plenum chamber. The system first was exercised by loading the cable in 50 lb increments up to 500 pounds. The readout then was zeroed and the plenum chamber was pressurized to the expected test pressure. The cable then was loaded in 10 lb increments over the expected range of test thrust. This procedure was repeated to establish the system repeatability. Calibration data were acquired in this manner for pressures of 10 and 20 psi above and below the expected test pressure. These data then were curve fit for use in reduction of test data. The calibration data are presented in Table II. These data are shown plotted in Figures 8 thru 10.

After completion of test 9, it became necessary to modify the power supply system in the Thiokol Aerodynamic Laboratory. It then was determined that the modifications produced a change in the calibration requiring recalibration of the force balance. This was accomplished in a manner similar to that discussed previously. The loading, however, was applied in 50 lb rather than 10 lb increments. The calibration data for all runs 10 thru 27 are presented in Table III and are shown plotted in Figures 11 thru 13.

TABLE II

CALIBRATION DATA
(Ten Pound Increments)

Force (lb)	Channel 5			Channel 6			Channel 7		
	Voltage (psi)								
	200	210	220	200	210	220	200	210	220
200					3.739				
210					3.938				
220	2.901	2.945	2.980	4.166	4.149	4.146			
230	3.041	3.083	3.109	4.357	4.334	4.336	2.668		2.637
240	3.181	3.204	3.227	4.541	4.527	4.531	2.782		2.752
250	3.317	3.338	3.347	4.747	4.740	4.727	2.895	2.886	2.876
260	3.442	3.465	3.482	4.930	4.949	4.921	3.027	3.015	3.002
270	3.572	3.580	3.598	5.141	5.135	5.121	3.143	3.147	3.132
280	3.695	3.708	3.728	5.330	5.336	5.321	3.263	3.258	3.252
290	3.821	3.837	3.847	5.521	5.526	5.521	3.393	3.388	3.382
300	3.951	3.973	3.991	5.721	5.725	5.717	3.517	3.509	3.508
310	4.082	4.103	4.118	5.911	5.915	5.910	3.632	3.623	3.622
320	4.202	4.225	4.247	6.115	6.110	6.110	3.752	3.742	3.746
330	4.332	4.349	4.362	6.321	6.303	6.298	3.878	3.868	3.872
340	4.459	4.477	4.491	6.517	6.513	6.494	4.017	3.998	4.002
350	4.581	4.595	4.622	6.707	6.701	6.697	4.143	4.134	4.127
360	4.711	4.693	4.745	6.907	6.925	6.890	4.258	4.291	4.247
370	4.831	4.827	4.871	7.117	7.121	7.090	4.387	4.395	4.362
380	4.951	4.963	5.010	7.300	7.306	7.300	4.508	4.512	4.493
390	5.087	5.099	5.132	7.500	7.505	7.487	4.632	4.632	4.618
400	5.216	5.237	5.251	7.691	7.696	7.697	4.752	4.752	4.738
410	5.337	5.355	5.381				4.872	4.877	4.868
420	5.465	5.484	5.627				5.002	5.008	5.002
430							5.133		5.112
440							5.258		5.242

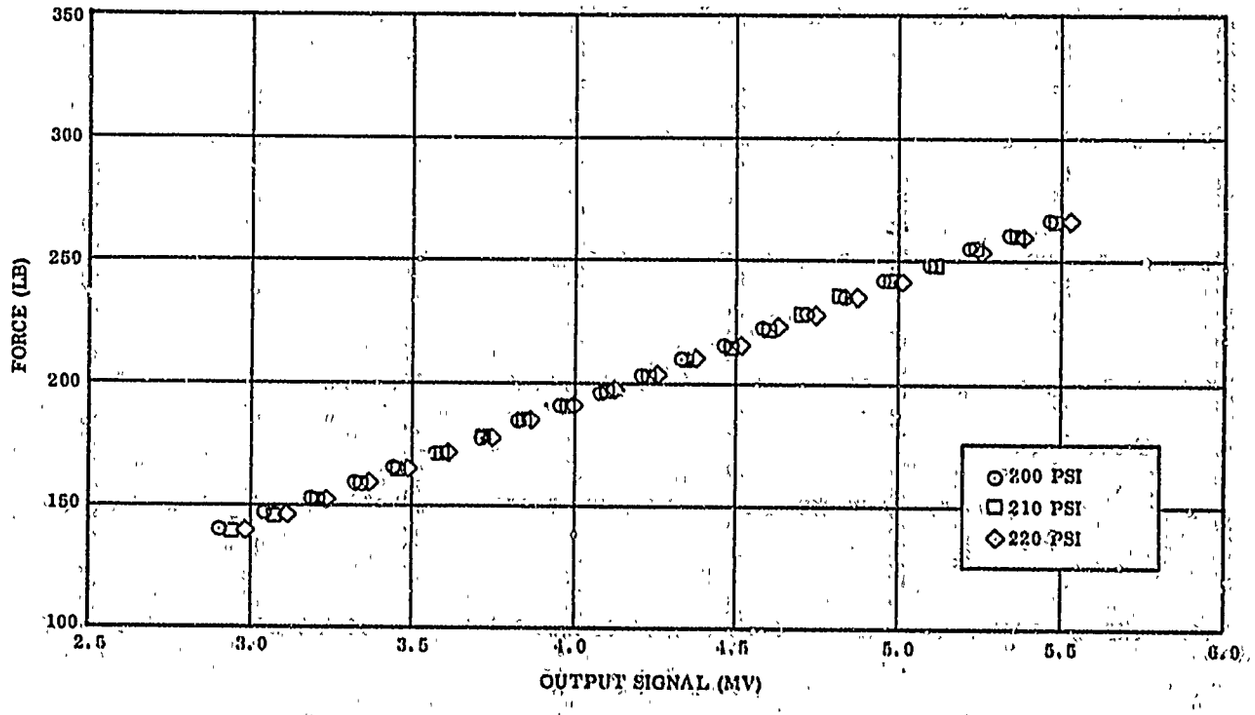

19523-2

Figure 8. Channel 5 Calibration

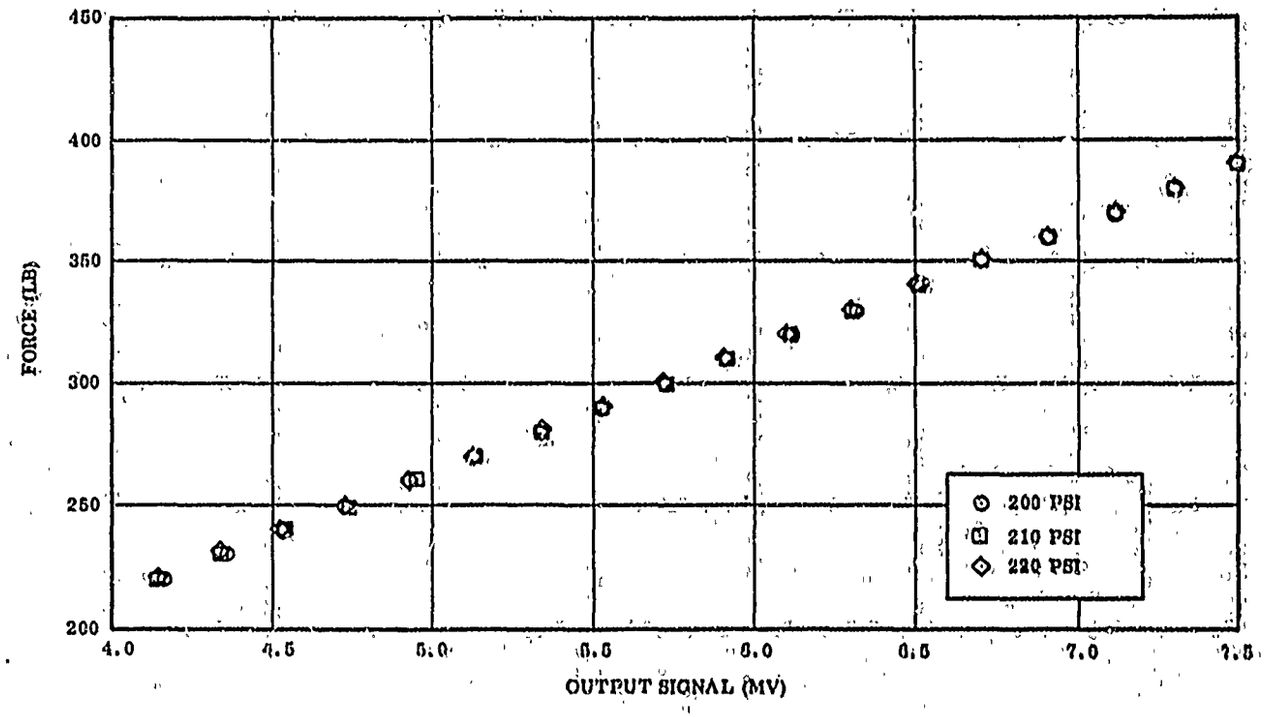

10523-3

Figure 9. Channel 6 Calibration

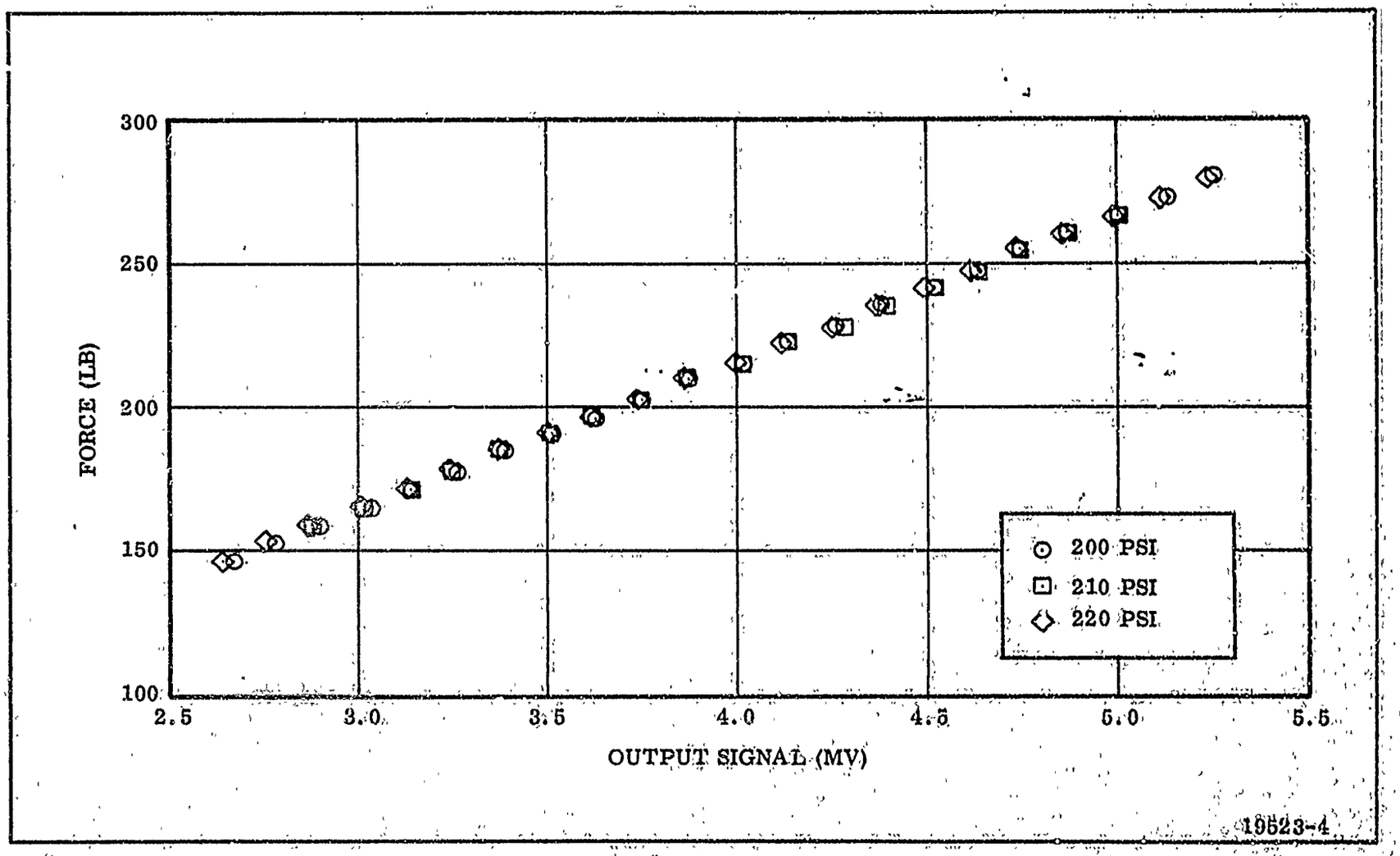

Figure 10. Channel 7 Calibration

TABLE III

CALIBRATION DATA
(Fifty Pound Increments)

Force (lb)	Channel 5				Channel 6				Channel 7			
	Voltage (psi)											
	200	210	215	220	200	210	215	220	200	210	215	220
0	0.204	0.239	-0.256	0.268	-0.206	-0.180	-0.203	-0.182	-0.235	-0.242	-0.274	-0.226
50	0.837	0.865	0.890	0.902	0.138	0.800	0.771	0.777	0.379	0.369	0.350	0.374
100	1.465	1.503	1.529	1.539	1.754	1.779	1.763	1.759	1.006	0.998	0.970	1.001
150	2.100	2.132	2.160	2.176	2.736	2.763	2.739	2.748	1.624	1.609	1.590	1.625
200	2.729	2.762	2.790	2.800	3.724	3.749	3.727	2.732	2.248	2.239	2.210	2.245
250	3.363	3.399	3.426	3.434	4.699	4.732	4.707	4.711	2.862	2.853	2.830	2.857
300	3.998	4.033	4.053	4.065	5.684	5.719	5.691	5.701	3.481	3.472	3.450	3.480
350	4.617	4.656	4.683	4.687	6.667	6.699	6.676	6.688	4.103	4.100	4.070	4.098
400	5.247	5.301	5.311	5.326	7.655	7.705	7.662	7.670	4.718	4.723	4.689	4.718

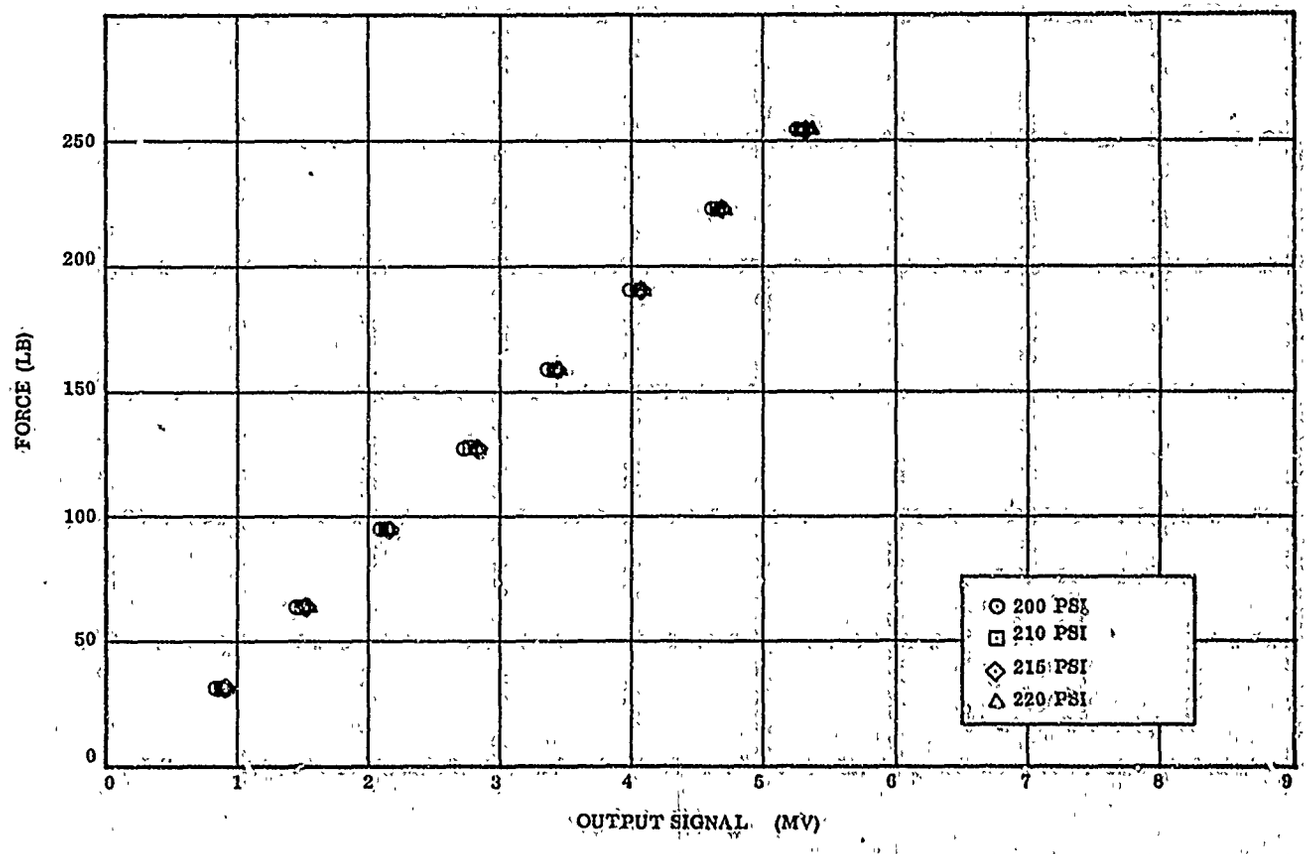

12523-5

Figure 11. Channel 5, Second Calibration

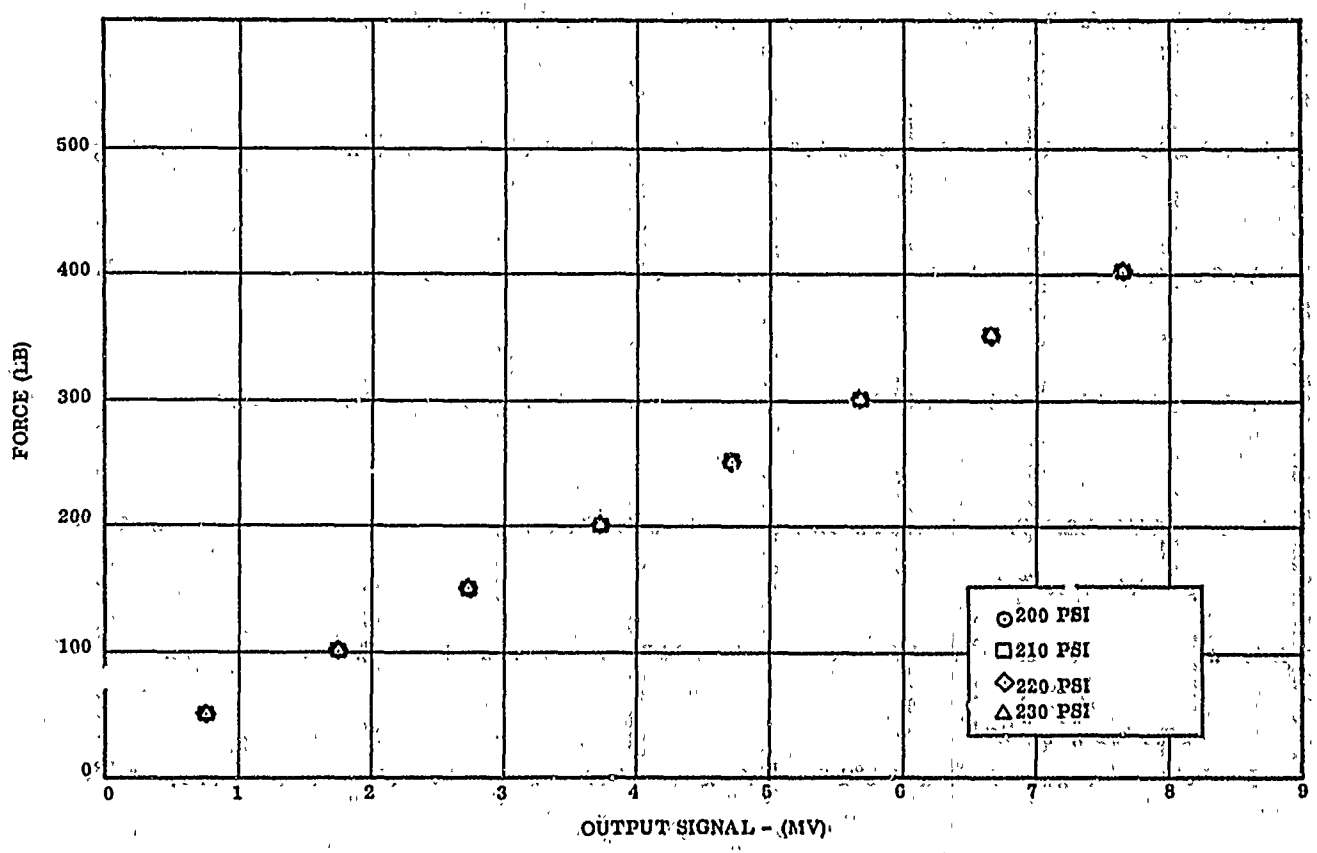

Figure 12. Channel 6, Second Calibration

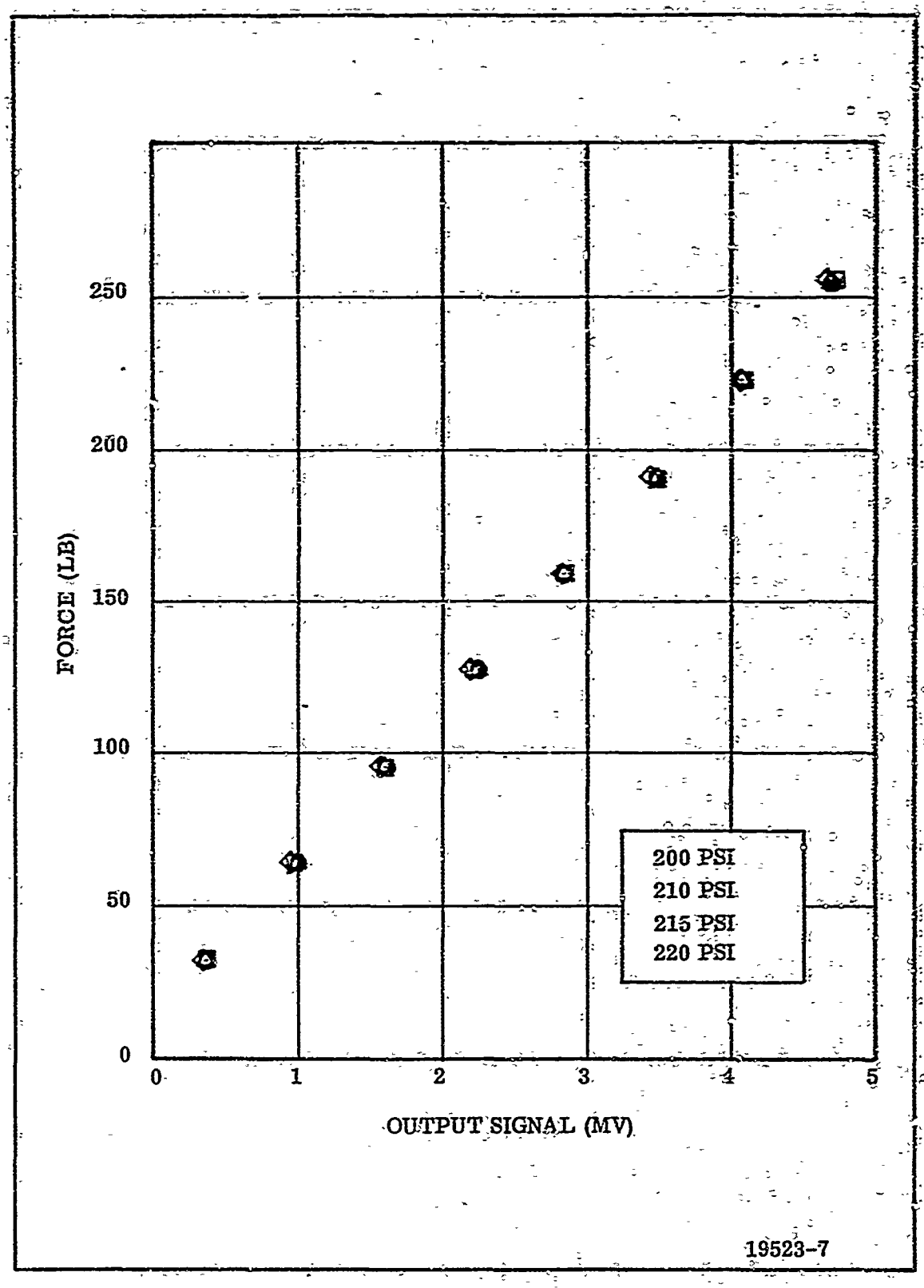

Figure 13. Channel 7, Second Calibration

The tabulated data present the deadweight force along with the recorded voltage. However, Channels 5 and 7 do not record the deadweight force as this force is axial only. These two forces act as a couple reacting against the moment produced by the dead weight. The force recorded on Channels 5 and 7 is 0.63514 of the dead weight. The scaled values are shown on the figures.

The accuracy of the data is as follows.

Measurement	Full Scale Accuracy (percent)
Axial Force	±0.32
Side Force	±0.70
Torque	±0.65

B. TEST MODELS

The test models were designed to allow investigation of the effects of variables unique to the flexible exit cone concept such as joint location and pivot location. In addition, variables such as cone angle and nozzle expansion ratio, which uniquely influence the performance of flexible exit cone nozzle, were considered. The inlet and throat design are not critical to performance of a supersonic flex nozzle; therefore, a common geometry was used for all nozzles.

The range of cone angle and expansion ratio to be considered was selected to bracket the values most commonly required for first stage and upper stage motors. The location of the joint was selected to avoid intersection of a shock wave with the opposite wall for all models. However, a more detailed analysis conducted after completion of model design indicates that this phenomenon can be expected to occur on the higher expansion ratio nozzles. The pivot point was allowed to vary from the point source to the farthest aft point structurally feasible on the flexible joint design. To reduce the test matrix, the joint length was not considered as a test variable.

The test model designs are shown in Figures 14 thru 18.

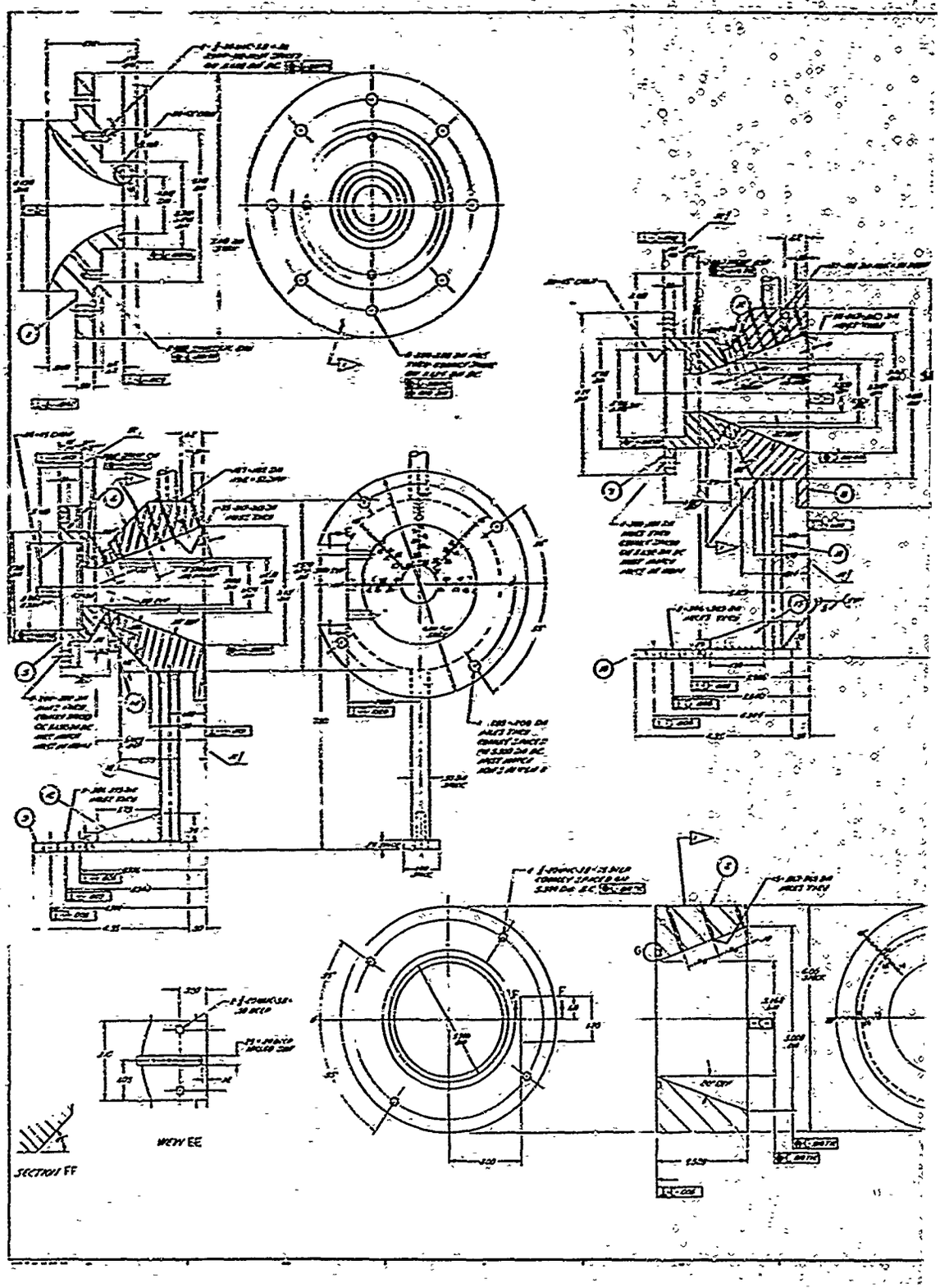
VIEW EE
SECTION FF

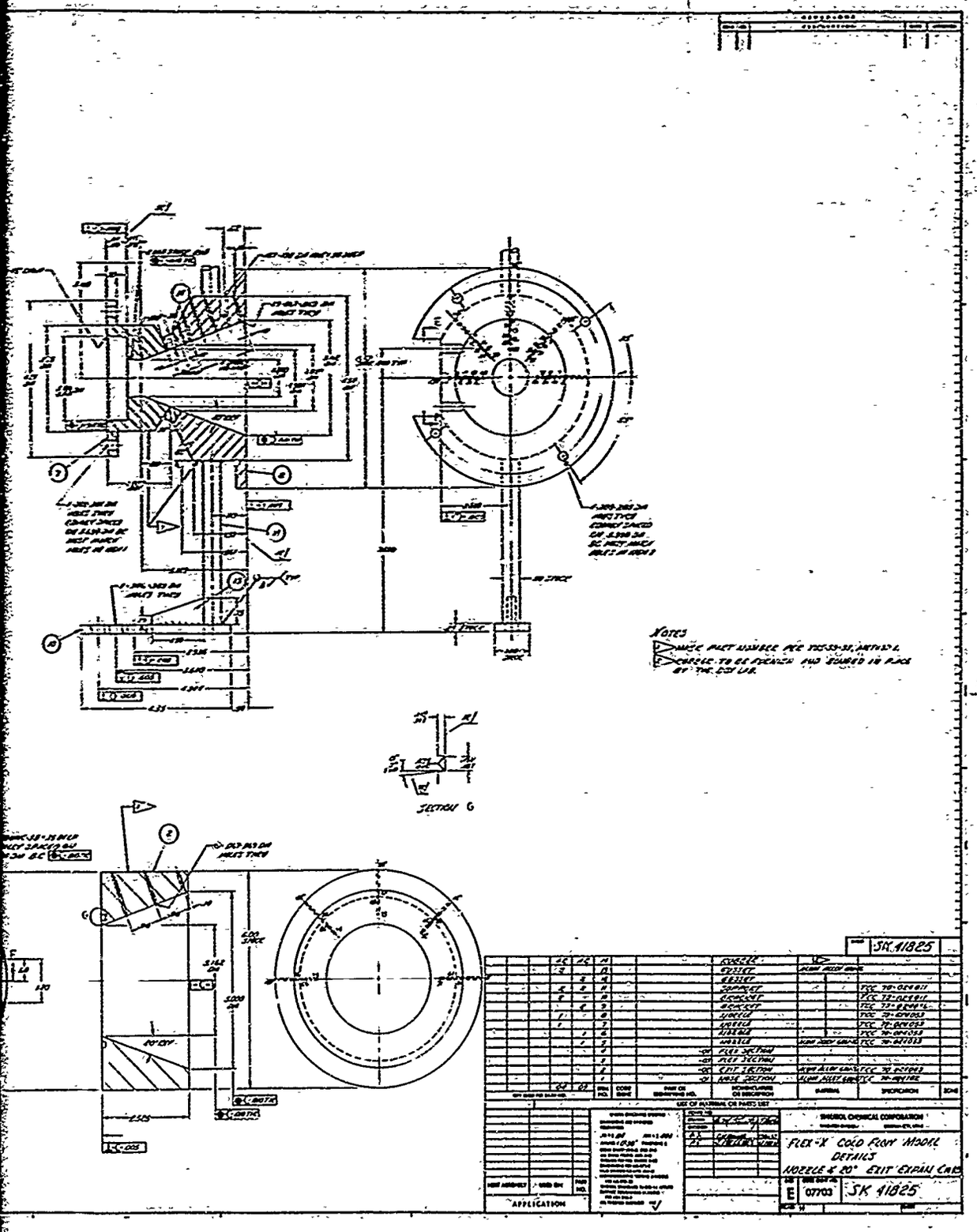

Figure 14. Flex-X Cold Flow Model Details

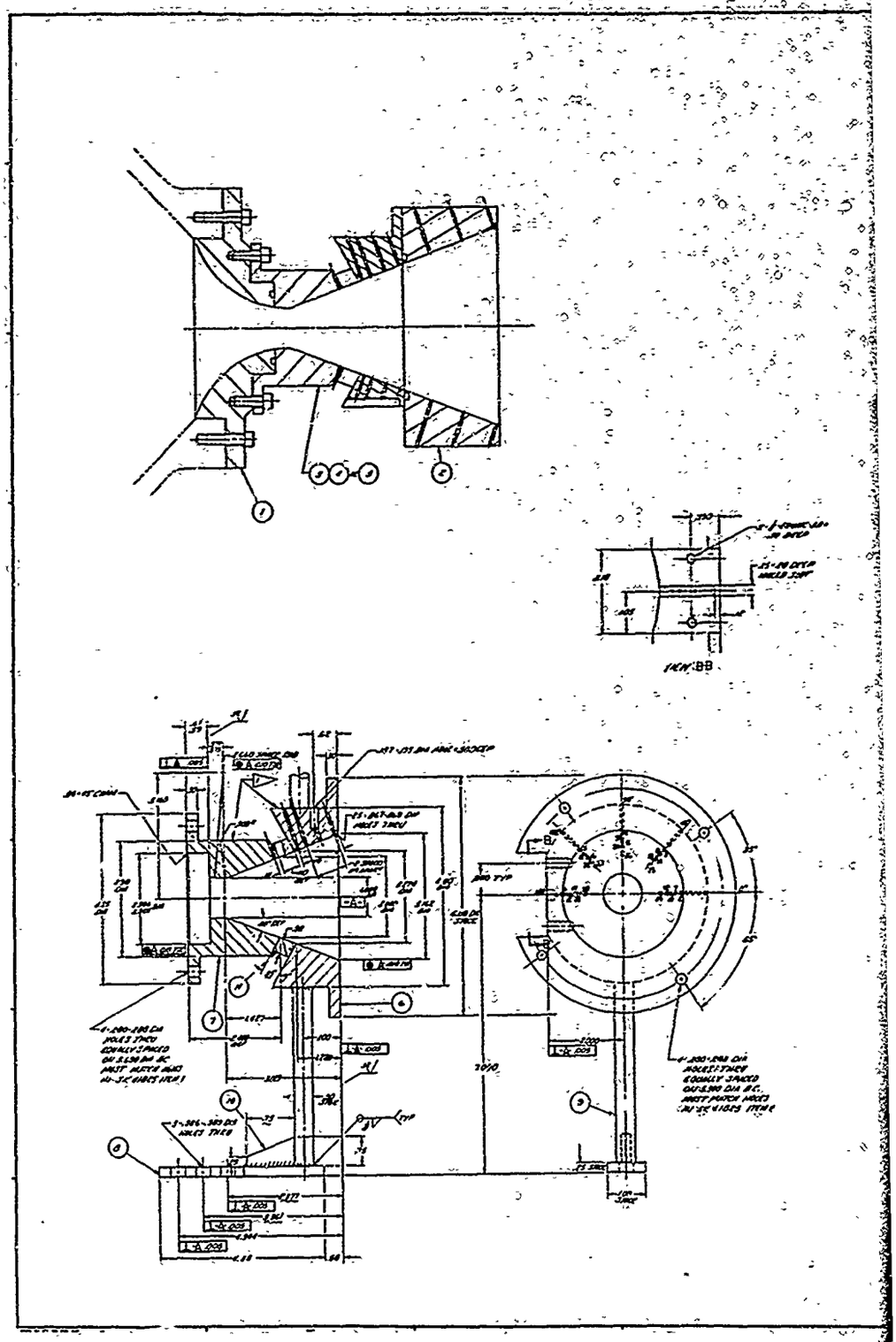

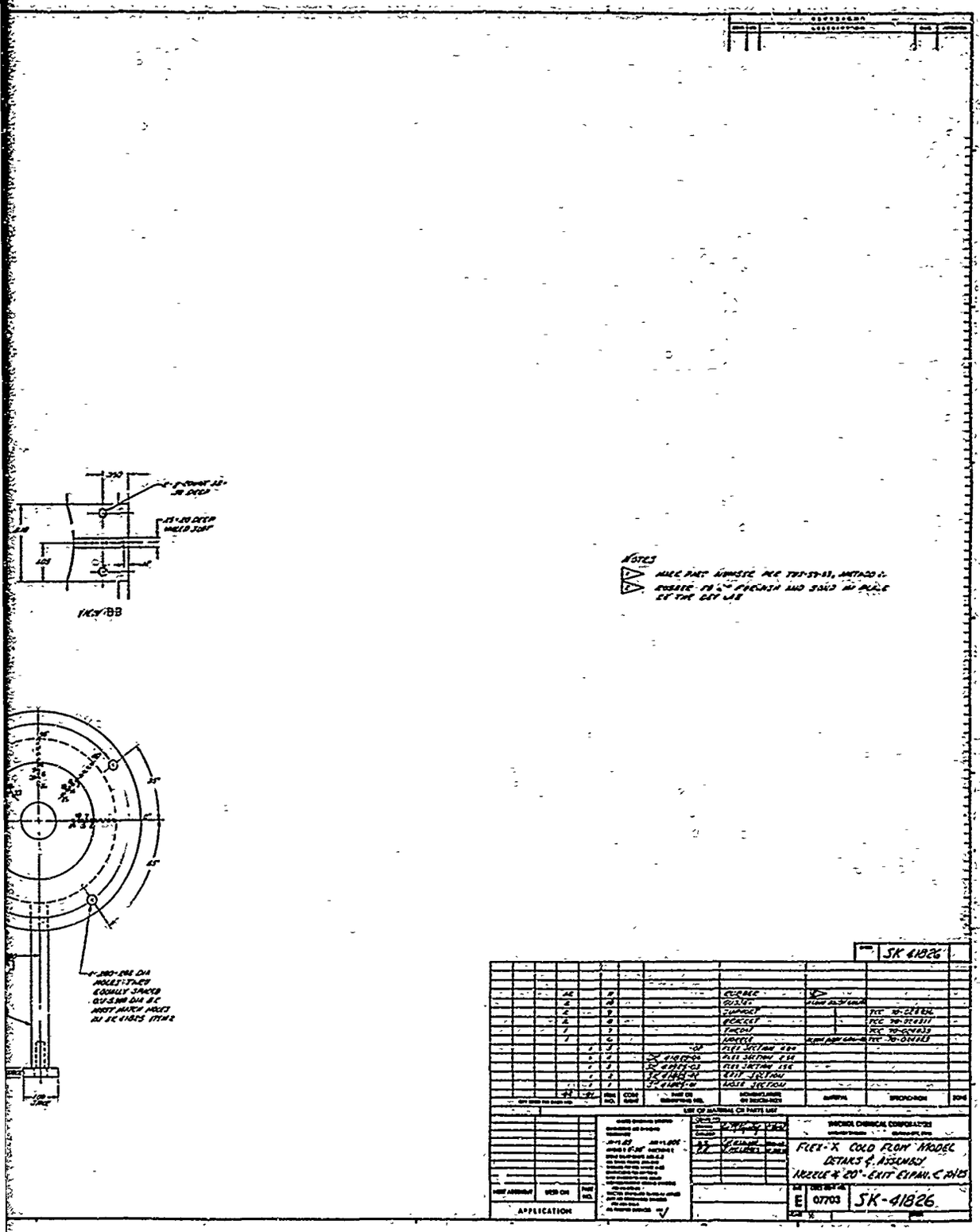

Figure 15. Flex-X Cold Flow Model Assembly

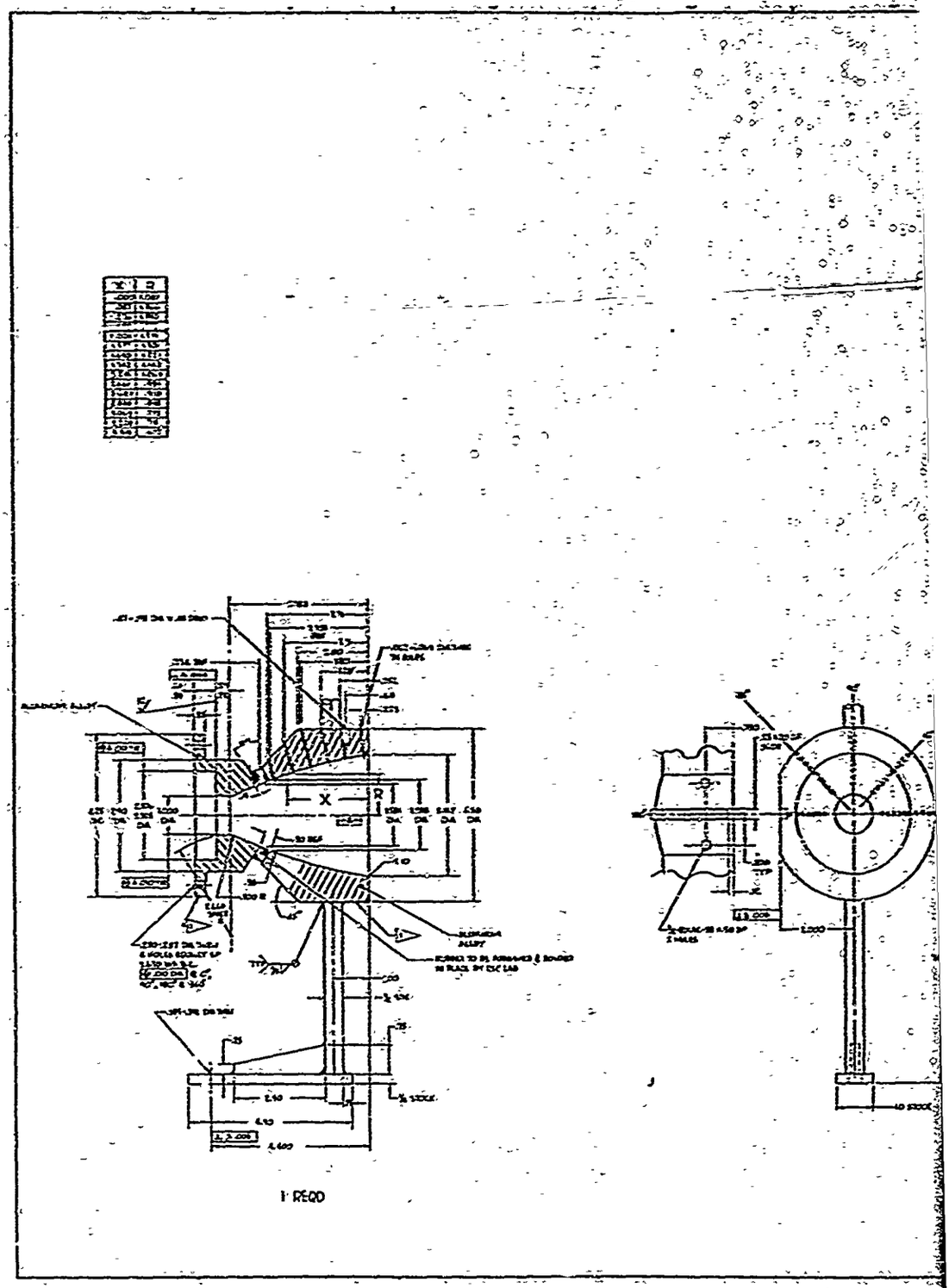

Figure 16.

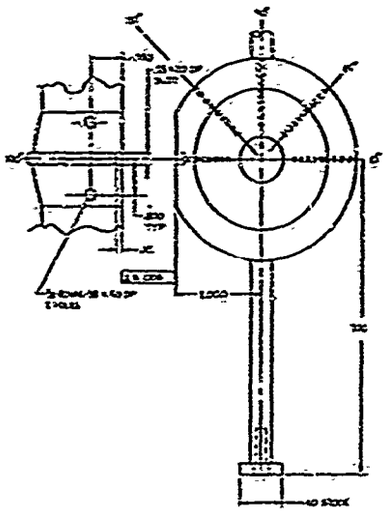

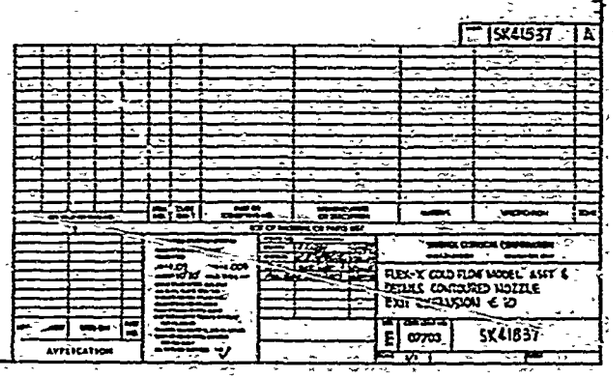

Figure 15. Flex-X Cold Flow Model Details at Exit Expansion ϵ 10

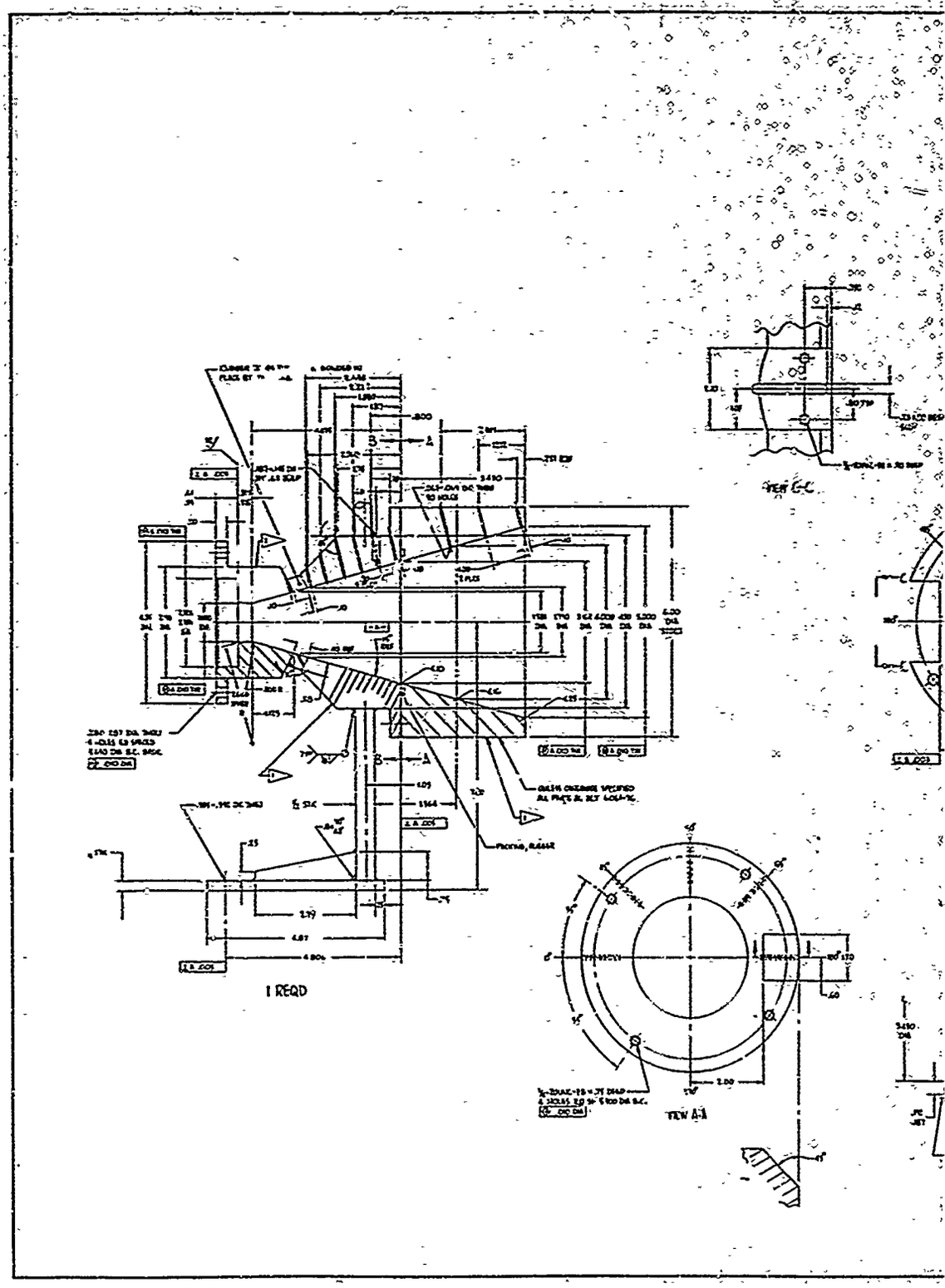

Figure 17. F

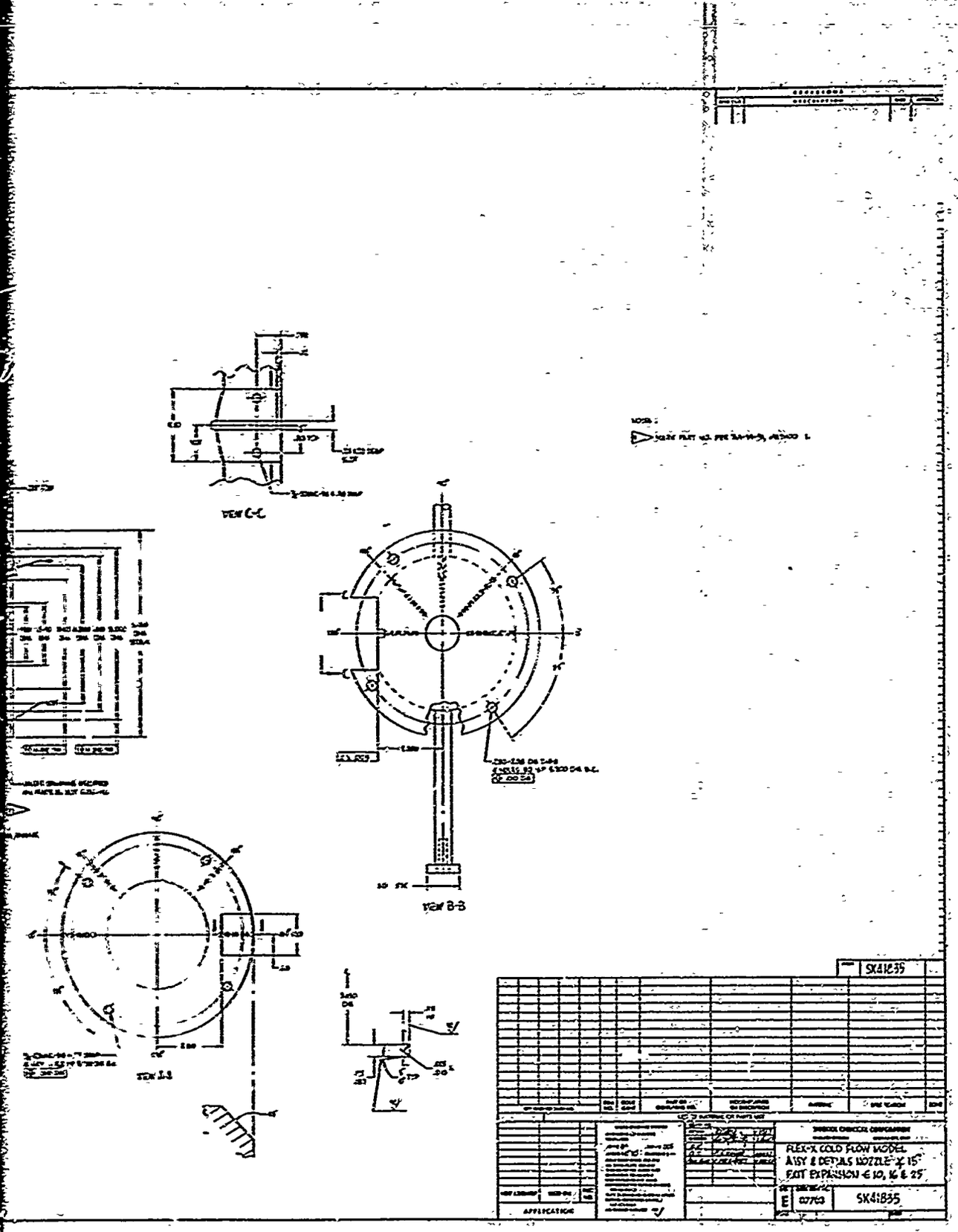

Figure 17. Flex-X Cold Flow Model Details, 15 Degree Nozzle Angle, Exit Expansion ε 10, 16, and 25

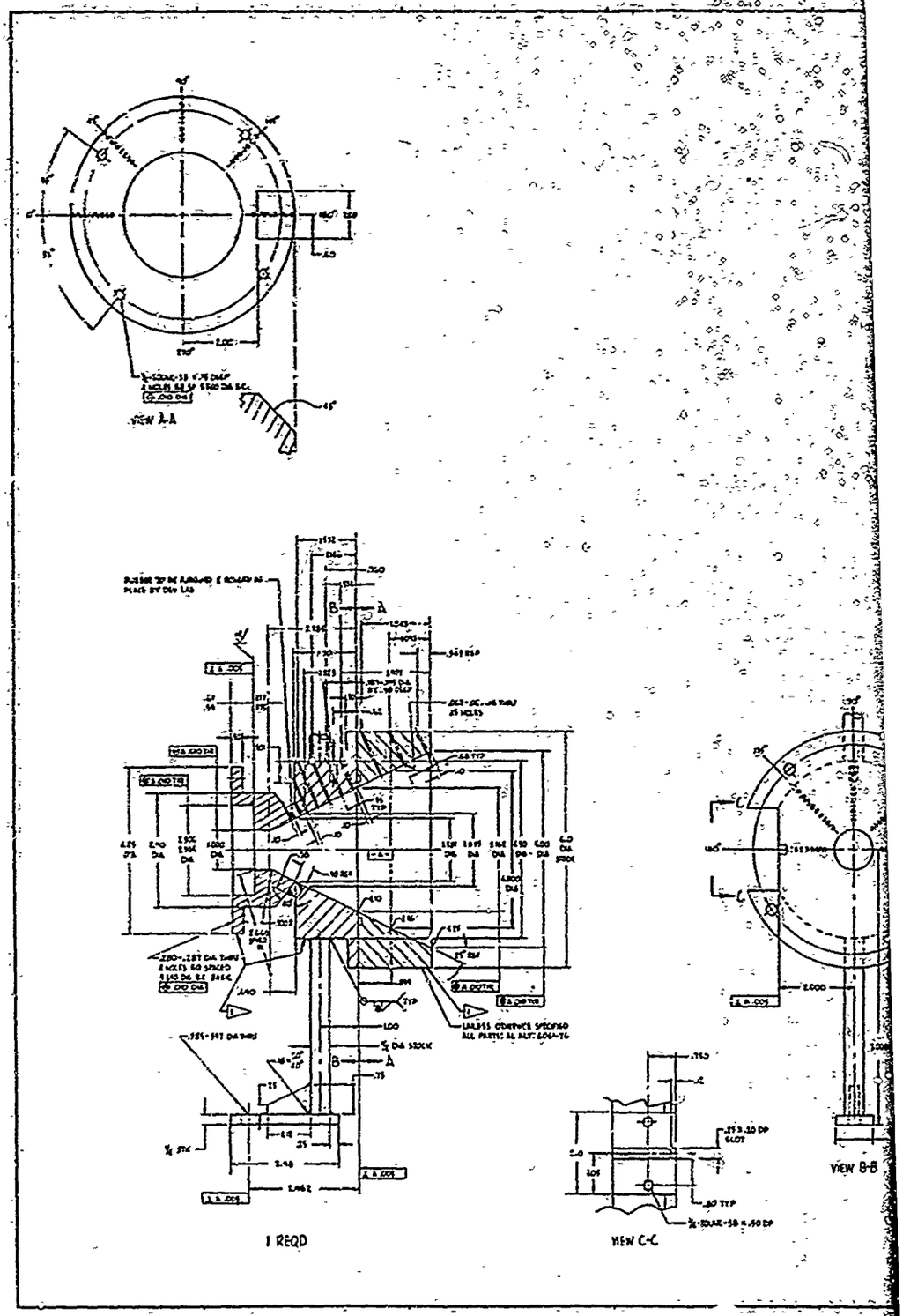

Figure

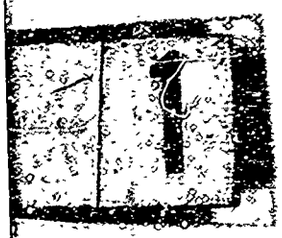

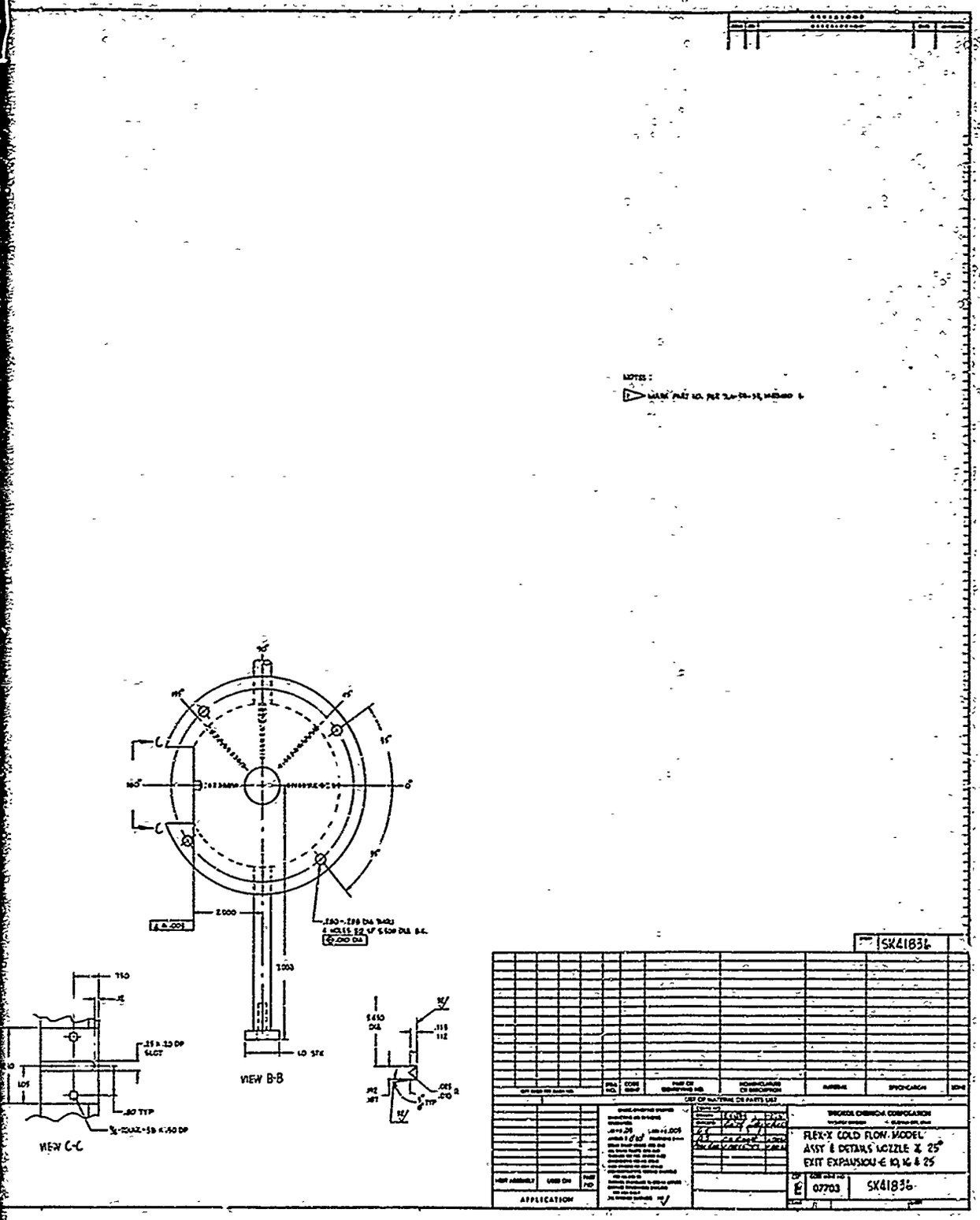

Figure 18. Flex-X Cold Flow Model Details, 25 Degree Nozzle Angle, Exit Expansion ε 10, 16, and 25

Two eroded nozzle configurations also were tested to examine the effect of erosion on nozzle performance. The test model having a 10:1 expansion ratio and a 2.5:1 joint and pivot point was machined to simulate the 30 and 60 sec eroded configurations. Sketches of the eroded nozzles are shown in Figure 19.

C. INSTRUMENTATION

The instrumentation consisted of the following:

1. Force balance.
2. Two force links for measuring nozzle torque.
3. Manometer boards.
4. Pressure transducers.
5. Precision gages used for pressure measurement.

The three parallelogram flexures of the force balance were oriented so that the flexures on each end read vertical loads in either tension or compression while the center flexure measured the axial force. The plenum chamber was supported on the upper balance platform, which was connected to the flex-cell blocks by three thin straps, each as wide as the block (Figure 20). Forces generated by the test model were carried through these straps to the flex-cell units. The thin straps further acted to reduce interaction between the three flex-cells to a minimum.

Two 2,000 lb Baldwin force links were initially used to measure torque. After tests 1, 4, and 7, it was determined that the range of these force links was too great, thus the accuracy was poor. They were, therefore, replaced with two 300 lb Transducer, Inc force links. The accuracy of these links, as measured in the Thiokol Metrology Laboratory, was within 0.46 and 0.6 percent of full scale.

A Tabor 500 psi pressure transducer was used to measure plenum chamber pressure. The accuracy of this transducer was within 0.17 percent of full scale.

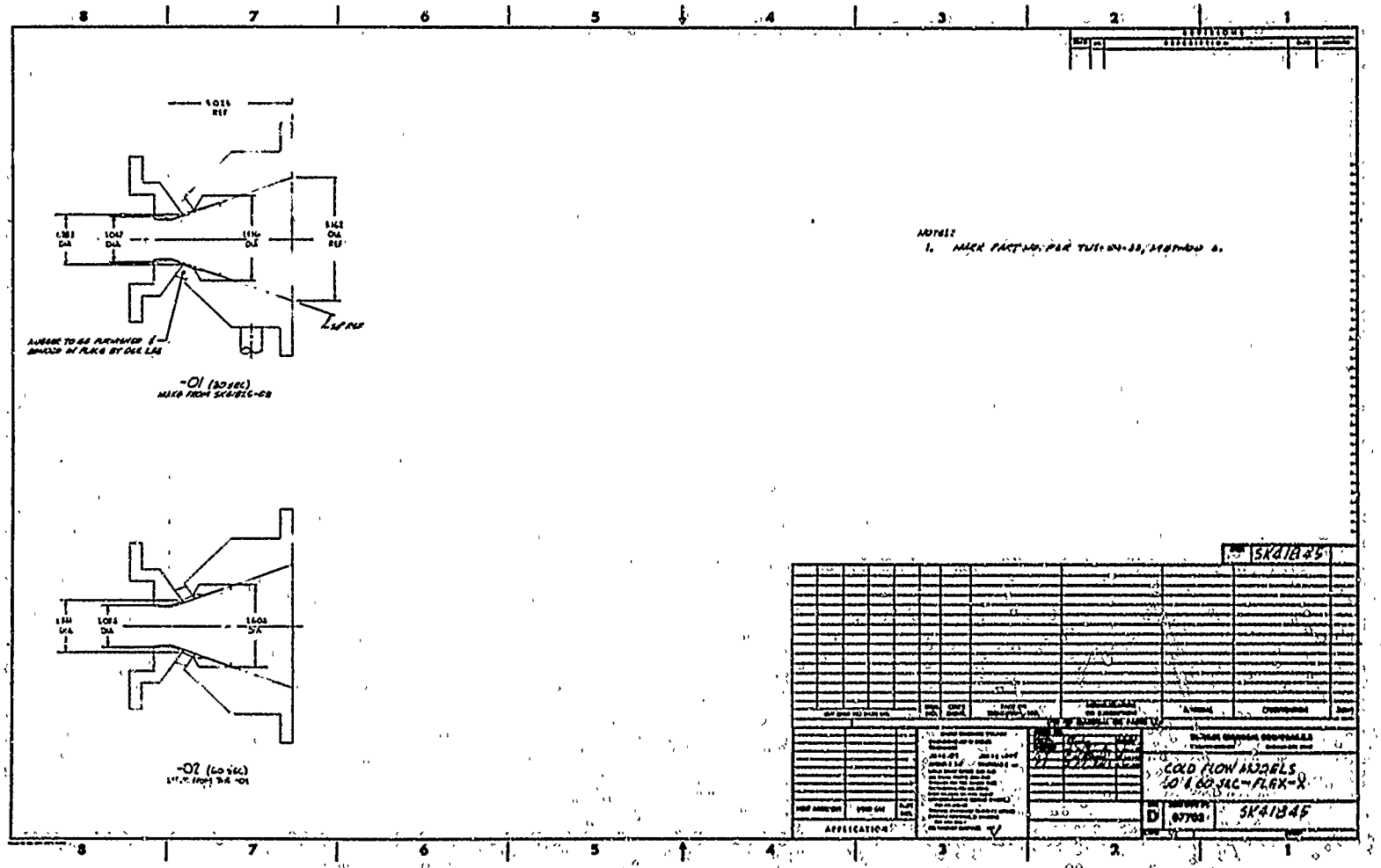

Figure 19. Sketch of Eroded Nozzles (30 and 60 Sec)

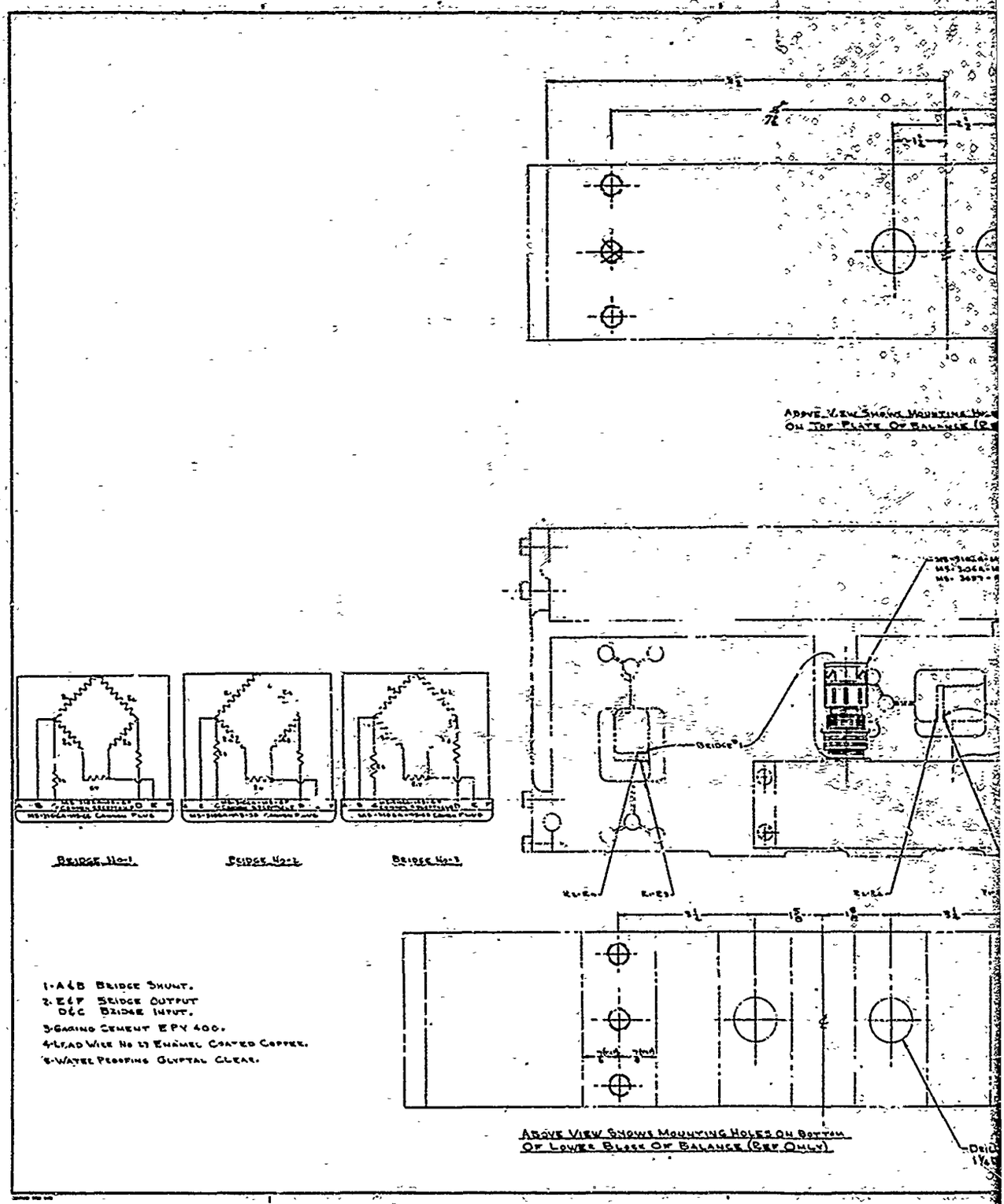
Above View Shows Mounting Holes On Top Plate Of Balance (Ref
Bridge No-1
Bridge No-2
Bridge No-3
Bridge 1
Fuses
Fuses
Fuses
1-A&B Bridge Shunt.
2-E&F Bridge Output
D&C Bridge Input.
3-Gaging Cement EPY 400.
4-Lead Wire No 23 Enamel Coated Copper.
5-Water Proofing Glyptal Clear.
Above View Shows Mounting Holes On Bottom
Of Lower Block Of Balance (Ref Only)

Figu

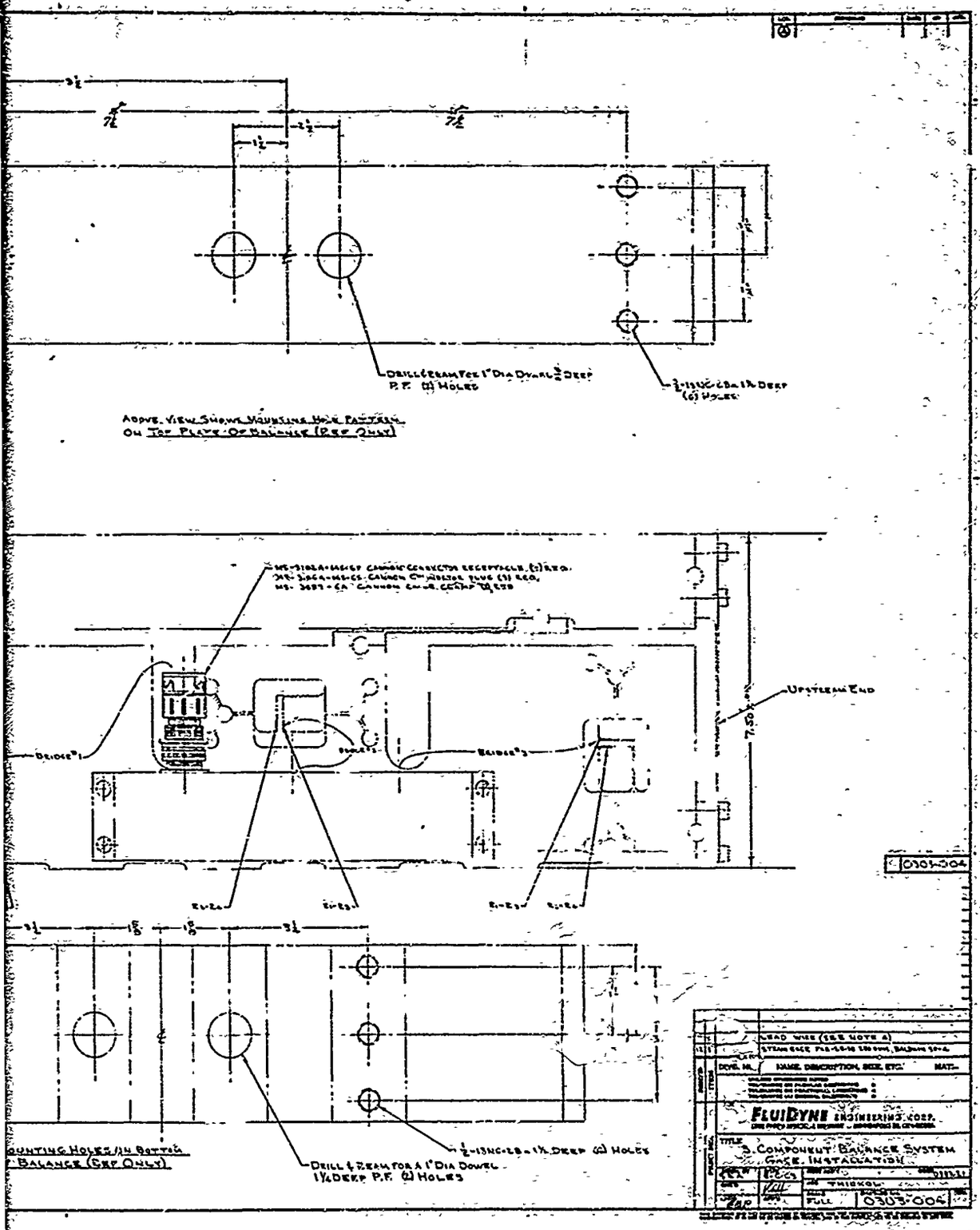

Figure 20. Three Component Balance System Gage Installation

Data from the force balance, force links, and pressure transducer were recorded on an Electro-Instruments digital data system. The error induced by this system is less than 0.05 percent. Most of the pressure measurements in the nozzle exit cone were read on mercury manometer boards. The boards were photographed (Figure 21) during the test and readings were then taken from the photograph. Pressures can be read in this manner to 0.024 in. of mercury or 0.025 psi. In addition to the mercury manometer board, precision Bourdon tube pressure gages were used to measure high pressures recorded near the seal on the vectored nozzles. These gages were calibrated at 70° F. The accuracy was determined to be 0.15 percent of full scale, which was 500 psi.

D. TESTING

Considerable effort was expended to establish a test procedure which would yield the best possible accuracy from the available test equipment. The procedure then was utilized throughout the test program. The following paragraph describes this procedure.

The force balance first was exercised by flowing air through the nozzle at a total pressure greater than the test pressure. The air flow then was shut-off and the data acquisition system was zeroed. This procedure was done twice at the start of each test day. The test was then conducted by gradually increasing the air flow to the required total pressure through the nozzle. Flow conditions were then allowed to reach steady state before test results were recorded. A minimum of five digital readings were recorded while maintaining a constant total pressure. A photograph of the manometer boards was taken simultaneous with third recording of the digital output. A zero reading was recorded after the test.

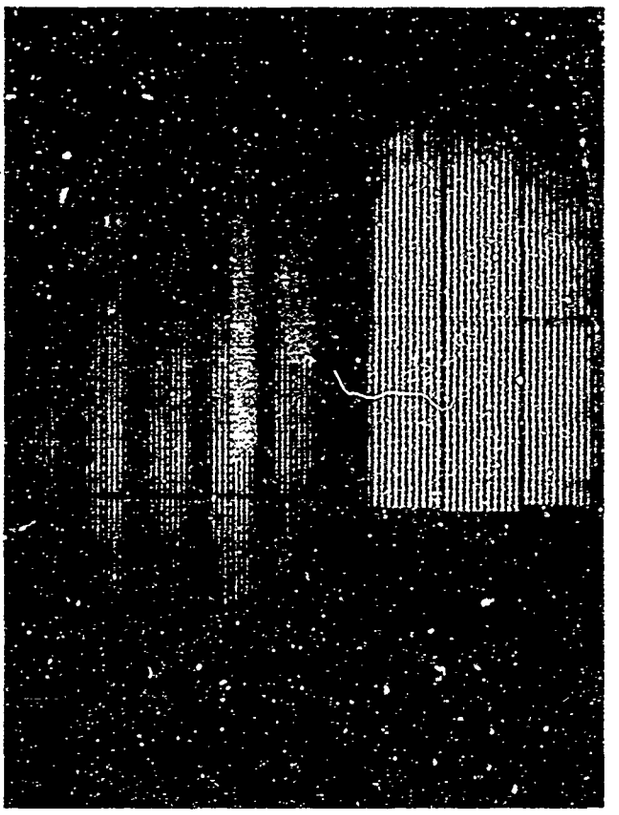

Figure 21. Photograph of the Mercury Manometer Board Run No. 1, 5 Deg Vector, Hg 25.71

SECTION VI

TEST RESULTS

A. DATA PRESENTATION

All test data are presented in tabulated form in Appendix I. The first page of data for each run contains the following information:

1. Run number,
2. Nozzle vector angle,
3. Area ratio of the nozzle at the upstream edge of the joint,
4. Pivot point number,
5. Expansion ratio of the nozzle,
6. Ambient pressure,
7. Test date,
8. Digital output channels,
9. Pressure data.

The pivot point number designation is as follows: (1) downstream pivot point, (2) middle pivot point (half-way between (1) and (3), and (3)) is the pivot point located at the point source.

The digital data includes a zero reading before the test, five readings recorded while testing, and a post-test zero reading. The five force readings were averaged and then converted to proper units. This value is presented for each channel in the load column. Channel 2 is the nozzle inlet total pressure in psig. Channels 3 and 4 are the force link readings in pounds.

Channels 5 and 7 are the vertical force measurements and Channel 6 is the axial force measurement. These measurements all have units of pounds force.

The first column under pressure data is the tap number as designated in Figure 14. Taps 1, 11, 21, and 31 recorded the pot levels of the manometer board. Tap 30 was the vacuum cell pressure. The second column was the mercury height in inches. The third column presented the difference between the pot level and the measured mercury level. The fourth column was the tap presented in psia units and column 5 shows the ratio of static pressure to total pressure.

The second page of data includes the thrust coefficient, side force, side force amplification, torque, torque amplification, axial thrust efficiency, and thrust vector angle.

The equations used to compute the above parameters are presented below.

Thrust Coefficient (C_F)

$$C_F = \frac{F}{P_t A_t}$$

Where:

F = Axial force (Channel 6)

P_t = Total pressure (psia)

A_t = Throat area (sq in.)

Side Force

F_s = Channel 7 - Channel 5

Side Force Amplification

$$AF = \frac{F_s}{C_{F_o} P_t A_t \text{ Sin Delta}}$$

$$AF_{corr} = \frac{F_s}{C_{F_{TH}} P_t A_t \text{ Sin Delta}}$$

Where:

$C_{F_{TH}}$ = Theoretical Thrust Coefficient

$$\lambda = \left(\frac{2\gamma^2}{\gamma - 1}\right)\left(\frac{2}{\gamma + 1}\right)^{\frac{\gamma+1}{\gamma-1}} \left[1 - \frac{P_e}{P_t}^{\frac{\gamma-1}{\gamma}}\right]^{1/2} + \left(\frac{P_e}{P_t}\right)\epsilon - \left(\frac{P_a}{P_t}\right)\epsilon$$

<u>Torque</u>

Torque = (Channel 3) (L_3) + (Channel 4) (L_4)

Where:

L_3 and L_4 are the respective moment arms of the load cells about the pivot axis

<u>Torque Amplification</u>

T_{amp} = Torque/C_{F_o} P_t $A_t^{3/2}$ Sin Delta

$T_{(amp)_{corr}}$ = Torque/$C_{F_{TH}}$ P_t $A_t^{3/2}$ Sin Delta

<u>Axial Thrust Efficiency</u>

F_{eff} = $C_F/C_{F_{TH}}$ Cos Delta

<u>Thrust Vector Angle</u>

Theta = ARCTAN (Side Force/Axial Force)

The torque and side force amplification and the axial thrust efficiency are essentially the ratio of measured nozzle performance to ideal nozzle performance. Initially, the measured thrust coefficient for the unvectored nozzle was used to represent the ideal nozzle in the torque and side force amplification calculation. However, examination of the data revealed that for several runs, the variation in back pressure produced a significant variation in the thrust coefficient. The variation in back pressure was due to the loss in diffuser efficiency when the nozzle was in the vectored position.

The back pressure variation produced a change in thrust coefficient which was not indicative of nozzle performance. It was therefore necessary to calculate theoretical thrust coefficients for each run using the measured back pressure in each calculation.

The axial thrust efficiency also was calculated using the theoretical thrust coefficient. These values have been added to the second page of each data sheet.

The plotted pressure data are presented in Appendix II. The pressure ratio versus axial location for each test run is plotted. In addition, these data are plotted circumferentially at each axial station for Runs 1 thru 9. These plots were used to study the pressure variation for development of an analytical program.

B. DISCUSSION OF TEST DATA

The force data provide a measure of the performance characteristics of the nozzle. Three parameters have been devised for comparing the performance of the Flex-X nozzle with that of an ideal nozzle. These parameters are side force amplification, torque amplification, and axial thrust efficiency. Each of these parameters are the ratio of the measured to the ideal force value.

1. SIDE FORCE AND TORQUE

The side force and torque amplification are of primary concern in this test program. These parameters are, therefore, considered first in this report. The effects of various geometric changes in the nozzle configuration on these parameters are discussed in the following paragraphs.

a. Effect of Pivot Location—The effect of varying the nozzle pivot location is shown in Figures 22 thru 24 for the 10:1 expansion ratio nozzles and in Figures 25 thru 27 for the 25:1 expansion ratio nozzles. Data are shown for three vector angles, 2.5, 5.0, and 10.0 degrees.

The force amplification is greatest for the upstream pivot (Pivot 3) and decreases in an almost linear manner with pivot axial location. The upstream pivot produces nearly the same side force amplification on all configurations. However, moving the pivot aft resulted in considerably larger reduction in side force on the configurations having the downstream joint location. In fact, a force amplification of less than 1.0 resulted with the downstream pivot and joint expansion ratio of 4.0 on the 10:1 expansion ratio nozzle.

The upstream pivot produces the largest side force because the larger radius of the joint results in increased travel of the movable portion of the nozzle during vectoring. A stronger shock is thus generated providing additional turning of the flow within the nozzle.

The combination of a downstream joint and a downstream pivot results in a minimal change in the wall slope which produces only a slight pressure differential in the plane of vector. This, coupled with the fact that only a small portion of the nozzle is affected, results in a side force degradation rather than amplification.

The side force amplification varies with pivot point on the 25:1 expansion ratio nozzle in a manner very similar to that experienced with the 10:1 expansion ratio nozzle. The 25:1 expansion ratio nozzle produces a slightly higher side force on most configurations. This is to be expected since the surface area affected by vectoring is appreciably larger on the high expansion ratio nozzle.

The torque amplification data exhibits considerably more scatter due to vector angle indicating that aerodynamic torque will not vary linearly with vector angle. However, the general trend is for torque amplification to decrease as the pivot is moved downstream. This is primarily due to the reduced moment arm.

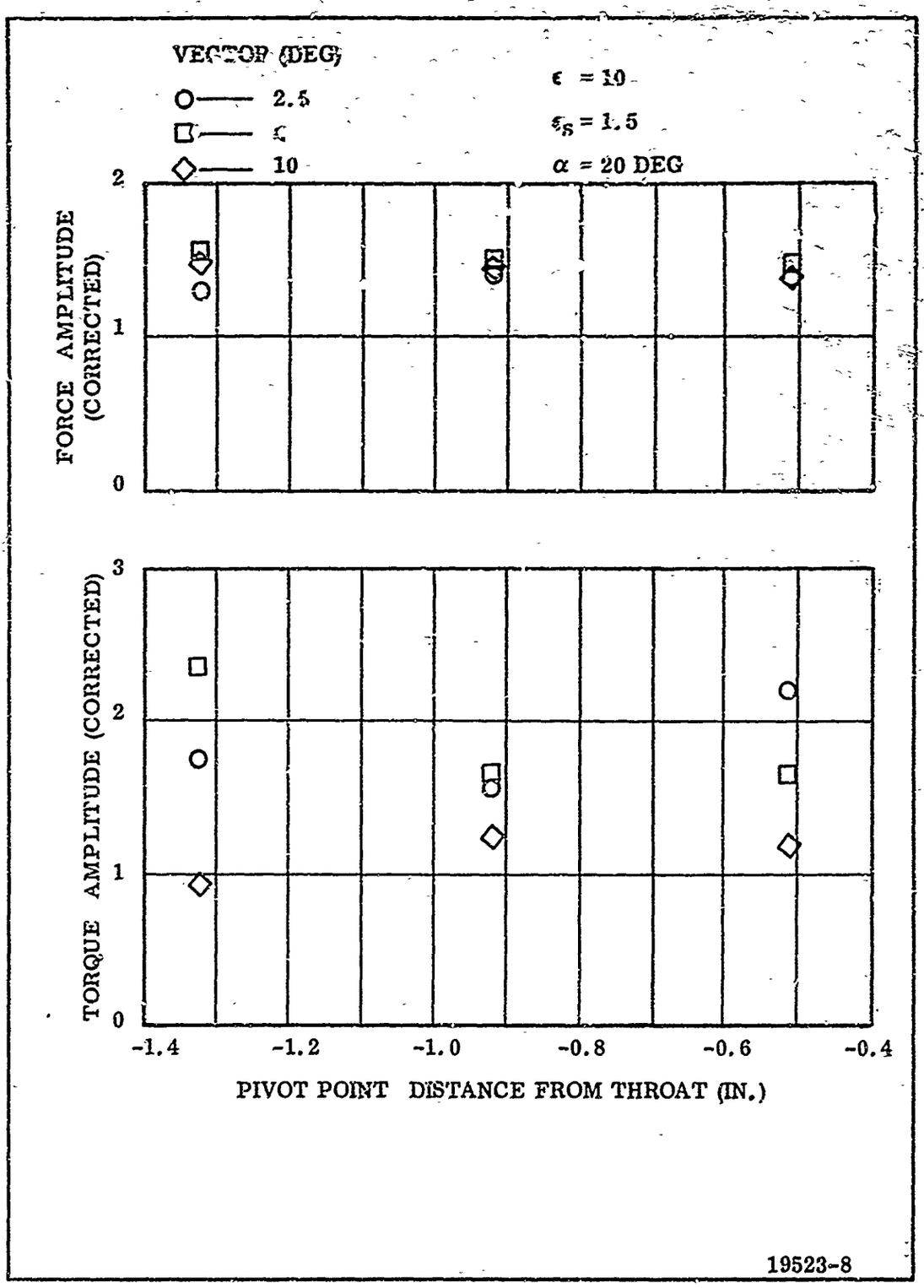

Figure 22. Effect of Pivot Location on Side Force and Torque Amplification (ϵ = 10, ϵ_s = 1.5)

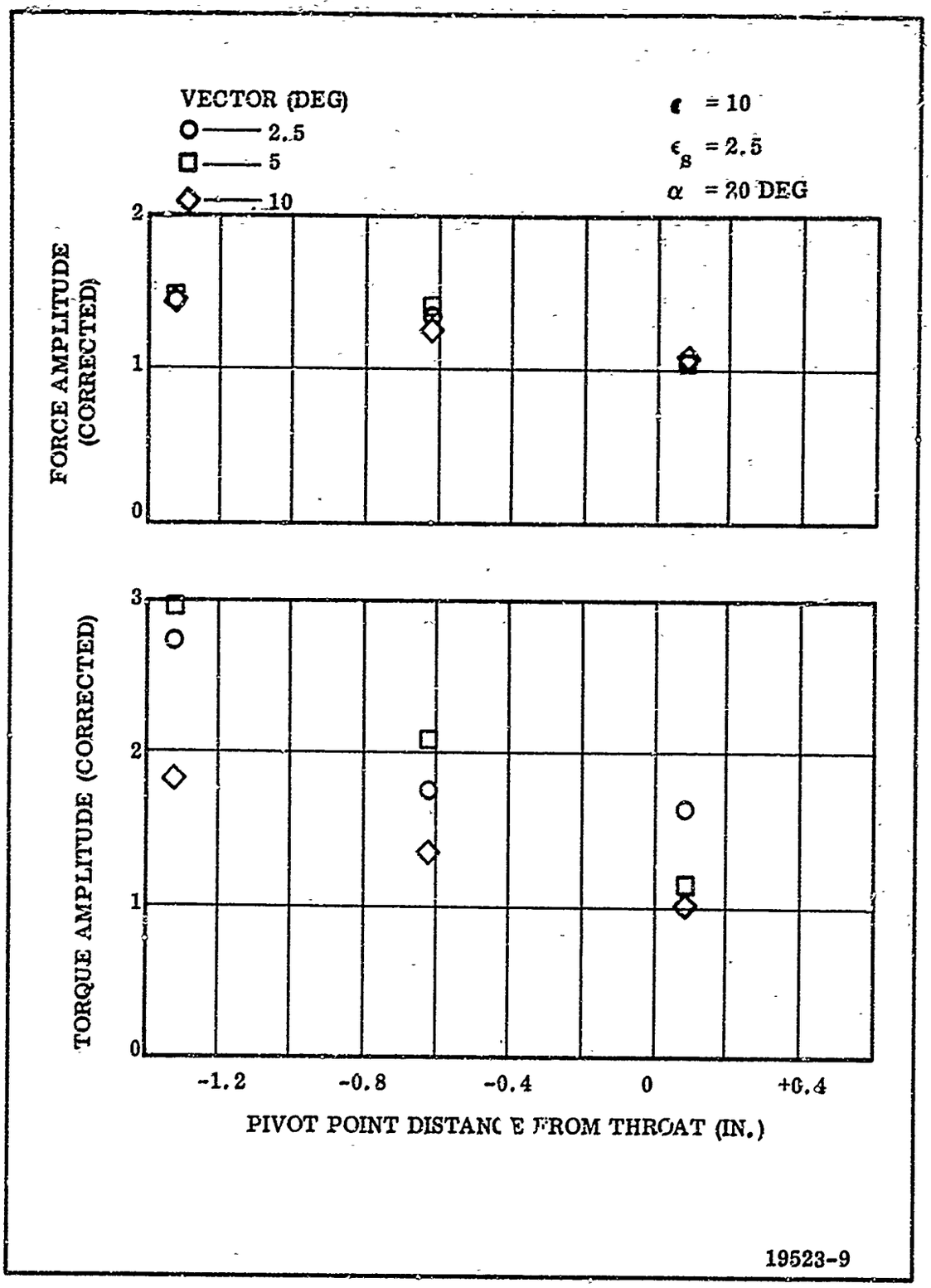

Figure 23. Effect of Pivot Location on Side Force and Torque Amplification (ϵ = 10, ϵ_s = 2.5)

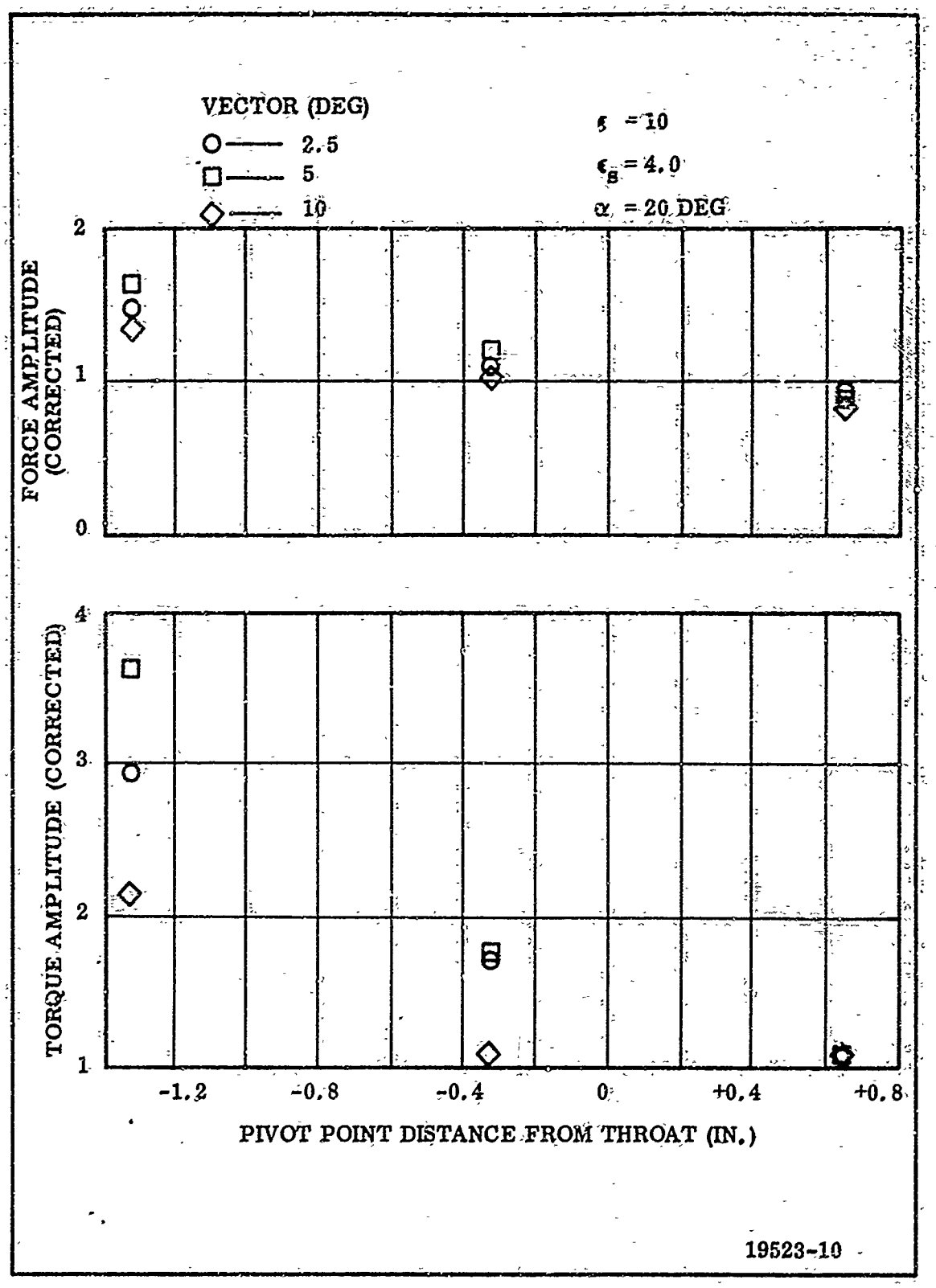

Figure 24. Effect of Pivot Location on Side Force and Torque Amplification (ϵ = 10, ϵ_s = 4.0)

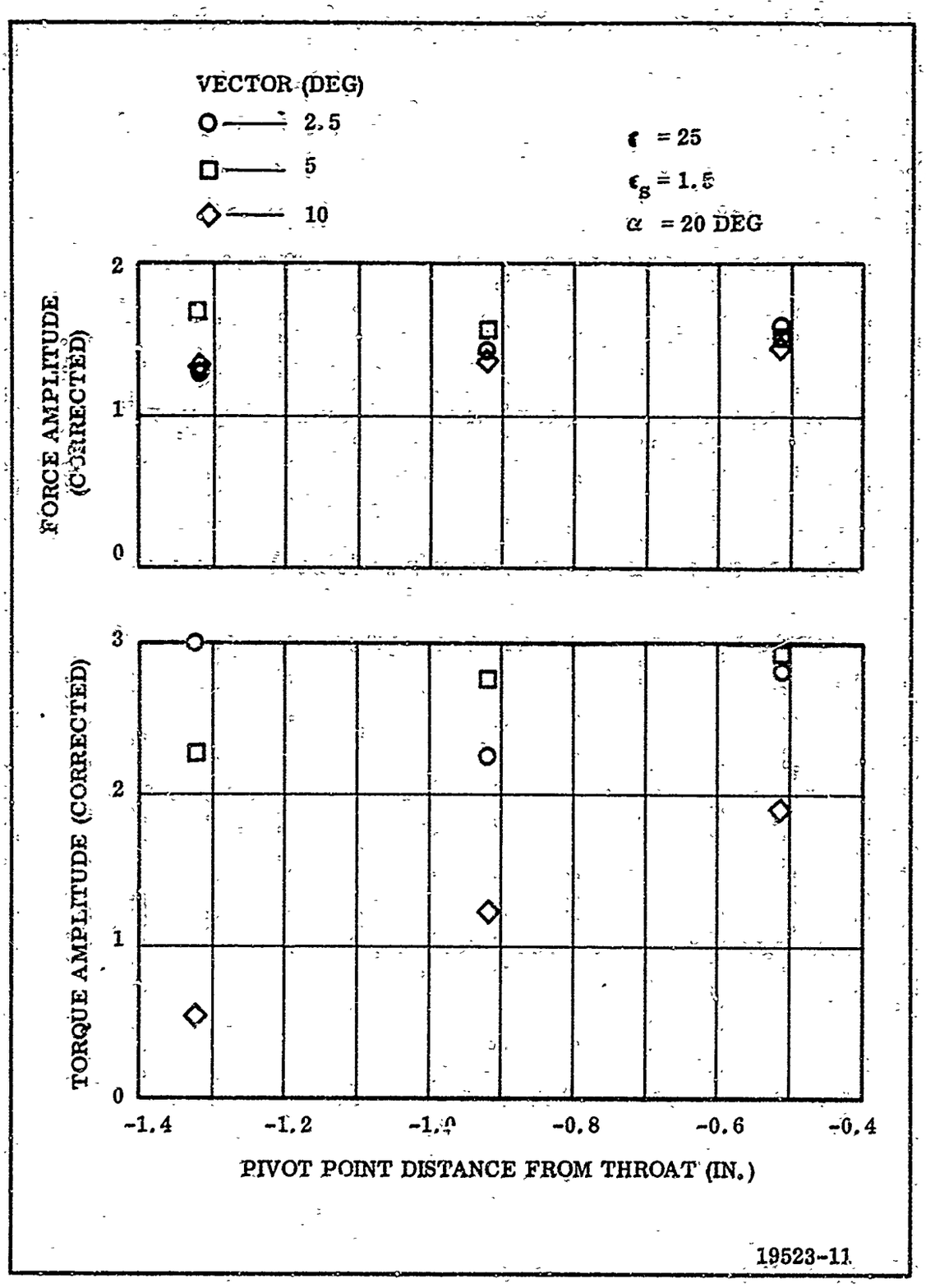

Figure 25. Effect of Pivot Location on Side Force and Torque Amplification (ϵ = 25, ϵ_g = 1.5)

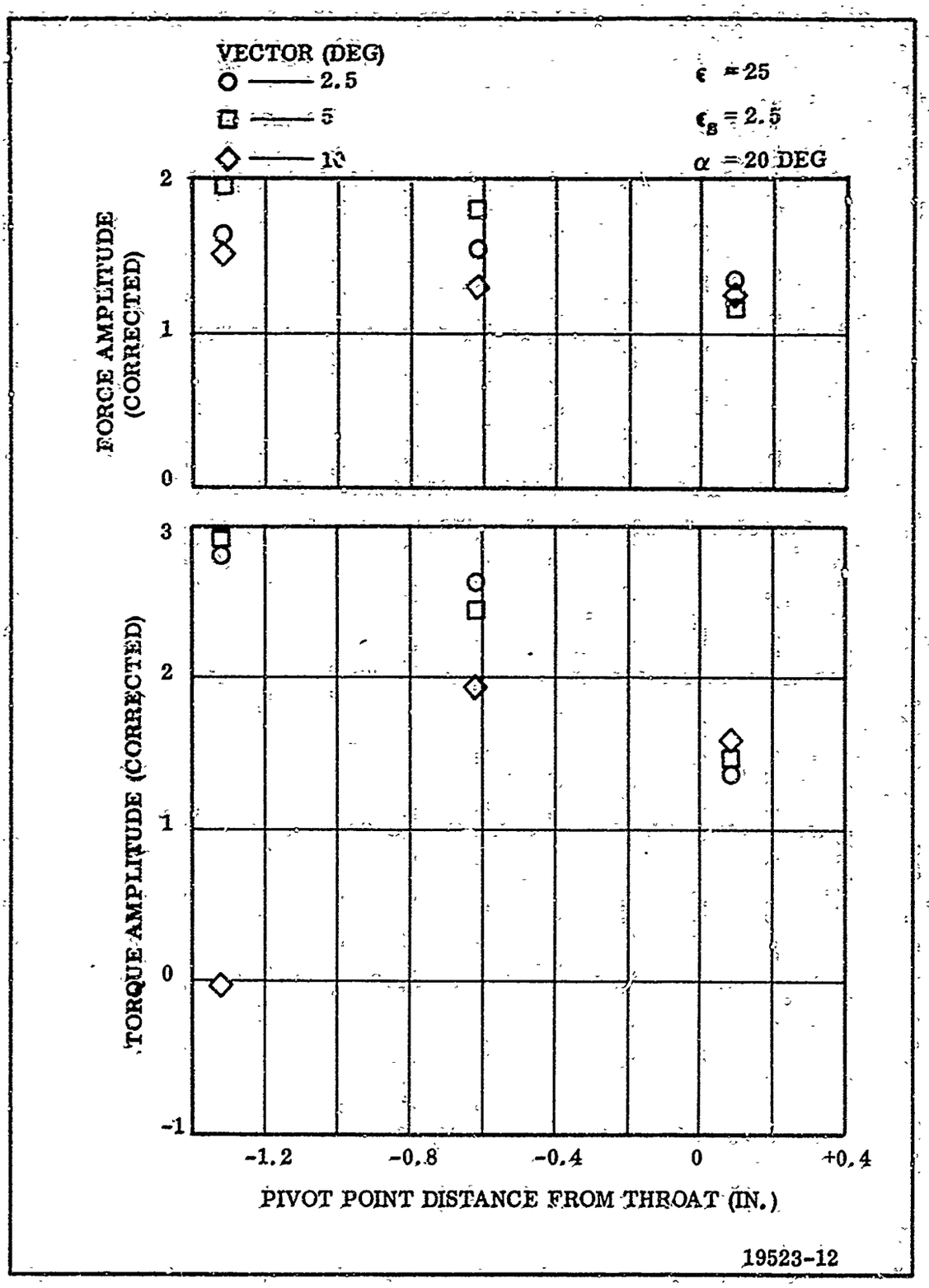

Figure 26. Effect of Pivot Location on Side Force and Torque Amplification (ϵ = 25, ϵ_s = 2.5)

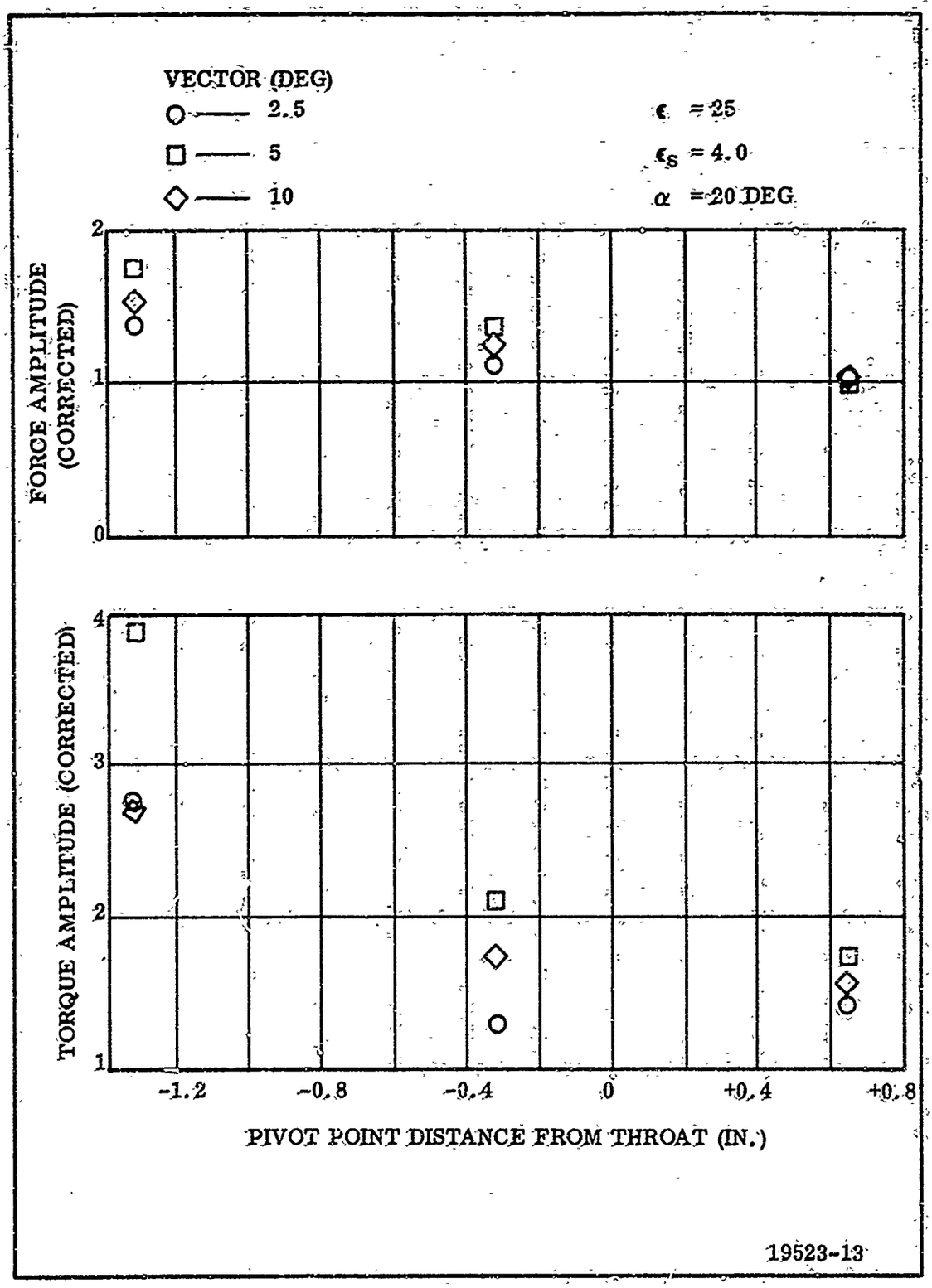

Figure 27. Effect of Pivot Location on Side Force and Torque Amplification (ϵ = 25, ϵ_s = 4.0)

The variation in torque amplification is somewhat more erratic with the upstream seal than with the other joint configurations. This is probably caused by the shock from the compression side of the nozzle influencing the flow on the opposite side of the nozzle. This phenomenon is dependent upon joint location, vector angle, and pivot location as well as several lesser variables. Since the Mach No. is lower at the upstream seal, a larger shock angle results. This allows the shock to affect the opposite half of the nozzle farther upstream in the nozzle. The upstream joint location also results in a larger portion of the nozzle being influenced by vectoring. However, the pressure ratio across the shock is reduced due to the lower Mach No. at the joint. All of these variables complicate the variation in torque such that a consistent pattern is unlikely.

The pressure data show evidence of the shock intersecting the opposite wall in the plane of vector on the high expansion ratio nozzle. The effects of this occurring is quite apparent in the torque data. Vectoring the nozzle 10 deg produces a large reduction in torque due to the influence of the shock. Some evidence of this phenomenon is also apparent in the side force data.

b. Effect of Joint Location--The effects of joint location on side force amplification and torque amplification are illustrated for the 10:1 expansion ratio nozzle in Figures 28 thru 30. The same data are presented for the 25:1 expansion ratio nozzle in Figures 31 thru 33.

The side force amplification is generally reduced, as the joint location is moved downstream. This is primarily due to the reduced surface area downstream of the joint.

The influence of joint location on force amplification is much less pronounced with the upstream pivot configuration. This is the result of a stronger shock generated with the upstream pivot increasing the pressure differential downstream of the joint which tends to reduce the effect of moving the joint downstream.

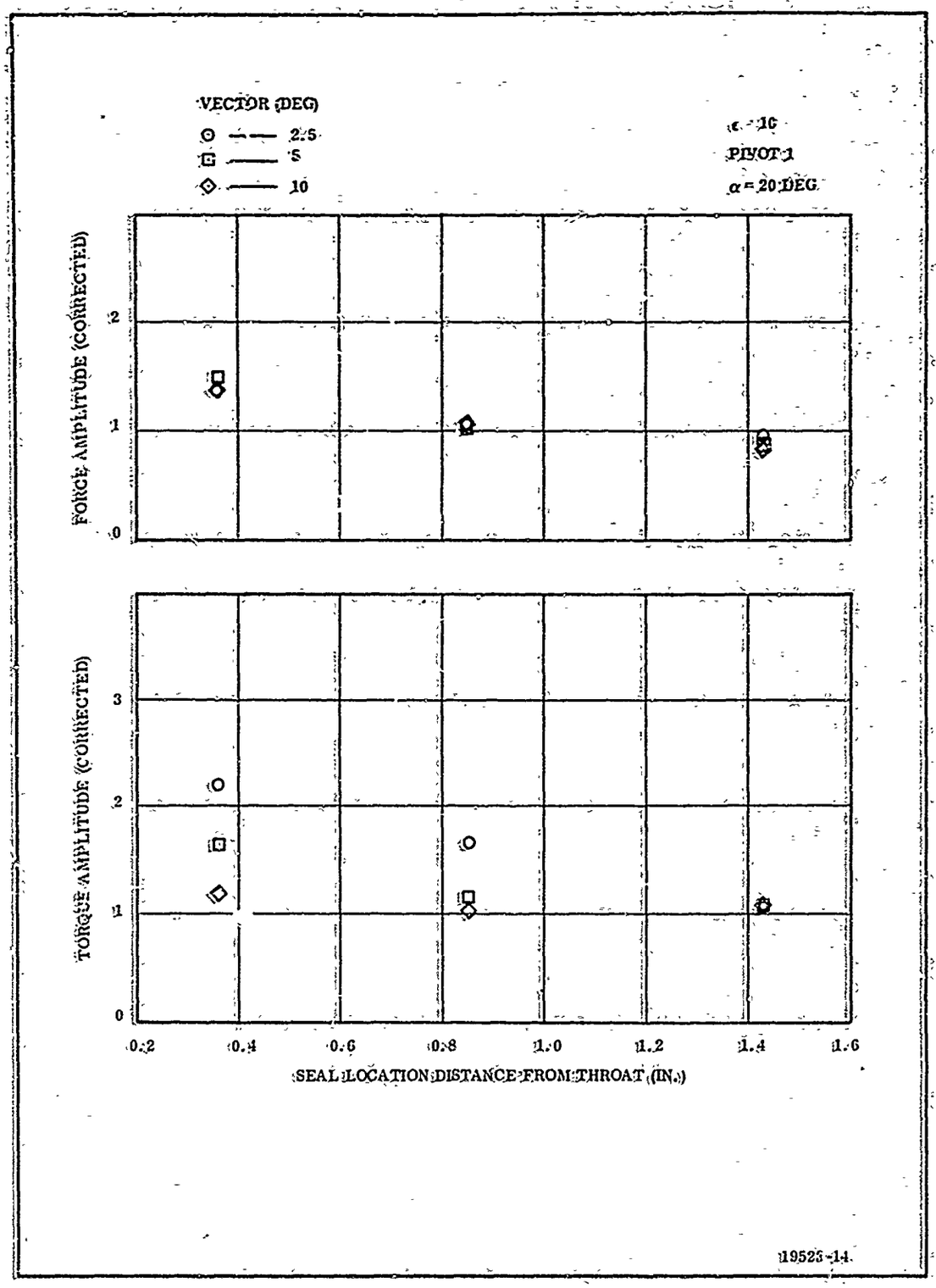

Figure 28. Effect of Joint Location on Side Force and Torque Amplification (ϵ = 10, Pivot 1)

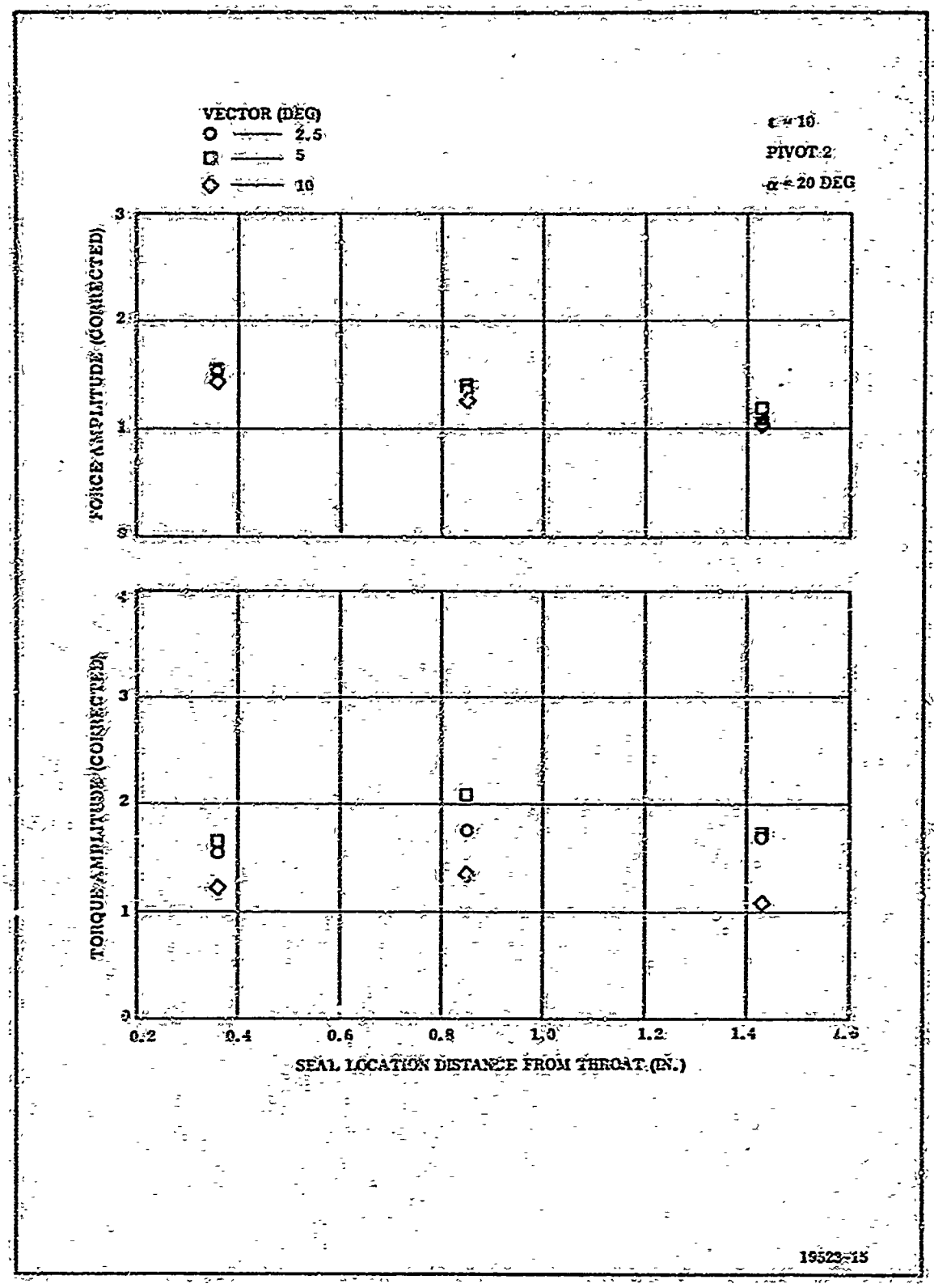

Figure 29. Effect of Joint Location on Side Force and Torque Amplification (ε = 10, Pivot 2)

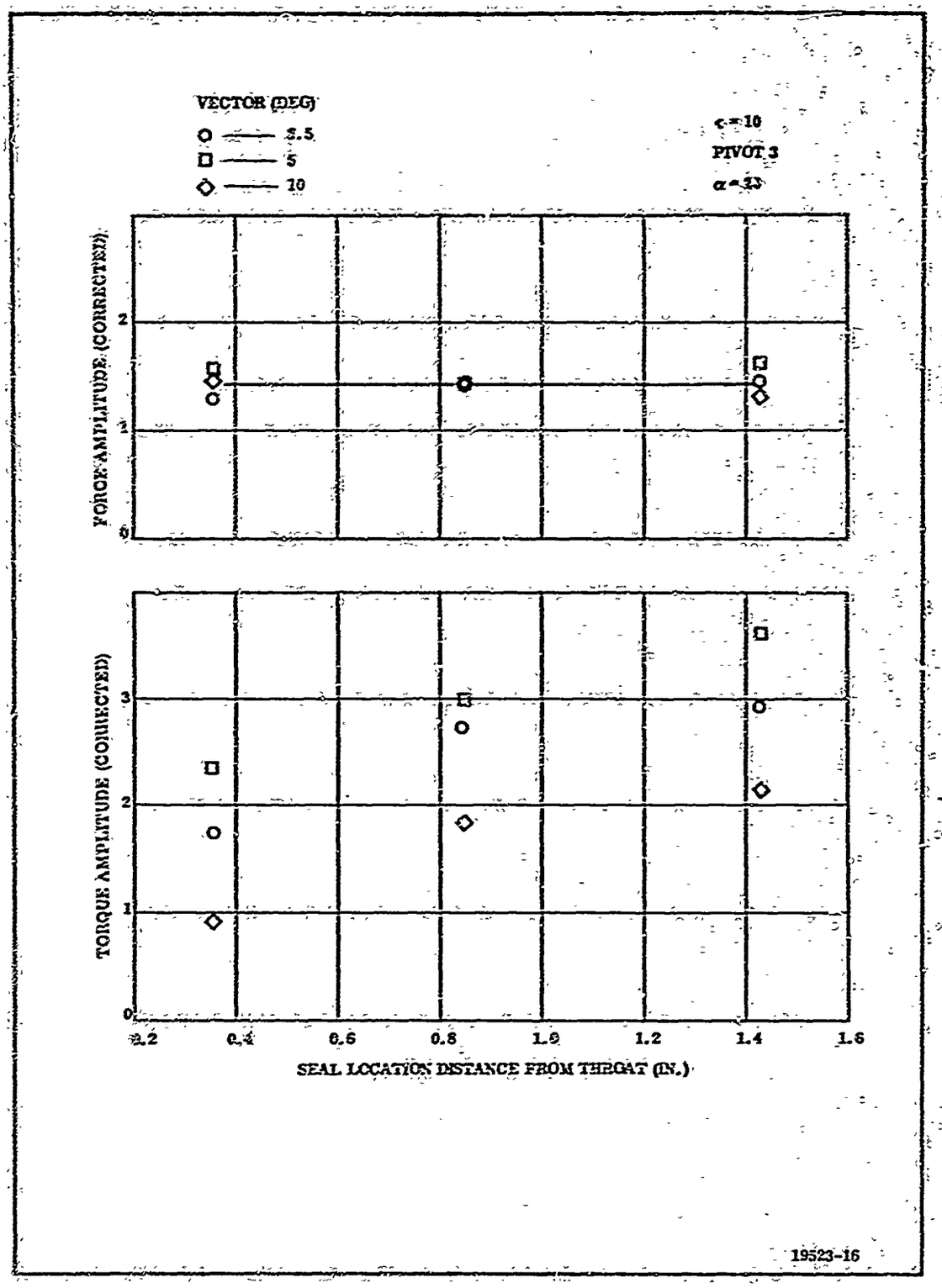

Figure 30. Effect of Joint Location on Side Force and Torque Amplification (ϵ = 10, Pivot 3)

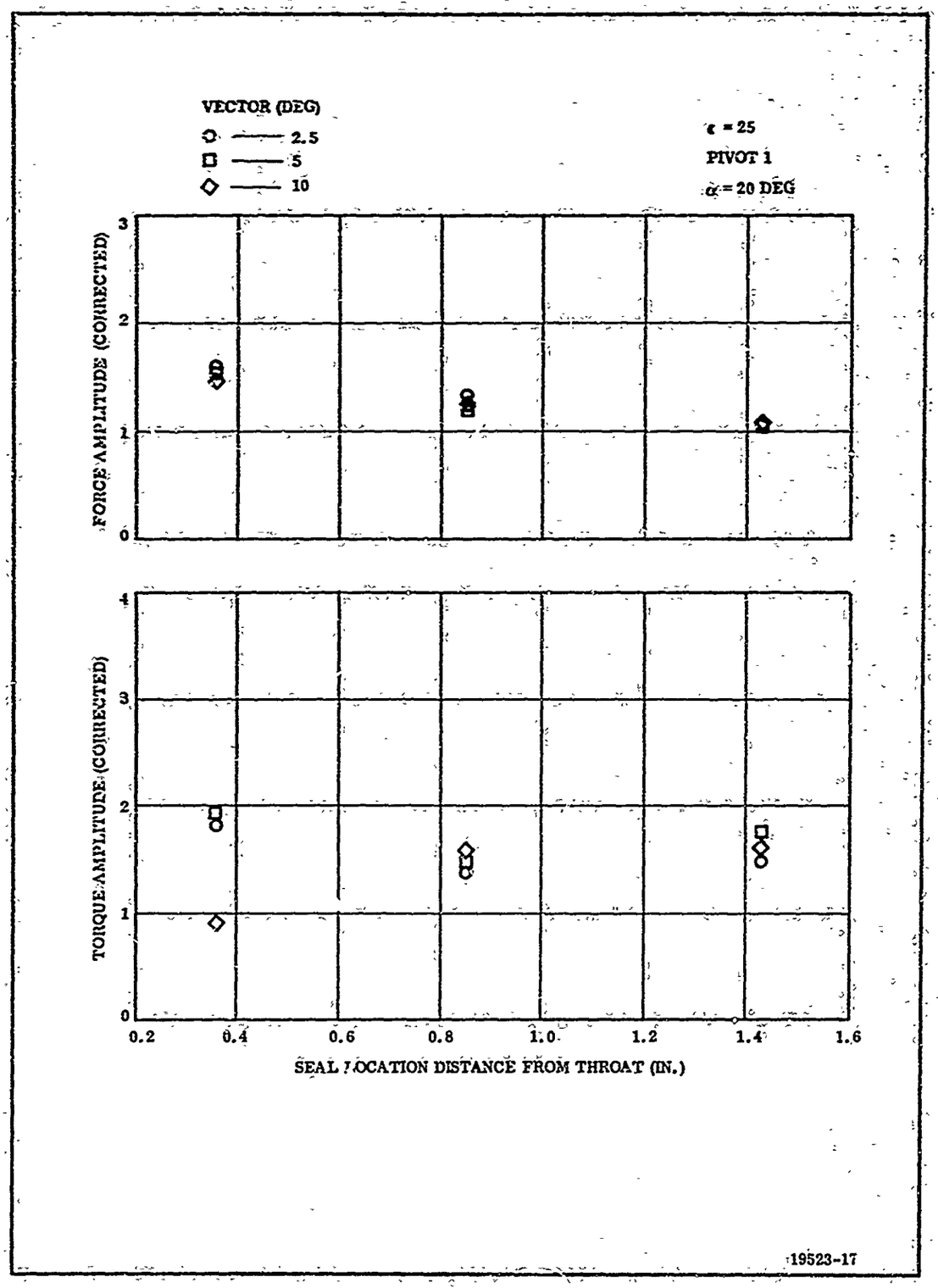

Figure 31. Effect of Joint Location on Side Force and Torque Amplification (ε= 25, Pivot 1)

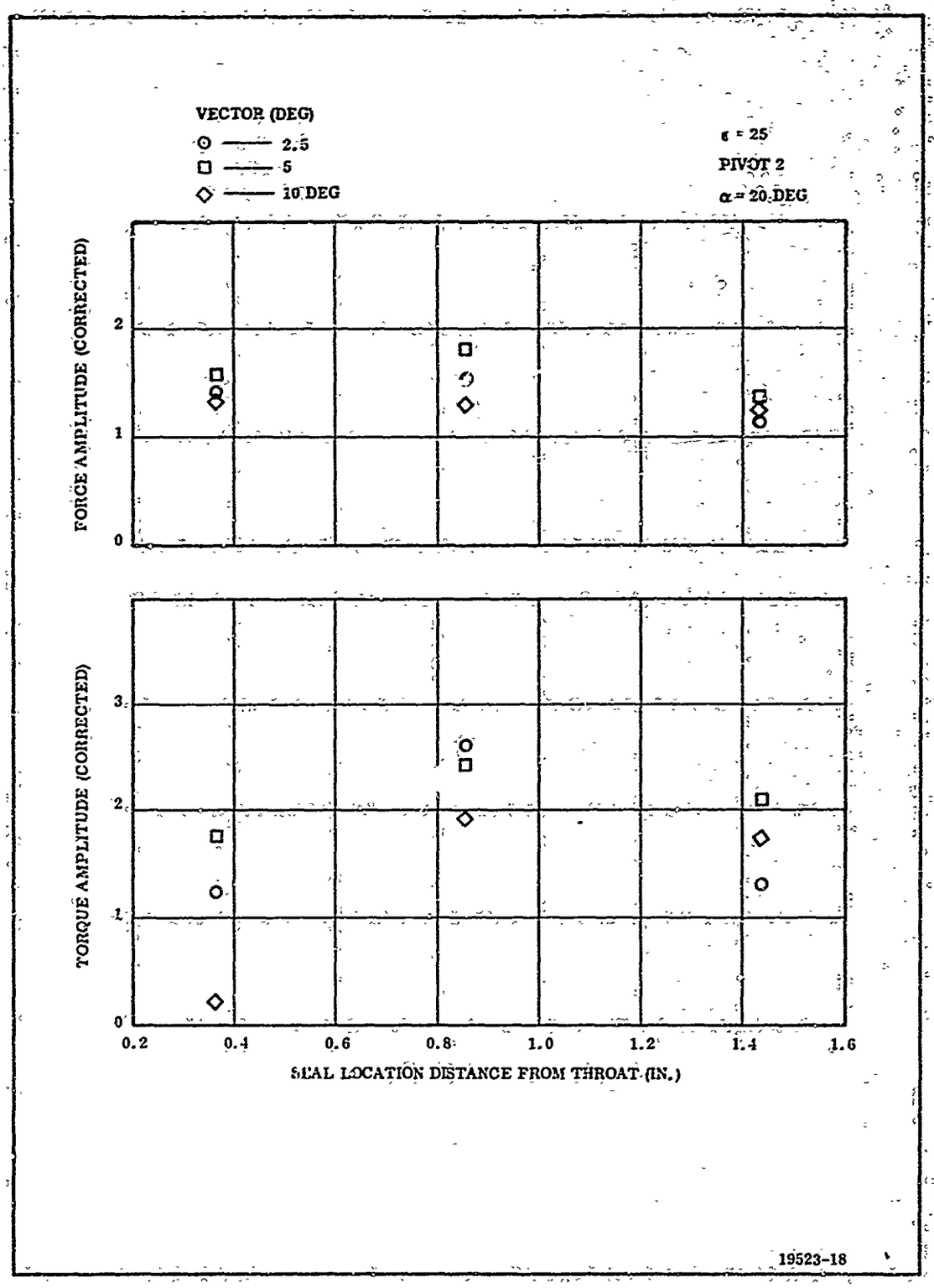

Figure 32. Effect of Joint Location on Side Force and Torque Amplification (ϵ = 25, Pivot 2)

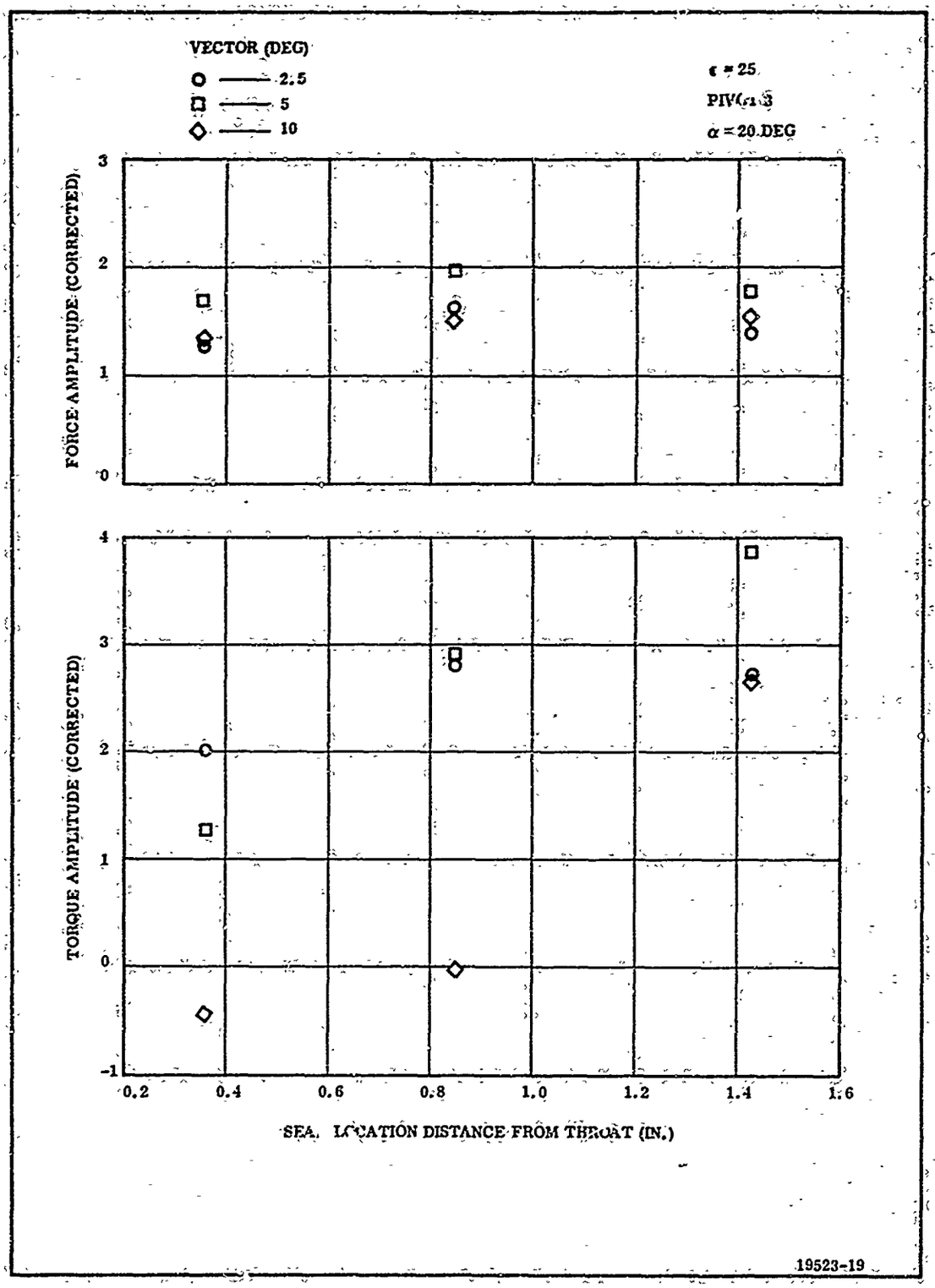

Figure 33. Effect of Joint Location on Side Force and Torque Amplification (ε = 25, Pivot 3)

The torque amplification tends to decrease as the joint is moved downstream on the aft pivot configuration. The opposite is true for the forward pivot configuration. The interaction of the effects of pivot and joint location on torque should be similar to that of the force data. However, the moment arm variation introduces an additional variable which further complicates the influence of these two parameters on nozzle torque.

c. Effect of Nozzle Expansion Ratio--The effect of varying the expansion ratio of the nozzle was investigated on the 15 deg and 25 deg cone configurations. The pivot 2, $E_s = 2.5$ nozzle was used. Expansion ratios of 10:1, 16:1, and 25:1 were examined. Force and torque amplification are shown as a function of expansion ratio in Figures 34 and 35.

Increasing the nozzle expansion ratio while holding all other parameters constant normally would be expected to produce an increase in side force due to the increased area downstream of the joint. On the nozzle having a 25 deg exit cone, the 16:1 expansion ratio does produce an increase over the 10:1 expansion ratio nozzle. However, the side force drops appreciably on the 25:1 expansion ratio nozzle. Pressure data indicate that this is due to the intersection of the shock wave from the compression side of nozzle with the opposite wall.

On the 15 deg exit cone, 16:1 expansion ratio nozzle, the shock wave intersection with the opposite wall was apparent in the pressure data. This explains the general decrease in side force with increasing expansion ratio on the 15 deg exit cone nozzle. The 2 1/2 deg vector angle data vary in the opposite manner on this nozzle because the smaller shock angle (due to reduced turning of the gas) did not result in the shock intersecting with the opposite wall. This also is verified by the pressure data.

The influence of the shock intersection was much more pronounced in the torque data. At the higher expansion ratios, the vector angle induced a wide spread in torque amplification. This was due to the larger vector angles increasing

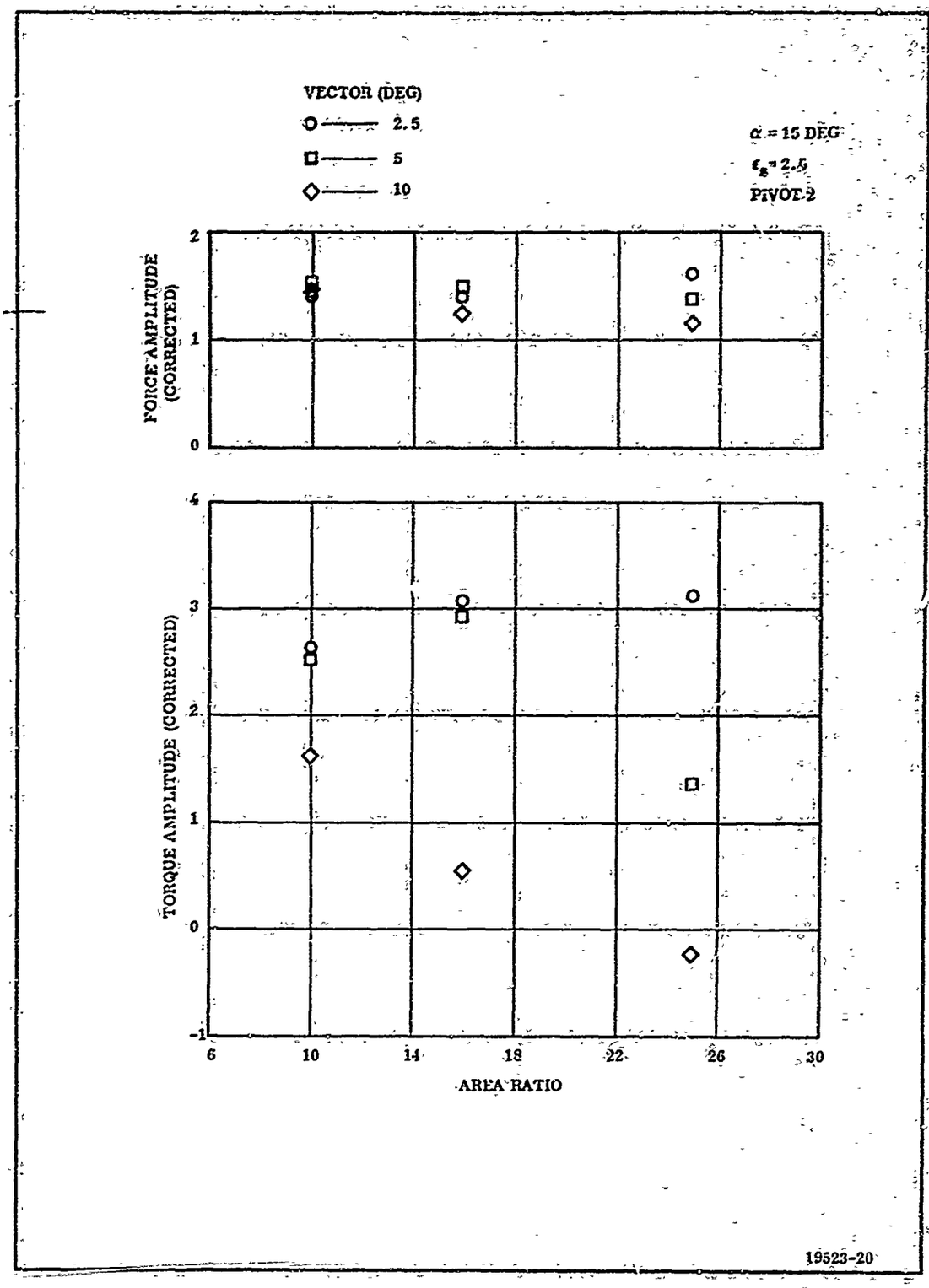

Figure 34. Effect of Nozzle Expansion Ration on Side Force and Torque Amplification (α = 15 Deg

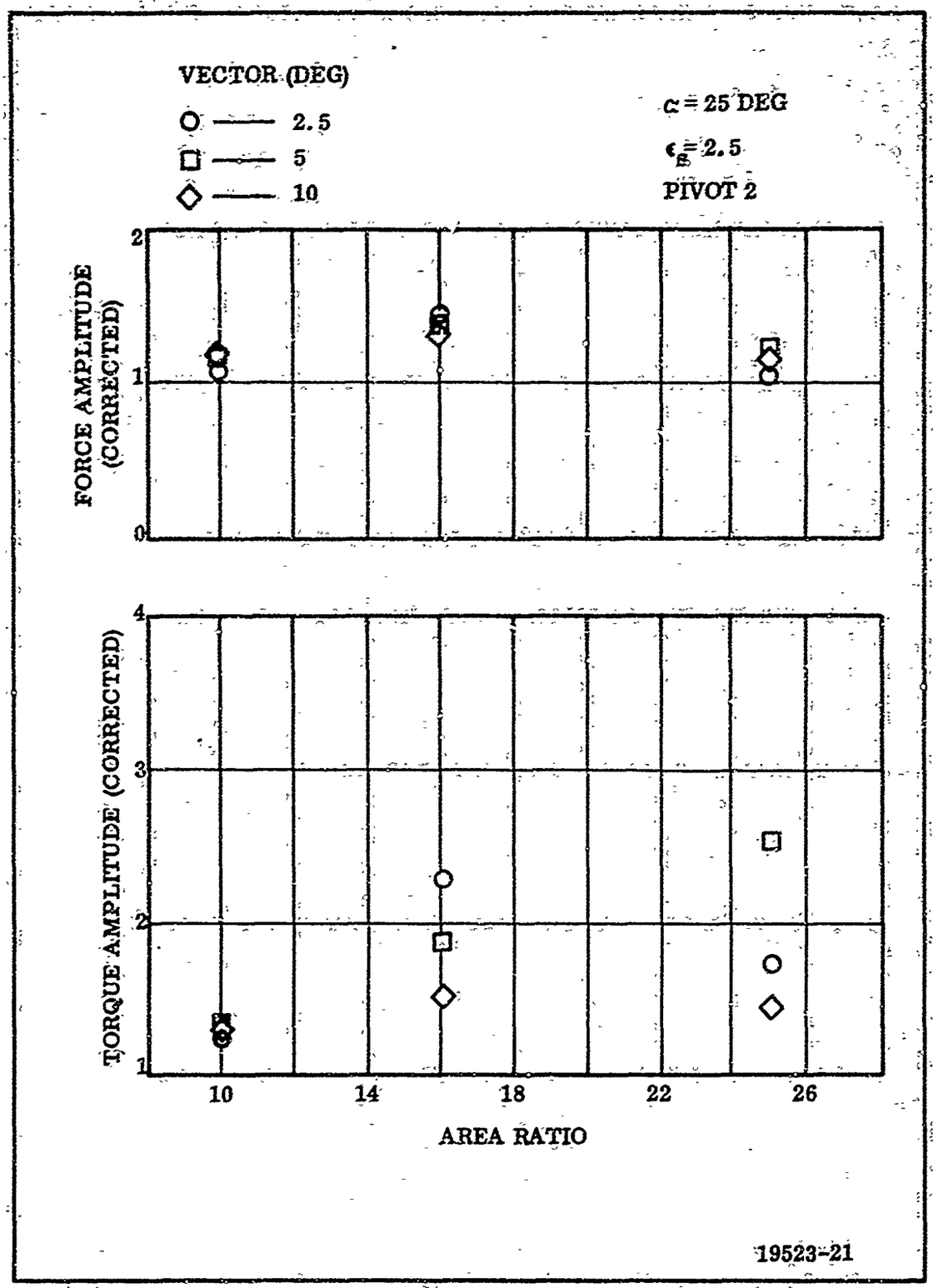

Figure 35. Effect of Nozzle Expansion Ration on Side Force and Torque Amplification (α = 250 Deg)

the shock angle such that the shock intersection point moved upstream. In fact, on the 15 deg cone, 25:1 expansion ratio nozzle, the area affected by the intersecting shock was large enough to produce a nonrestoring nozzle torque (Figure 34).

d. Effect of Cone Angle--The effect which varying the cone angle from 15 to 25 deg had on side force and torque is illustrated in Figure 36. Both the side force and torque increased appreciably as the cone angle decreased. Increasing the cone angle while holding the expansion ratio constant resulted in a shorter nozzle, thereby reducing the length of the movable portion of the nozzle. The surface area affected by vectoring being decreased, reduces the side force and torque.

The effect of cone angle was examined on the 10:1 expansion ratio nozzle only. This trend would not be expected on high expansion ratio nozzles, due to crossover of the shock wave.

e. Effect of Nozzle Erosion--Two eroded nozzles were tested to evaluate the effect of burn time on nozzle performance. Force data are presented for these nozzles in Figure 37. Torque and side force increase with burn time.

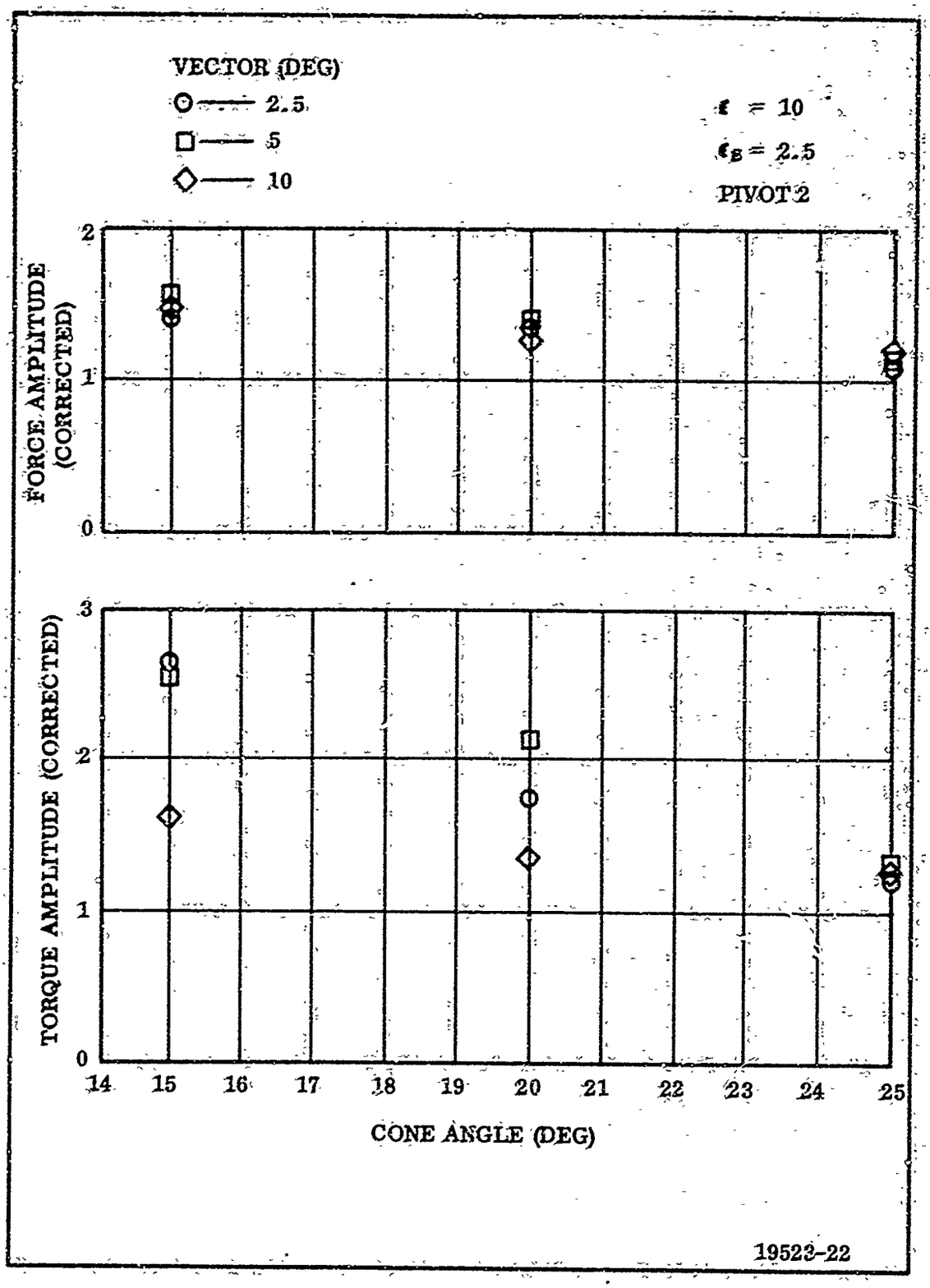

Figure 36. Effect of Nozzle Cone Angle on Side Force and Torque Amplification

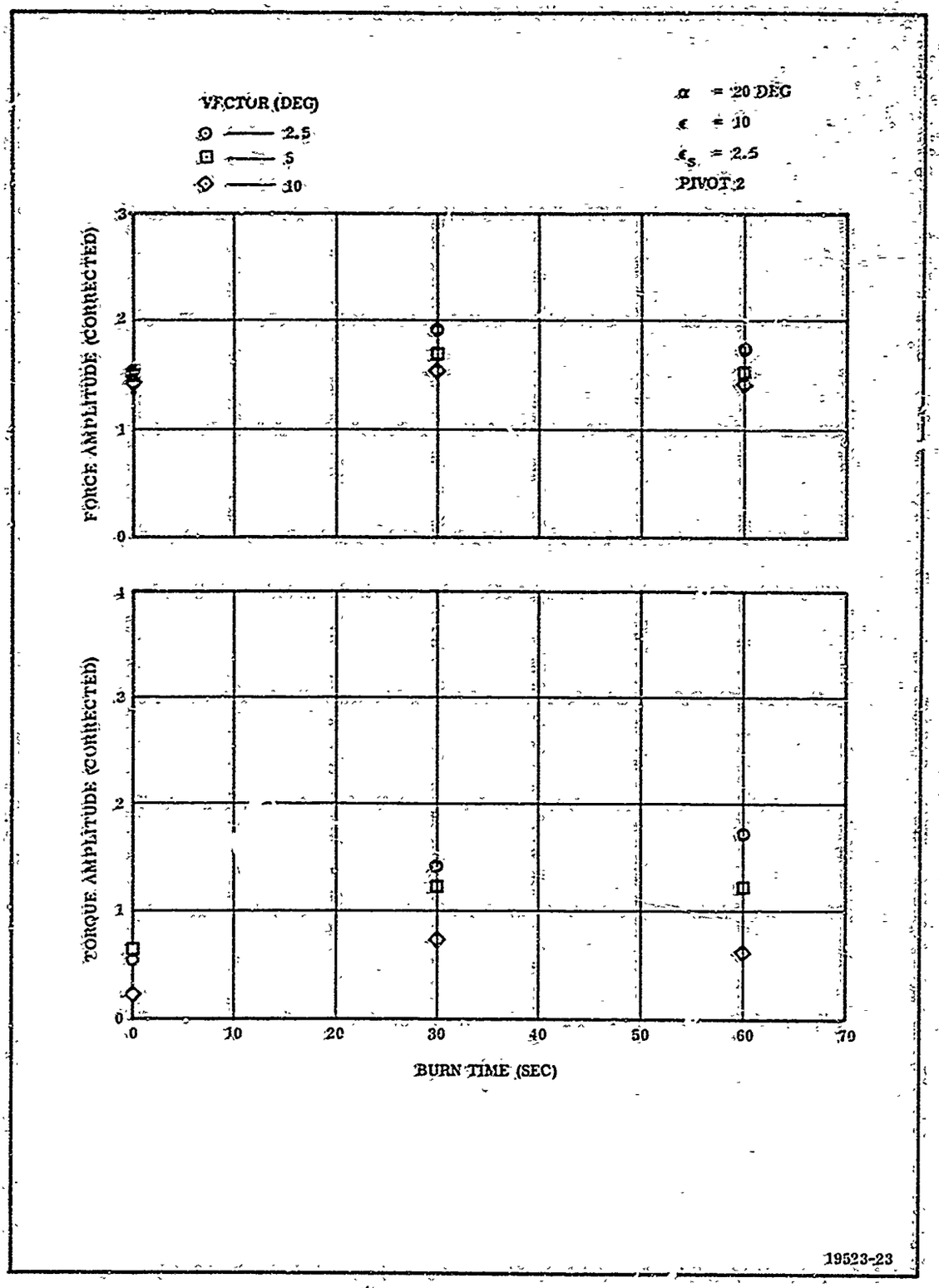

Figure 37. Effect of Nozzle Erosion on Side Force and Torque Amplification

2. AXIAL FORCE DATA

The axial thrust efficiency is presented for each test run on the data sheets presented in Appendix I. These data are also plotted on Figures 38 thru 41.

The axial thrust efficiency is the ratio of measured thrust to the ideal thrust of a vectoring nozzle. This parameter decreases with increasing vector angle due to losses incurred when turning a supersonic gas stream.

Moving the pivot upstream or the joint downstream tends to reduce nozzle efficiency. Moving the pivot upstream increases the shock strength due to the larger turning of the flow in the vicinity of the joint thus increasing the losses in the nozzle. The losses also are increased with the downstream joint due to the stronger shock associated with the higher Mach No. of the flow being turned.

The higher expansion ratio nozzles are more efficient than the 10:1 expansion ratio nozzle indicating that some of the losses are recovered with the longer nozzle. the thrust efficiency data is somewhat more irregular on the 10:1 than on 25:1 expansion ratio nozzle. This is primarily due to the measured back pressure affecting the ideal nozzle thrust rather than irregularities in the measured thrust. Four pressure taps recorded back pressure on the 25:1 expansion ratio nozzle, whereas a single tap was used with the 10:1 expansion ratio nozzle. Tap 30, which measured back pressure on both nozzles was found to be erratic during testing and during reduction of data on the 25:1 expansion ratio nozzle.

The effect of erosion on axial thrust efficiency is illustrated in Figure 41. The efficiency of the 30 second configuration is nearly the same as for the uneroded configuration. However, the loss experienced became significant with the 60 second configuration. The model reflected a highly erodable flexible joint.

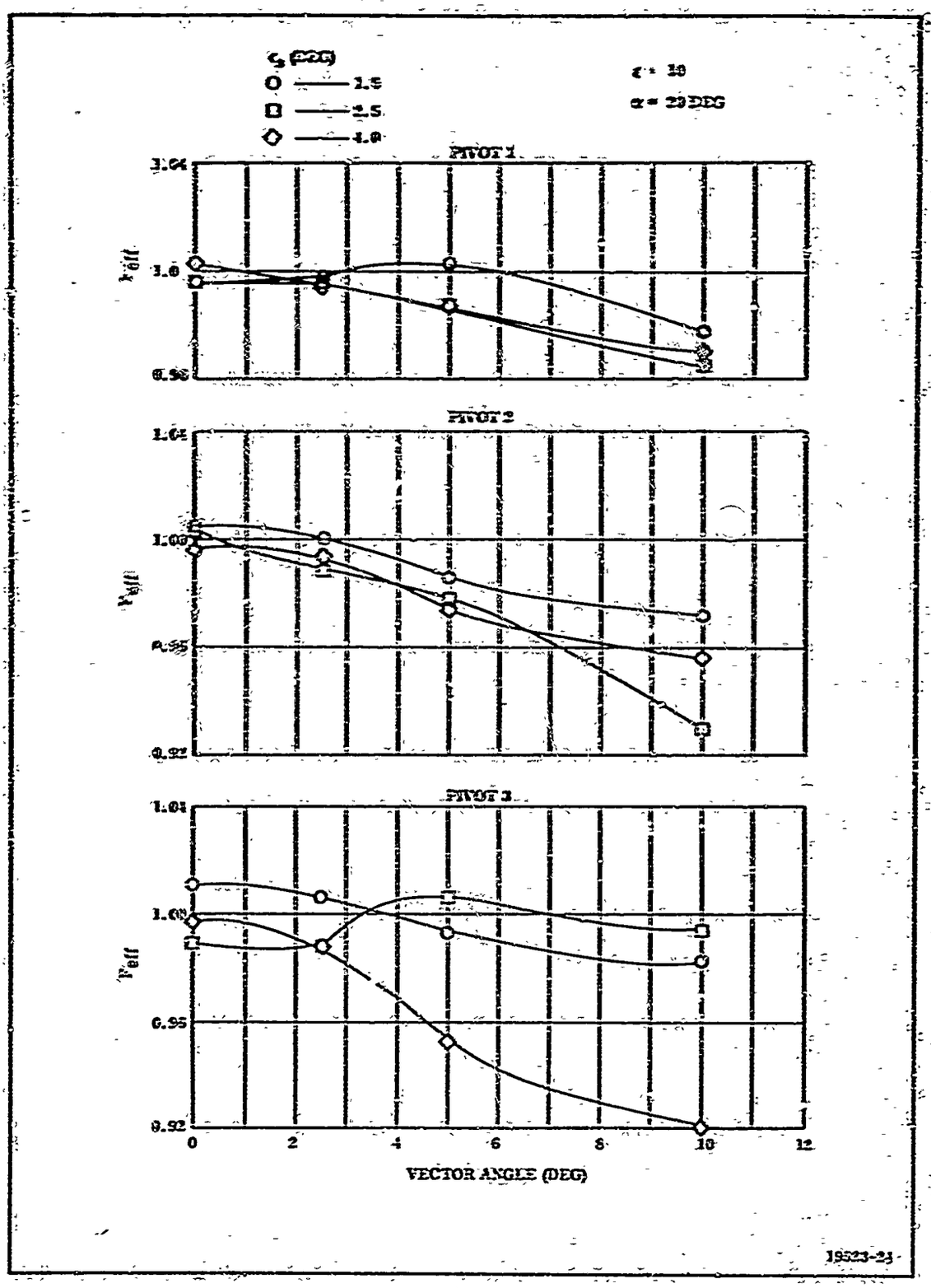

Figure 38. Axial Thrust Efficiency vs Nozzle Vector Angle

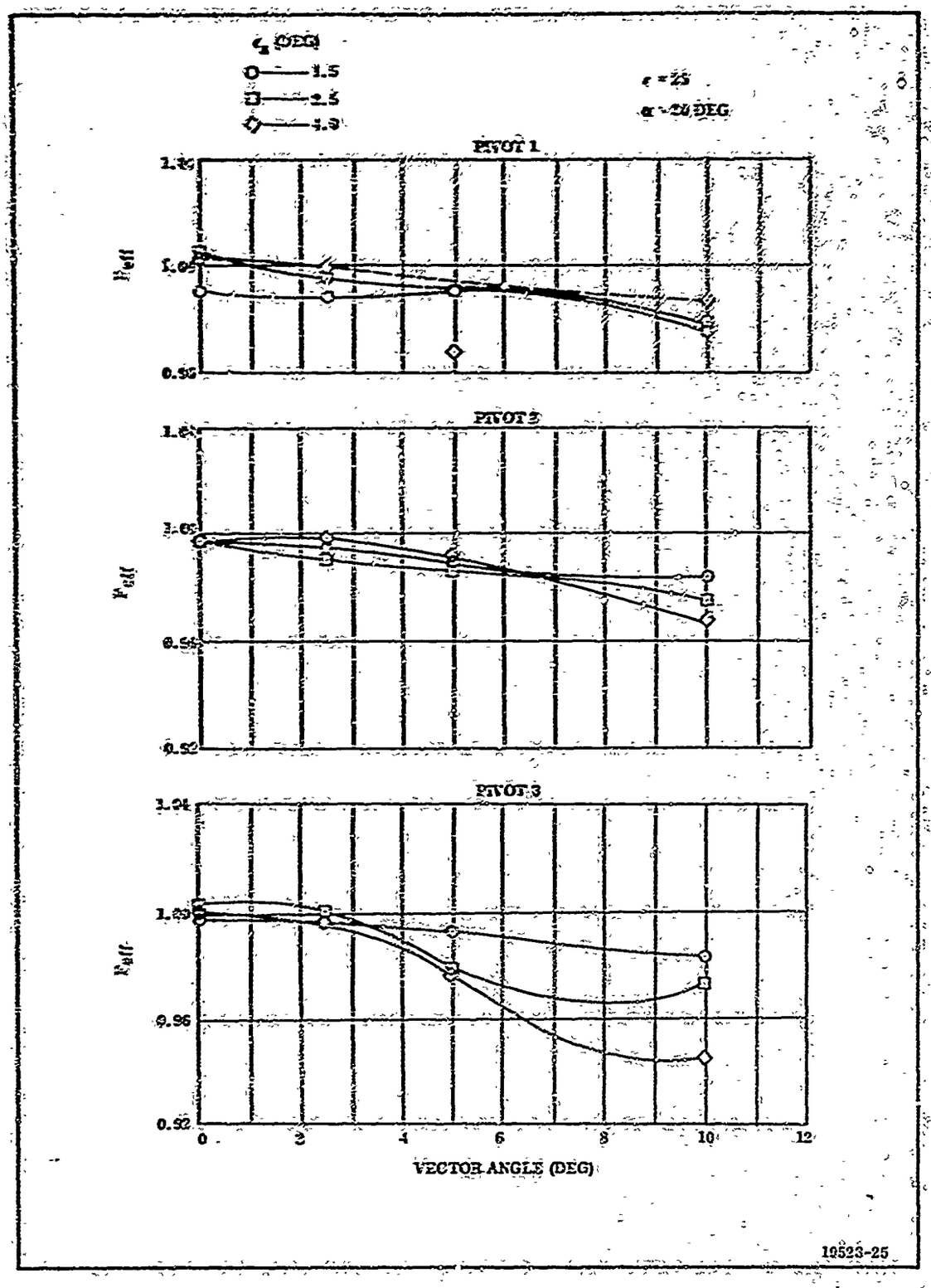

Figure 39. Axial Thrust Efficiency vs Nozzle Vector Angle

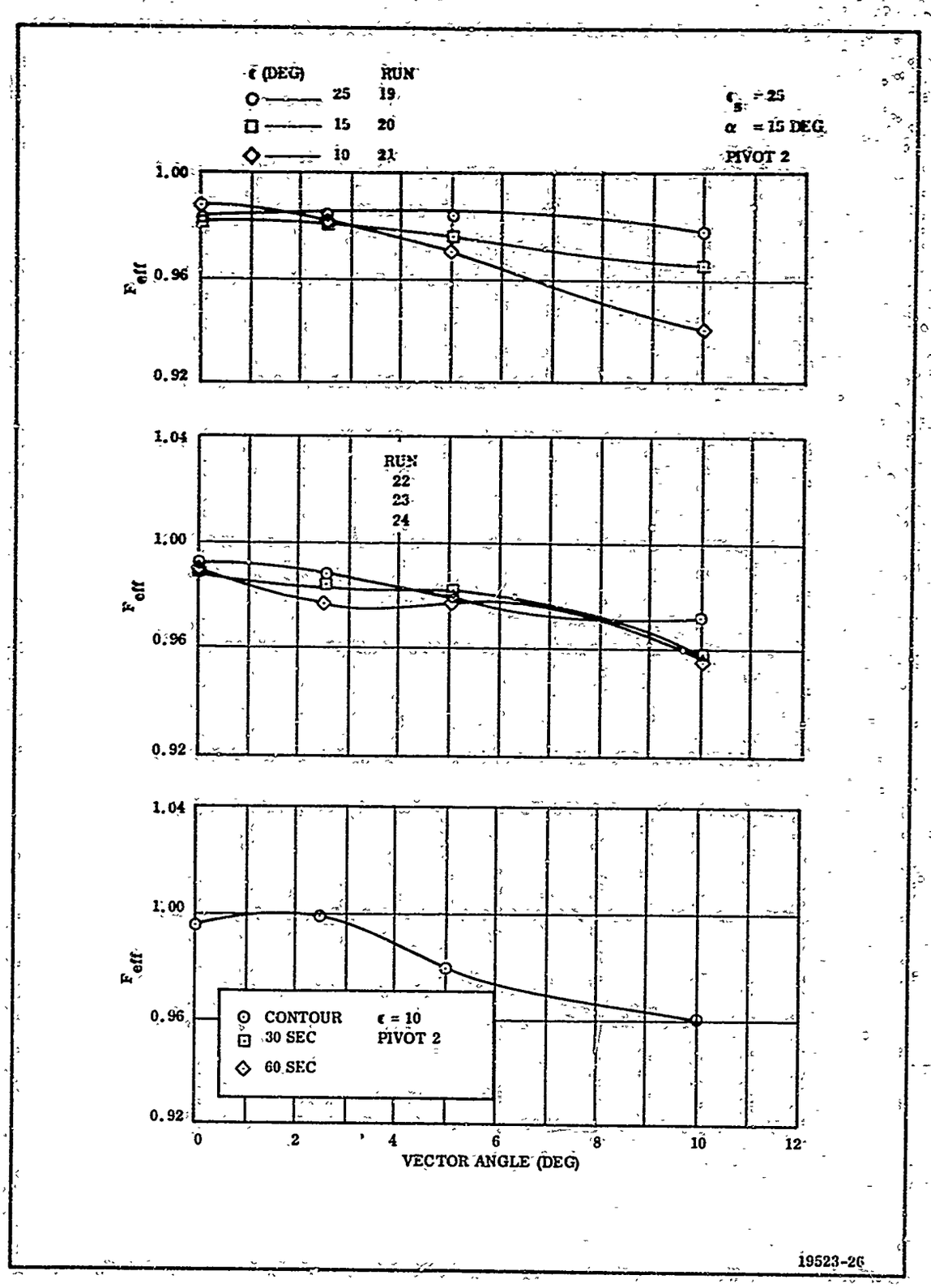

Figure 40. Axial Thrust Efficiency vs Nozzle Vector Angle

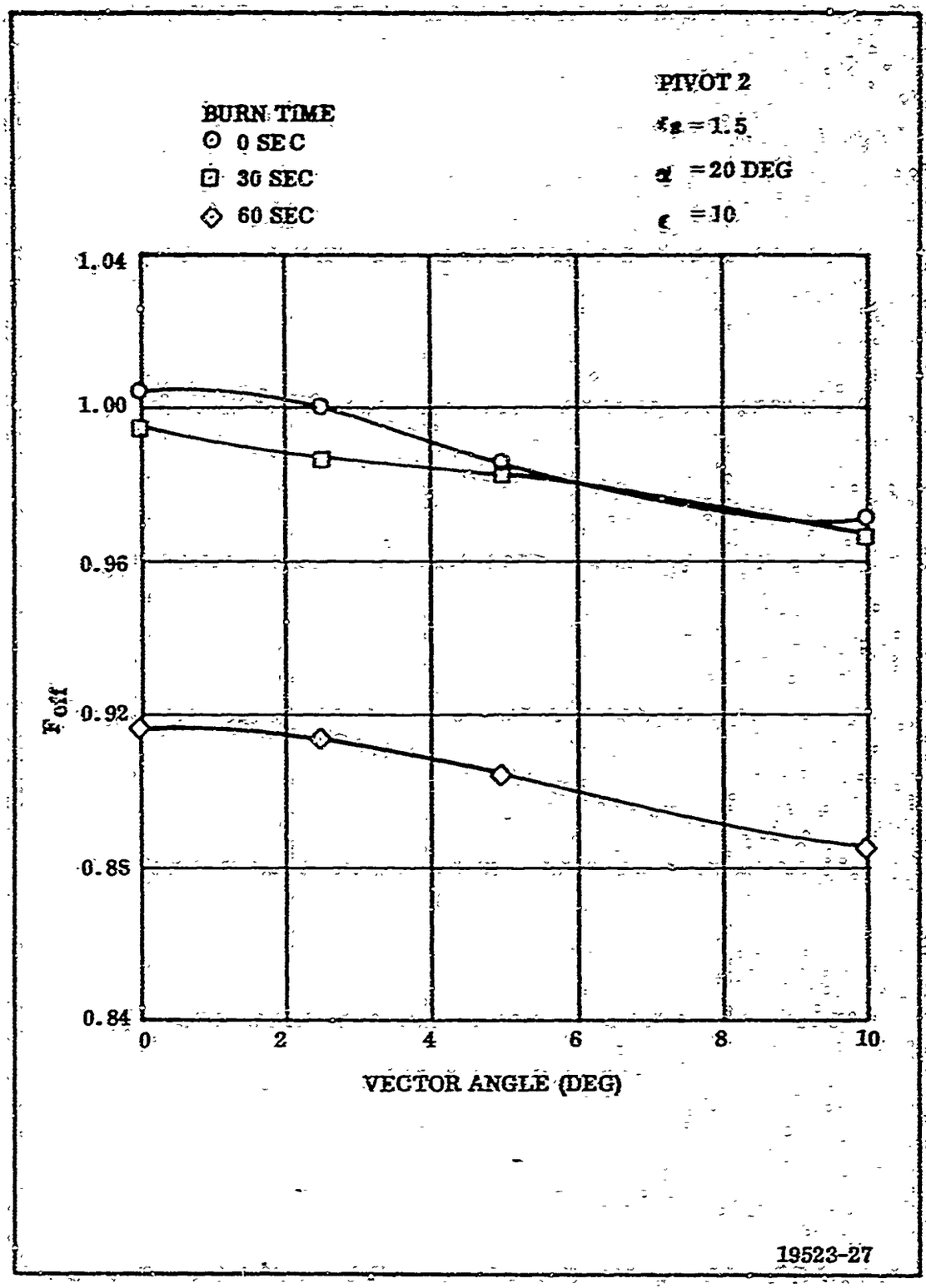

Figure 41. Axial Thrust Efficiency vs Nozzle Vector Angle

3. PRESSURE DATA AND FLOW VISUALIZATION DATA

All pressure data are presented in Appendix II. For Runs 1 thru 9, the data are plotted axially and circumferentially. Only the axial plots are presented for the remaining runs.

The circumferential plots were used to support development of the analytical flow model and to perform a pressure area integration to obtain side force and torque for purposes of checking with the measured test data.

Integration of pressure data produced torque and side force values significantly less than the measured data. Investigation showed this to be due to insufficient pressure data in the vicinity of the joint. Figures 42 and 43 show a comparison of test data with pressures calculated using the analytical flow model being developed under this program. From these plots it is apparent that pressure data are not adequate to define the flow field in the joint region. Therefore, side force and torque could not be accurately determined in this manner.

Figure 42 shows a point of separation occurring upstream of the forward edge of the joint. Theory indicates that this phenomena occurs when the turn angle at the wall is greater than the angle which the flow can negotiate through an attached oblique shock. This results in shocks being generated at the point of separation and at the reattachment point.

Evidence of separation occurring ahead on the vectored seal was obtained from flow visualization. Stipples of lampblack and glycerin were placed in the model to examine the separation phenomena and also to assure that separation did not occur near the nozzle exit.

Figures 44 thru 46 are photographs of flow visualization data obtained in this manner. The line of separation is clearly evident in each of these photographs. Separation distances were measured on various runs to assist in establishing a separation criteria to be used in the analytical model.

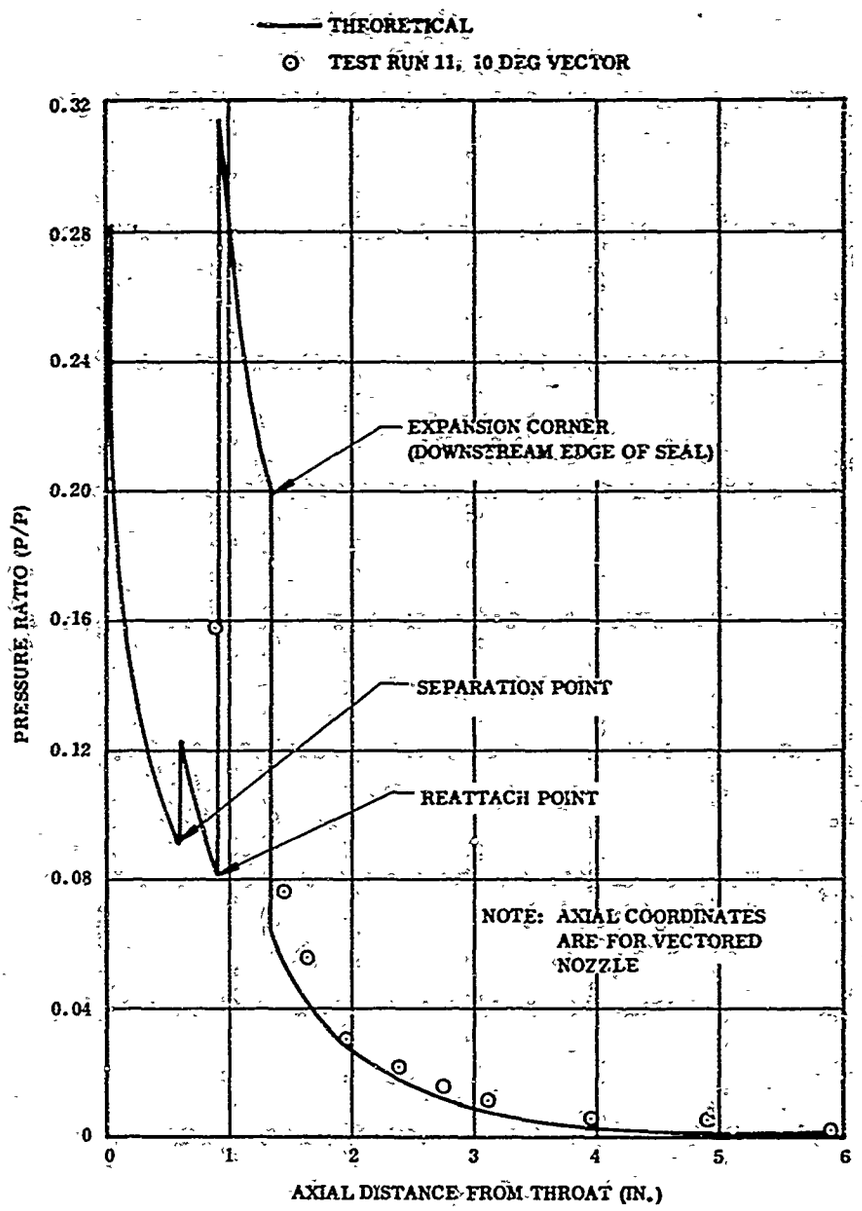

Figure 42. Comparison of Test Data with Theory, Compression Side of Nozzle

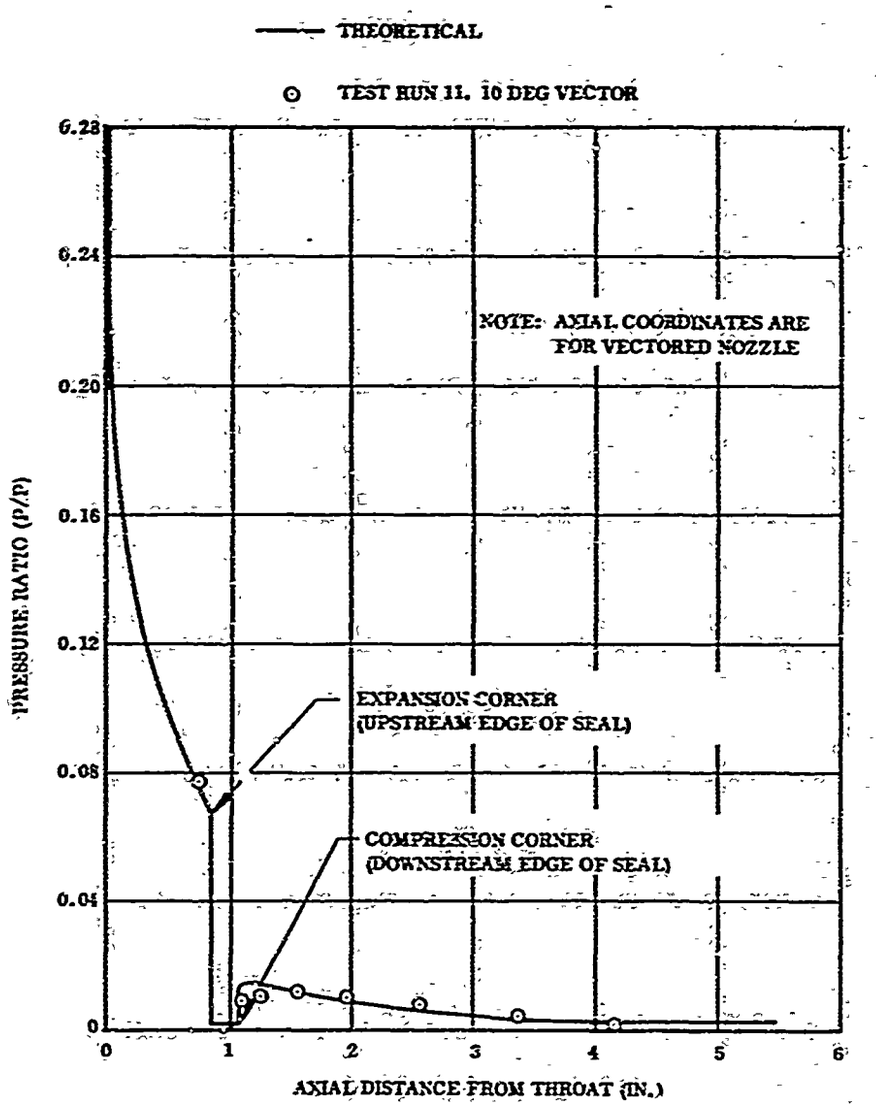

Figure 43. Comparison of Test Data with Theory, Expansion Side of Nozzle

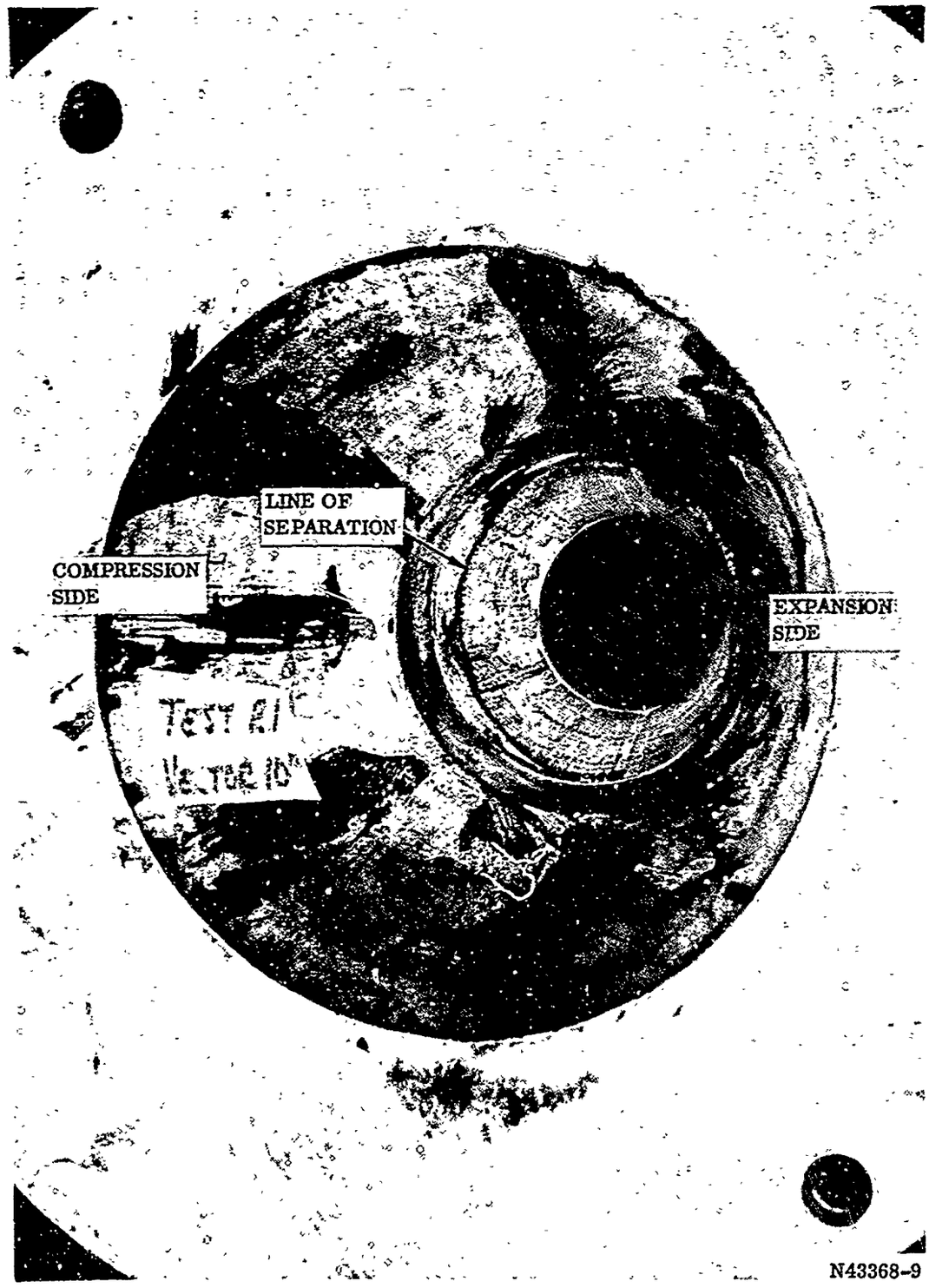

Figure 44. Flow Visualization Showing Separation Upstream of the Joint (Test 19)

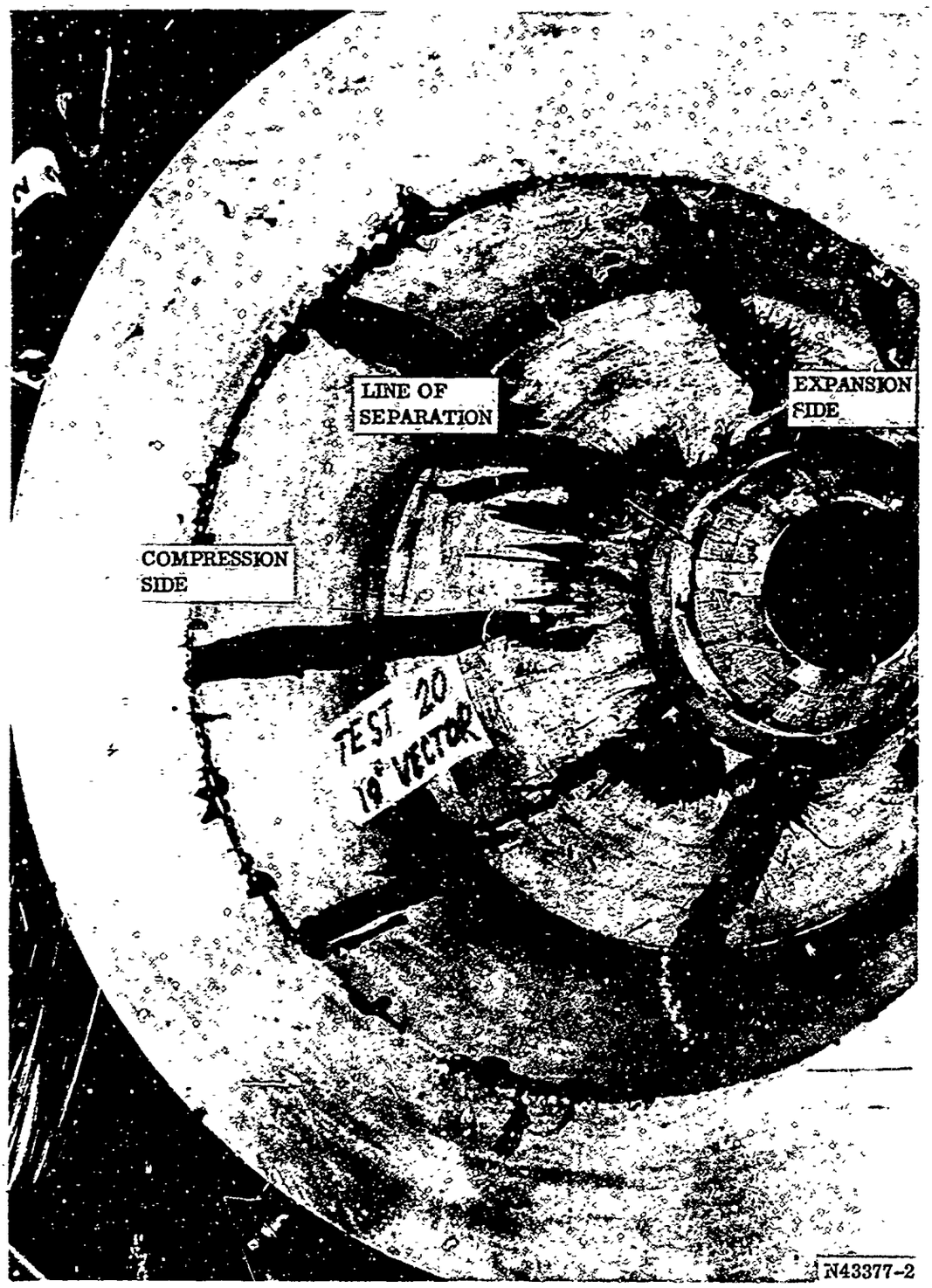

Figure 45. Flow Visualization Showing Separation Upstream of the Joint (Test 20)

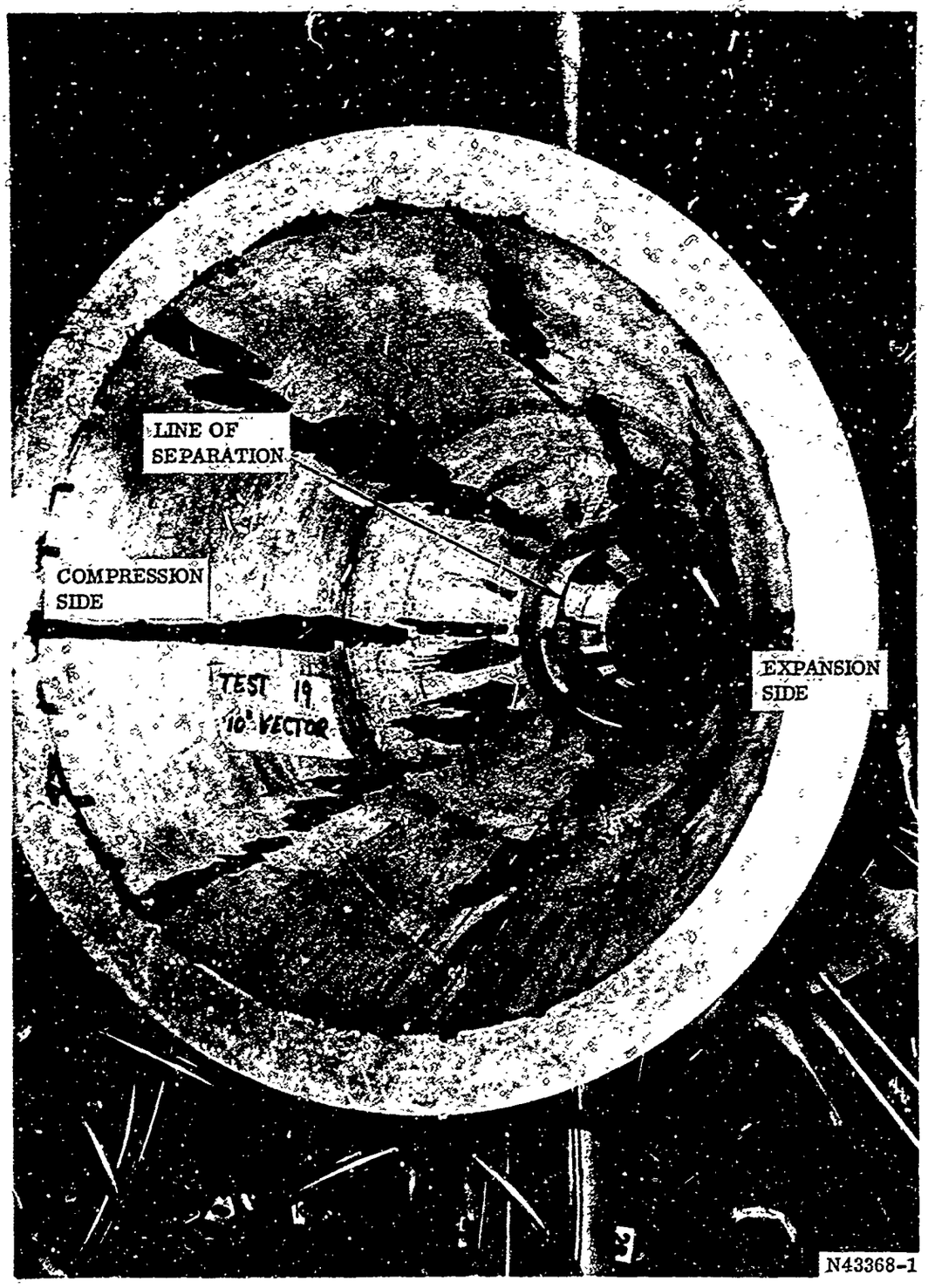

Figure 46. Flow Visualization Showing Separation Upstream of the Joint (Test 21)

Flow separation near the nozzle exit also was discovered using smear data. Pressure data were used to verify this occurrence, in which event, a repeat run was performed.

On the high expansion ratio nozzle, the 10 deg vector angle resulted in the shock wave from the compression side of the nozzle intersecting with the wall on the expansion side of the nozzle. This caused pressure on the expansion side of the nozzle to be appreciably higher than that of the compression side which results in a reduction in torque and side force. This phenomenon can be seen in the pressure plots of Appendix II. The 10 deg vector configuration of Run 10 is a good example of this occurrence.

SECTION VII

CONCLUSIONS

The performance parameters considered in this program were:

1. Side force
2. Axial thrust
3. Actuation torque

The influences of nozzle expansion ratio, nozzle vector angle, joint location, pivot location, exit cone half angle and nozzle erosion on each of the performance parameters were evaluated. Performance data are presented as a function of each of these geometric parameters. These data show that with proper design, appreciable amplification of side force can be achieved with a relatively small loss in axial thrust.

Nozzle internal pressures were recorded for each of the test runs. These data are plotted versus axial station at five circumferential locations around the nozzle. Flow visualization data were also taken to further investigate the flow field.

It was determined that a separated region exists ahead of the joint on the large vector angle configurations. The pressure data are not adequate to properly define flow conditions in this region.

The pressure data as well as flow visualization data are used extensively in the development of an analytical model. A comparison of analytical results with test data is presented in this report.

Data from tests 1 thru 9 were utilized in establishing the design for the demonstration nozzles.

Data from the Cold Flow Test Program will be used for refining the TVC Computer Program. These data will be supplemented with analytical results so that a matrix defining the interaction of various geometries can be developed. The effects of hot gas will also be computed. A regression analysis then will be run so that expressions for each of the performance parameters as a function of the variables mentioned can be included in the TVC Computer Program.

SECTION VIII

RECOMMENDATIONS

The data obtained in this study should be used to evaluate optimum designs for various application. These data should then be verified in cold flow and hot firing tests.

The effect of joint length was not considered in this program. The effects of the parameter should be investigated analytically and verified in cold flow.

A cold flow program in which pressures in the separated area ahead of the joint can be measured should be accomplished. The effects of separation on heat transfer and erosion in this region also should be investigated.

The analytical model presently being developed assumes an ideal gas. Future development should include consideration of real gas effects.